Development of Graphene Reinforced Ultra High Molecular Weight Polyethylene (UHMWPE) Nanocomposite Coatings for Mechanical Bearing Applications

BY

Ismaila Kayode Aliyu

A Dissertation Presented to the

DEANSHIP OF GRADUATE STUDIES

KING FAHD UNIVERSITY OF PETROLEUM & MINERALS

DHAHRAN, SAUDI ARABIA

In Partial Fulfillment of the
Requirements for the Degree of

DOCTOR OF PHILOSOPHY

In

MECHANICAL ENGINEERING

December 2017

KING FAHD UNIVERSITY OF PETROLEUM & MINERALS

DHAHRAN- 31261, SAUDI ARABIA

DEANSHIP OF GRADUATE STUDIES

This thesis, written by **Ismaila Kayode Aliyu** under the direction of his thesis advisor and approved by his thesis committee, has been presented and accepted by the Dean of Graduate Studies, in partial fulfillment of the requirements for the degree of **DOCTOR OF PHILOSOPHY IN MECHANICAL ENGINEERING.**

Dr. Amro Mohammad Al-Qutub
(Advisor)

Dr. Zuhair Mattoug Gasem
Department Chairman

Dr. Mohammed Abdul Samad
(Co-Advisor)

Dr. Salam A. Zummo
Dean of Graduate Studies

Dr. Necar Merah
(Member)

6/6/18
Date

Dr. Saheb Nouari
(Member)

Dr. Zuhair Mattoug Gasem
(Member)

ACKNOWLEDGMENTS

I thank Allah, for making it possible to do this thesis work. My parents provided me guidance, encouragement, and sponsorship to acquire basic and further education. I appreciate their efforts. Also, I thank my wife, children and the rest of my family members for their patience and support.

I really appreciate the input of Dr. Amro Al-Qutub, my thesis advisor. He helped me a lot by providing invaluable guidance and advice throughout my research. Through him, my research experience has been flavored with great engineering concepts. My co-advisor, Dr. Mohammed Abdul Samad was very helpful too. He provided a lot of assistance and he is readily available. I also acknowledge the contributions of all the members of my thesis committee, Prof. Necar Merah, Dr. Saheb Nouari and Dr. Zuhair Gasem.

My profound gratitude goes to Mr. Romeo Agua, the mechanical engineering workshop technician. He used cutting-edge technical experience to fabricate samples and devices for my research. Mr. Ali Saber of the same unit was also very assisting. I thank Mr. Latif Hashmi for his support that I got in the Materials Science Laboratory.

I thank Akeem Yusuf, Muhammad Umar Azam, Osman Kaleem, and Annas bin Ali for their assistance in various forms.

I commend King Fahd University of Petroleum and Minerals (KFUPM) and the Ministry of Higher Education (MoHE), Saudi Arabia for awarding me the scholarship to undertake this degree. My appreciation also goes to Advanced Manufacturing Technology Program (AMT-P), NASENI, Jalingo, Nigeria for granting me a study leave to embark on my Ph.D. degree.

Financial support for this work from King Abdulaziz City for Science and Technology (KACST) through the KACST Annual Program (KAP) Unit at King Fahd University of Petroleum & Minerals (KFUPM) through research project number ART 34 – 47 is highly acknowledged.

Finally, I express my gratitude to anyone I did not mention that has assisted or contributed to the success of this research in one way or the other.

TABLE OF CONTENTS

LIST OF TABLES

LIST OF FIGURES

ABSTRACT

Full Name : Ismaila Kayode Aliyu

Thesis Title : Development of Graphene Reinforced UHMWPE Nanocomposite Coatings for Mechanical Bearing Applications

Major Field : Mechanical Engineering

Date of Degree : December 2017

The main cause of plain bearing failure is the excessive wear during the starting of internal combustion engines due to insufficient lubrication. Various additives are added to lubricants to decrease the wear. Unfortunately, additives pose some dangers to the environment. To minimize these dangers, polymers are used as coatings on metallic bearings because of their ability to provide low friction and wear in dry sliding. However, at high temperature and high compressive stress, polymers cannot survive. Therefore, the main objective of this research is to develop an environmentally friendly self-lubricating Ultra High Molecular Weight Polyethylene (UHMWPE) nanocomposite coating reinforced with graphene nanoplatelets (GNPs) with improved tribological performance. Ultra-sonication was used to achieve uniform dispersion of the GNPs in the UHMWPE matrix. Bulk UHMWPE/GNPs nanocomposites with different compositions of GNPs were first developed and tested as a preliminary study. Then GNPs (0, 0.25, 1 and 2 wt. %) reinforced UHMWPE nanocomposite coatings were developed. An appropriate surface preparation was employed to achieve high adhesion strength. Dry wear tests were conducted on the coatings. The effect of contact pressure, sliding speed, test temperature and lubrication were investigated. The results showed that the optimum amount of GNPs reinforcement was 1 wt. %, which improved UHMWPE wear resistance by 51 % and the coating was able to sustain contact pressures up to 6 MPa. It also sustained pressure and velocity (PV) factor up to 4 MPa.m/s and temperatures up to 115 ^{o}C as compared to pure UHMWPE that failed at 75 ^{o}C. An aluminum thrust bearing was coated with pure and 1 wt. % GNPs reinforced UHMWPE and tested at room temperature. In the dry test, UHMWPE/1 wt. % GNPs coating withstood contact pressures up to 0.8 MPa as compared to pure UHMWPE that withstood 0.3 MPa. In the boundary lubrication test, UHMWPE/1 wt. % GNPs coating withstood 2.7 MPa as compared to pure UHMWPE that withstood only 0.5 MPa. Also, the coating was compatible with various types of lubricants.

ملخص الرسالة

الاسم الكامل: إسماعيل كايودى عليو

عنوان الرسالة: تطوير طلاءات مركبات ال UHMWPE المدعمة بالجرافين لتطبيقات الرمان الميكانيكي

التخصص: هندسة ميكانيكية

تاريخ الدرجة العلمية: ديسمبر 2017

السبب الرئيسي لفشل الرمان المسطح هو التآكل المفرط أثناء بدء تشغيل محركات الاحتراق الداخلي بسبب عدم كفاية التشحيم. تضاف الإضافات المختلفة إلى مواد التشحيم لخفض التآكل. للأسف ، تشكل الإضافات بعض المخاطر على البيئة. لتقليل هذه المخاطر ، يتم استخدام البوليمرات كطلاء على الرمانات المعدنية بسبب قدرتها على توفير الاحتكاك و التآكل المنخفض أثناء الانزلاق الجاف. ومع ذلك ، في درجات الحرارة العالية والأحمال الشديدة ، لا يمكن للبوليمرات أن تستمر في العمل. ولذلك، فإن الهدف الرئيسي من هذا البحث هو تطوير طلاء من البولي ايثيلين ذو الوزن الجزيئي المرتفع للغاية و المكون من مركبات متناهية في الصغر (UHMWPE) والمدعمة بشرائح نانو من الجرافين (GNPs)، بحيث يكون ذو قدرة محسنة لمقاومة إحتكاك المفاصل. تم إستخدام طريقة ultrasonication لتحقيق تشتت منتظم. تم تطوير أول مجموعة من مركبات ال (UHMWPE/GNPs) من مركبات مختلفة من GNPs وتم إختبارها كدراسة أولية. ثم ، تم تجهيز مجموعة من طلاءات ال UHMWPE و المدعمة بال GNPs بتركيزات وزنية مختلفة (0، 0.25، 1 و 2%). تم اعتماد إعداد سطح مناسب لتحقيق قوة التصاق عالية. أُجريت إختبارات الاحتكاك الجافة على الطلاء. تم دراسة تأثير ضغط التلامس وسرعة الإنزلاق ودرجة حرارة الاختبار والتزييت. وأظهرت النتائج أن الكمية المثلى من تعزيز ال GNPs كانت عند نسبة تركيز وزنية 1% و التي حسنت مقاومة ال UHMWPE للتآكل بنسبة 51 ٪ وتمكنت من الحفاظ على الضغوط المتواصلة والتي تصل إلى 6 ميجا باسكال. كما أيضا حافظت على عوامل ضغط و سرعة (PV) تصل إلى 4 ميجاباسكال / ثانية ودرجات حرارة تصل إلى 115 درجة مئوية بالمقارنة مع UHMWPE النقي الذي فشل عند 75 درجة مئوية. تم طلاء رمان دفع من الألمنيوم بال UHMWPE النقي و كذلك بالمدعم بنسبة وزنية 1% من ال GNPs واختبر في درجة حرارة الغرفة. في الإختبار الجاف ، تحمل ال UHMWPE المدعم بنسبة وزنية 1% من الGNPs ضغوط اتصال تصل إلى 0.8 ميجا باسكال مقارنة بـ UHMWPE النقي و التي تحملت 0.3 ميجا باسكال. في إختبار التشحيم الحدودي ، ال UHMWPE المدعم بنسبة وزنية 1% من ال GNPs تحمل 2.7 ميجا باسكال مقارنة بـ UHMWPE النقي والتي تحملت 0.5 ميجا باسكال. أيضا ، كان الطلاء متوافق مع أنواع مختلفة من مواد التشحيم.

CHAPTER 1

INTRODUCTION

Mechanical bearings are widely used in automotive and industrial applications to provide relative rotational or sliding motion between pairs of components. However, due to high friction and wear, there is a high rate of bearings failure. The United States of America spends over $700 billion, 7 % GNP, yearly on friction and wear [1]. It is reported that poor lubrication constitutes 80 % of failures in bearings [2].

Therefore, lubrication is extensively relied on to minimize friction and wear. However, it was observed that the lubricants are only effective during normal operation of the engine. Up to 90 % of bearing wear occurs during the engine startup/shutdown when metal-to-metal contact is unavoidable as a result of lubrication starvation, which is termed as boundary lubrication regime [3]. As a result, additives in various kinds are being added to lubricants to reduce wear occurring during the boundary lubrication.

The success in this regard resulted in a great boom in the lubricant additives market with the United States spending about US $ 3.1 billion on automotive lubricant additive in the year 2012 [4]. The enormous efforts to improve the performance of additives in base oils have resulted in their high cost even though their performance is still limited by operating conditions, such as high pressure and temperature. In addition, a couple of activities in the life cycle of oil additives poses danger to our environment. National and international

regulations are put in place in various countries to limit the use of additives and regulate emissions from automotive engines.

In order to overcome these problems, bearing surfaces are being modified by application of hard coatings, such as TiN and diamondlike carbon coating (DLC). However, these coatings are expensive and incompatible with most bearing counterparts. Hence polymers, due to their excellent properties, are being explored to overcome these challenges. Polymers have light weight, corrosion resistance, low friction, and moderate wear at low temperature and pressure. They also have self-lubricity, fabrication ease, relatively low cost and softness as counterpart [5,6]. Hence polymers are being used to replace metallic bearings. However, polymers cannot be used in place of metals for bearings operating at relatively high compressive stresses and temperatures. Yet the benefits of the self-lubricating polymers can be tapped for high stresses and temperatures applications by applying the polymers as coatings on metallic bearings. As such, the substrate bears the load while the coating provides friction and wear protection, thereby conserving energy and minimizing failures respectively. Within the polymer family, it is also important to carefully select a candidate polymer for use as coatings on a metallic substrate for mechanical bearing applications. Some polymers have much lower friction when sliding against metals such that the friction is close to a liquid lubricated contact. These are called self-lubricating polymers and examples include PTFE and Ultra High Molecular Weight Polyethylene (UHMWPE). Although polytetrafluoroethylene (PTFE) has very low friction it has high wear rate, therefore a suitable selection to solve the current problem would be UHMWPE. It has attractive properties, such as high impact strength, low friction, and high wear resistance compared to other polymers [5,7]. However, UHMWPE has a high

viscosity, which poses fabrication challenge [8,9]. A suitable or improved processing technique has to be used to overcome this problem. Also, UHMWPE has a low load-bearing capacity [5]. Therefore, its tribological properties are being improved by the addition of reinforcements, such as carbonaceous fillers. Graphene has been specifically identified as a new material that can enhance the tribological properties of UHMWPE by providing improved strength and reduced friction. This is due to its very high mechanical strength, thermal conductivity and large surface area [10,11]. Limited research work has been done on graphene reinforced UHMWPE for mechanical bearing applications as bulk and as coatings [7,11–14]. Also, its performance has not been explored for applications involving base oil lubrication and elevated temperature.

Despite the identified potentials of UHMWPE/graphene nanocomposite as boundary lubricant, poor processing, such as inhomogeneous dispersion, non-uniform coating thickness, and poor adhesion can prevent attainment of targeted properties. Ultra-sonication and magnetic stirring with the correct selection of mixing medium and steps have been identified as means of obtaining uniformly dispersed graphene in UHMWPE [11,14,15]. Also, electrostatic spray coating has shown excellent suitability for depositing polymer nanocomposite powders on conductive substrates [16]. It is cost effective with a limited waste of materials and the powders can be deposited at room temperature.

In order to realize the goals of the current research, bulk UHMWPE with different composition of graphene will be developed first by hot pressing. Pin on disc wear test will be carried out on the nanocomposites to identify the optimum graphene reinforcement. The observations and learnings made from the tests will be applied to develop UHMWPE/graphene coatings. The optimum composition will then be further tested to

establish load-bearing capacity and PV limit of the coatings. Also, wear tests at elevated temperature and under base oil boundary lubrication will be carried out on the developed coatings.

The following are important backgrounds necessary for the success of the current research.

1.1 Mechanical Bearings

A Bearing is a component used to provide relative rotational or sliding motion between pairs of components, thereby avoiding contacts that have high friction and wear. The use of bearings enables smooth transfer of contact load, minimize friction and wear, thereby increasing the components operation life since bearings can be replaced after their specified lifetime. There are several ways to classify bearings and a specific bearing may belong to a particular group in most classifications. For instance, a bearing may belong to metallic bearings and also belong to sliding contact bearings. The following are some of the ways bearings are classified.

1.1.1 Metallic vs Polymer Bearings

Metallic bearings are made of ferrous or nonferrous metals. Examples of metallic bearings are bearings made with cast iron, steel, copper alloy and aluminum alloy [17]. Care should be taken when using these bearings to avoid a galvanic cell, which can result in corrosion depending on the environment of the application. Polymer bearings are made with polymeric materials. Examples of polymeric bearings are those made with elastomers and other rubber materials. They may be bonded to steel laminate in some applications. In some applications, the aim of using polymer bearing is its elastic property, which allows much deformation without fracture. Polymeric materials have much lower friction and wear

compared to metallic materials; however, metallic materials can withstand higher load and temperature.

1.1.2 Sliding vs Rolling Contact Bearings

Bearings are also classified based on the type of contact they make in operation. Sliding contact bearings are those that slide over their counterpart with minimal or no relative rotation. They make plain contact with their counterparts during a linear translational motion or rotational motion. The failure modes of this type of bearing include abrasive, adhesive and corrosive wear. Examples of plain bearings are journal bearings, spherical plain bearings, and plain thrust bearings. Rolling element bearings consist of rolling elements, such as balls or rollers, held in retainers, which roll during operation to prevent sliding. As a result, they can withstand higher contact pressure and provide very less friction such that they are also called anti-friction bearings. Some of the rolling element bearings, such as thrust roller bearings are used to support axial load while others are used to support the radial load. Other examples are the spherical roller bearing and the tapered roller bearing, which can handle a combination of axial and radial load. The typical failure mode in rolling element bearings is fatigue spalling. However, when there is significant sliding, severe adhesive wear can occur. The rolling element bearings operate in an elastohydrodynamic mode.

1.1.3 Hydrodynamic vs Hydrostatic Bearings

Thrust and journal bearing can be operated in hydrostatic or hydrodynamic mode. Thrust bearing supports axial load while journal bearing supports radial load. In the hydrostatic mode, a pump is needed to supply lubricant and support the load on the bearing. However, in hydrodynamic bearings, convergent clearance and sufficient hydrodynamic pressure

generated by high speed are needed to separate contacting surfaces. This is why there is metal-to-metal contact in bearings during startup or shutdown of engines called boundary lubrication. In this period the engine is running at low speed. In journal bearings, the convergence is created by small eccentricity between the shaft and the journal, while in the thrust bearings, it is created by pads with convergent clearance. Some of the examples of bearings mentioned in the previous classification can also fall into one of the groups mentioned here. The current classification is about liquid lubricated bearings, it should be noted that there are unlubricated bearings, which are used alone or with the help of solid lubricants. Solid lubricants include Molybdenum disulfide (MoS_2), graphite and Hexagonal boron nitride. These materials have layered crystal structure, which explains why they have low friction [18]. Some metallic materials also exhibit the capability of solid lubrication due to their softness. These include lead, silver, and tin to mention a few [19]. Also, Self-lubricating polymers are used as unlubricated bearings. Figure 1.1 shows some examples of the types of bearings that have been discussed.

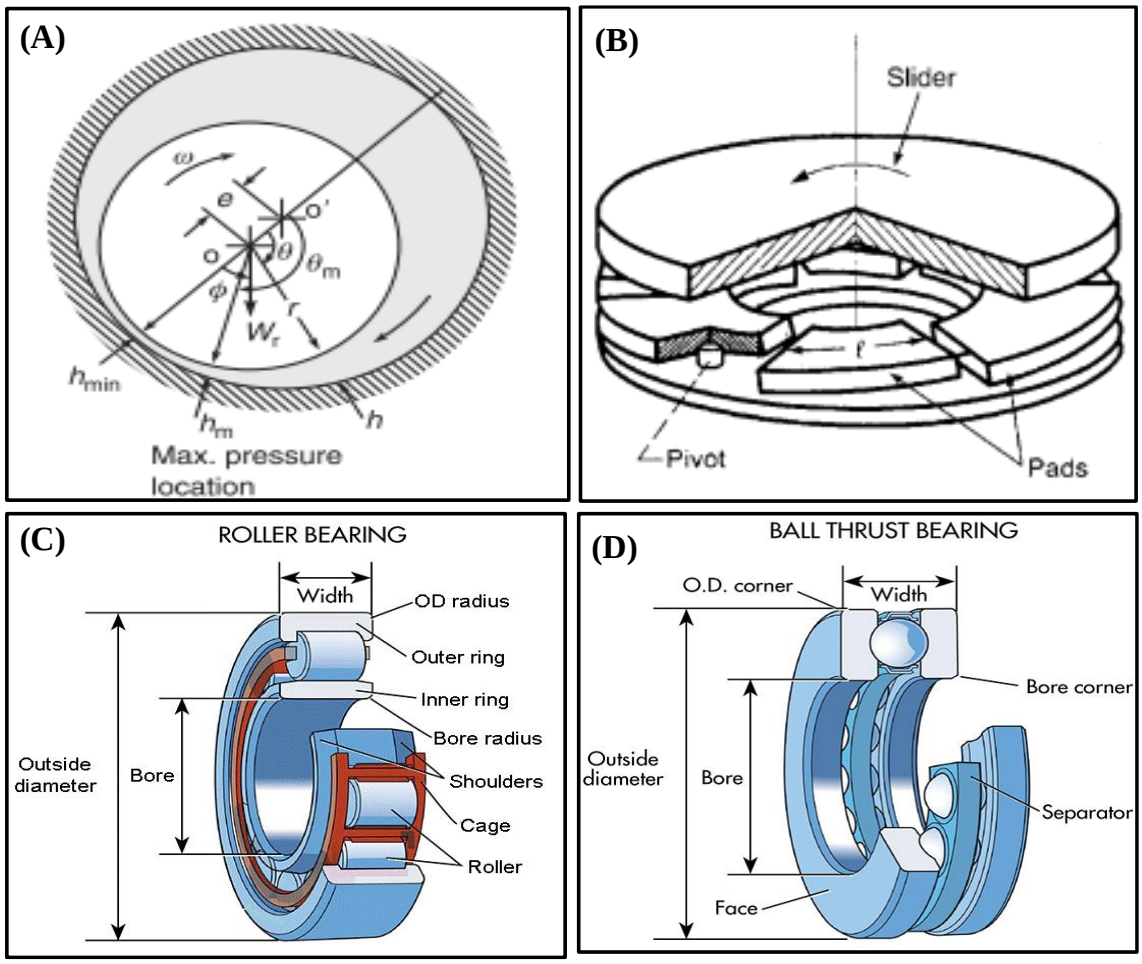

Figure 1.1: Plain bearings (A) Journal, (B) thrust [18] and rolling element bearings, (C) radial [20], and (D) thrust [21]

In this research, a nanocomposite plain bearing material is developed due to the important role it plays in a couple of applications, such as the combustion engines, other automotive machines, and in many industries. Due to the low friction and wear of polymer bearings compared to the metallic bearings, this research focuses on taking the advantage of polymeric material as bearings. However, there are some challenges such as low thermal stability and low compressive strength of polymers. In order to overcome these challenge, a nanocomposite polymer-based coating is applied on a metallic substrate. The coating

provides friction and wear protection while the metallic substrate provides resistance to stress.

1.2 Lubricants and Additives

Lubricants are introduced between rubbing parts in an engine to minimize friction, wear and provide a cooling effect. Figure 1.2, known as Stribeck curve, shows the importance of lubrication in bearings. When the engine is starting or stopping, velocity is low, hence the lubrication type is termed boundary lubrication regime where the lubricant film thickness is very small and cannot prevent metal-to-metal contact. Therefore, despite lubrication, friction is very high as can be seen from the figure and usually there is high wear rate. After the starting period, oil film with sufficient thickness to create separation between contacts is formed. Hence friction reduces tremendously through the mixed lubrication regime to the hydrodynamic lubrication regime.

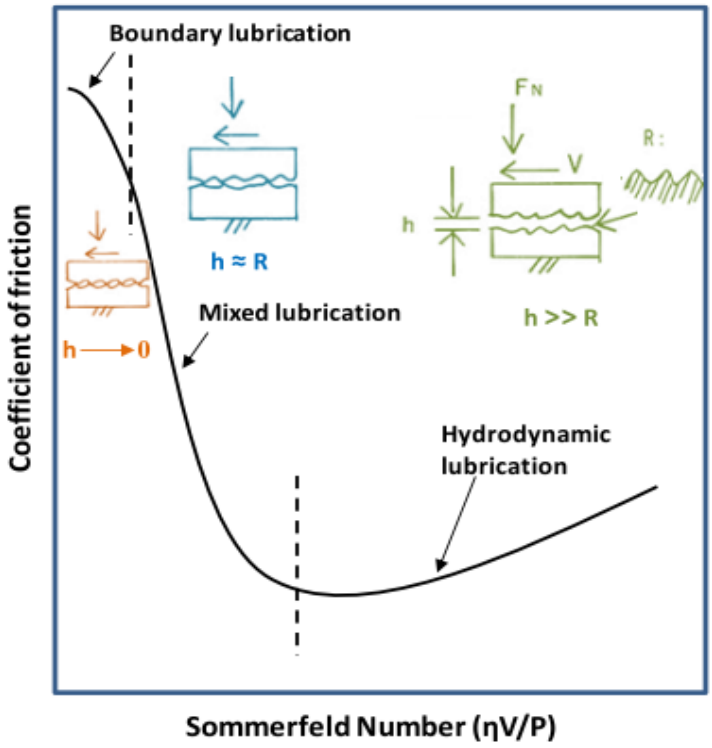

Figure 1.2: A Stribeck curve showing different lubrication regimes in liquid lubricated pair. *R* is the roughness of the surfaces, *h* is the oil film thickness, η is the viscosity of the lubricating oil, V is velocity and P is contact pressure [22]

The term lubricant may refer to a pure base oil or a base oil already mixed with additives depending on the context. In this section, base oil will be first discussed then followed by the discussion of lubricants mixed with additives. Base oil also referred to as base stock are lubricants without any additive. They are classified into two broad categories, such as natural and synthetic lubricants. Sometimes a lubricant is made by the mixture of the two types above. Examples of natural organics include; vegetable oils, animal fat, and petroleum fractions while examples of synthetic organics are; synthetic hydrocarbons, esters, silicones, and polyphenyl ethers. Synthetic oils can withstand extreme operating conditions than natural oil; however, it is costlier. For instance, while synthetic oil can withstand up to 370 ^{o}C, well refined natural oil can only withstand 200 ^{o}C [18].

The American petroleum institute (API) has further classified natural and synthetic oils into five groups as shown in Table 1.1. Respective production method, sulfur contents, saturates and viscosity index are given.

Table 1.1: API classification of base stock [23]

	API BASE OIL CATEGORIES				
	BASE OIL CATEGORY	Sulfur (%)		Saturates (%)	Viscosity Index
Mineral	Group I (solvent refined)	> 0.03	and/or	< 90	80 to 120
Mineral	Group II (hydrotreated)	< 0.03	and	> 90	80 to 120
Mineral	Group III (hydrocracked)	< 0.03	and	> 90	> 120
Synthetic	Group IV	PAO Syntehtic Lubricants			
Synthetic	Group V	All other base oils not included in the above groups			

The Stribeck curve (Figure 1.2) has shown that although lubrication can help to minimize friction and wear, it cannot during the boundary lubrication regime. Nowadays automotive base stocks are hardly used without additives. Additives are commonly long chain alcohols, amines, and fatty acids. They are normally added to lubricants to perform specific functions, such as friction and wear reduction, protection against corrosion, oil oxidation prevention, viscosity enhancer, extreme pressure application, and pour point depression [24]. Additives are greatly used for wear protection during the boundary lubrication regime. Some of the functions of additives are directly for the metallic rubbing parts while others are for the improvement of the lubricant performance. The mechanism of protection is either adsorption or reaction of the additive with the protected surface. Adsorption leads to the formation of a monolayer, with low shear strength limited to friction reduction while reaction leads to the formation of a thicker film, which can serve as friction and wear

reducer. The kind of additive selected for a specific purpose depends on the base oil used, the type, and surface nature of the protected metal. Table 1.2 is a list of commonly used additives and the functions they are used for.

Table 1.2: A table of additives and corresponding function [18,25,26]

Additives	**Function**
Oleic acid	Friction modifier; minimize friction
zinc dialkyl dithiophosphate (ZDDP), Zinc dithiophosphate (ZDP), tricresyl phosphate (TCP), ethyl stearate, and Sulphur compounds	Anti-wear; reduce friction and wear
sulfurized olefins, ZDDP, and TCP	Extreme pressure agent; when subjected to a high load, prevent increase scuffing resistance and prevent seizure
Sulfur-phosphorus compounds, Aromatic amine compounds, Organo-zinc compounds, and Organo-copper compounds	Anti-oxidant; increase the stability of lubricants to oxidation
Alkaline compounds, Esters, Organic acids and Amino-acid derivatives	Corrosion inhibitors; prevents metal surface from corrosion.
Polyisobutylene Succinimides and polyamides	Dispersants; disperse foreign particles, sludge or deposits in the lubricants
Polymethacrylates (PMA), Polyacrylates	Pour point depression; reduce the lowest flow temperature of lubricants
Acrylate polymers	Viscosity index improvers; minimize the drop in viscosity due to high temperature.
Dimethylsiloxanes	Anti-foaming; prevents the formation of air bubbles, which leads to oxidation of lubricants

Due to the harmful nature of additives, calls have been made to develop new additives that are biocompatible. Also, government regulations are in place to control the use of additives while some are prevented. Therefore, there is need to develop a means whereby the use of additives can be totally avoided or greatly minimized.

1.3 International environmental regulations

The world is yearning for a green and healthy environment with less pollution and a healthy climate. However, the environment is currently threatened by various types of pollution. The magnitude of various kinds of pollution is on the rise yearly. Air pollution is a major type of environmental pollution one of which is gas emissions from automobiles, such as passenger's cars and commercial vehicles. CO_2 is one of the leading emitted gas that is affecting the environment. The transportation sector is a major contributor to CO_2 emission. It contributes 27 % of CO_2 emission of which about 40 % is from light-duty vehicles [27]. Another source of environmental pollution, in connection with automotive, is the outcome of activities of the manufacture and use of lubricant additives. Unlike mineral base oils with mild exposure effect, handling and use of additives pose some concerns. The following are various ways in which additives production or use affects our environment and health [24,28].

i. Operators' exposure during mixing and reactions when processing additives.
ii. The tendency to inhale highly crystalline silica during filtration.
iii. Noise during additives processing.
iv. Human exposure during mixing of additives with base oils that can affect the skin and eyes.

v. Many additives are either skin and eye irritant, toxic or skin sensitizer.

vi. The release of harmful pollutants, such as Heavy metals, dioxins, and polychlorinated biphenyl (PCBs) into the atmosphere after combustion, which can affect human and wildlife health.

As a result of these, top global and powerful organizations, such as G20 Nations, World trade organization (WTO), and United Nations Environment Program (UNEP) have expressed their concerns at various occasions. The G20 has identified environmental pollution as a major global concern. Therefore, members of the group are continuously developing, adopting and enforcing regulations to minimize CO_2 in their various countries. Respective governments ensure that the regulations are adhered to by original equipment manufacturers (OEMs). Defaulting OEMs are penalized by fines or restriction of sales [29].

European Union is the leading body in green gas emission regulation. It seeks to reduce CO_2 emission from 130 g/km in 2015 to 95 g/km in the year 2021. Japan has adopted a regulation to reduce CO_2 emission from 127 g/km in 2010 to 105 g/km in the year 2020 while the United States targets 97 g/km in the year 2025 from a base value of 178 in 2010. Saudi Arabia with a total car sale of 828,200 in 2014 applies the Euro 2 emission standard developed in 1996. It targets to reduce CO_2 emission by 17 % between 2016 and 2020 [27]. However, in 2015, many of the G20 members have already started applying the Euro 6 standard developed in 2014. The summary of these regulations can be seen in Table 1.3. It should be noted that the data for Saudi Arabia are under study. Figure 1.3 shows a graphical representation of the G20 Nations emission regulation historically.

Table 1.3: Base CO_2 emission regulation for four G20 members [27] and [29]

Country	Base regulation		Future target	
	CO_2 (g/km)	Year	CO_2 (g/km)	Year
European Union	130	2015	95	2021
Japan	127	2010	105	2020
United states	178	2010	97	2025
Saudi Arabia	158*	2012	142*	2020

*proposed or under study

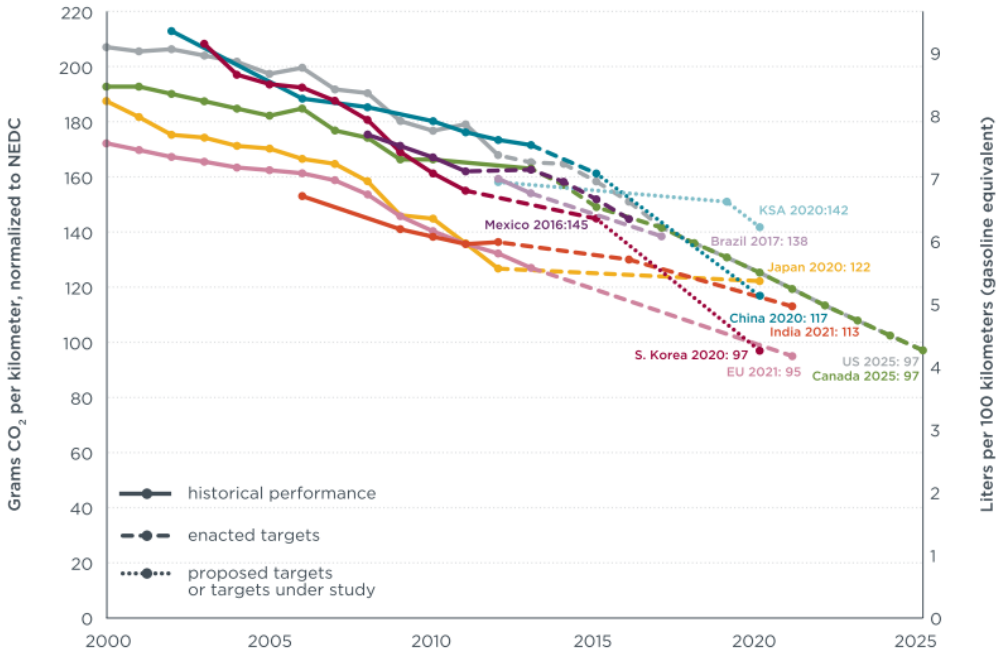

Figure 1.3: A chart on CO_2 emission regulation in the G20 member nations [27]

There are also measures in place to regulate the use of lubricant additives in automobiles. Lubricants are screened and then classified. The European legislation has classified zinc dialkyl dithiophosphate (ZDDP) and some calcium alkaryl sulphonates as dangerous. In order to grant a lubricant a blue angel label, a Germany regulation, which signifies that a product is environmentally friendly, the type of additive is inspected to ensure it meets some requirements and the total additive in a lubricant must be less than 5 % with each constituting additive having a biodegradability greater than 20 % [30]. According to the Stockholm Convention, Persistent Organic Pollutants (POPs) should be restricted. Some POPs, such as dioxins, and polychlorinated biphenyl (PCBs) are released from automotive lubricant combustion.

There isn't any technology yet that can convert emitted CO_2 into less harmful gases, such as NO is converted to N [27]. Therefore, alternative means have to be adopted towards solving the adverse effect of CO_2, from vehicles emission, on the environment. Several technologies are being used to minimize emissions to meet the governments' requirements. These include sequential multipoint fuel injection, turbocharging, engine downsizing, faster burn combustion chamber, and the three-way catalytic converter [31]. Irrespective of the methods used, vehicle weight and machine elements' friction reduction are used to achieve a realistic emission reduction. Weight reduction in vehicles implies that fuel consumption decreases, consequentially reducing green gas emission. Fuel consumption can also be reduced by design of machine systems with low friction. Friction opposes motion in the desired direction. Hence higher energy is required to overcome friction before achieving desired motion. Therefore, a system with less friction will require less energy to drive.

1.4 Research Methodology

A preliminary study was carried out to define the current problem and identify the goal of the research. In order to fulfill this goal, an extensive literature review was carried out. Research gap and specific objectives were arrived at. Methods, principles, and mechanisms of dispersion and coating deposition were studied, thereby selecting specific dispersion and coating methods. To implement the methodology, a systematic stepwise approach was used to disperse the GNPs in the polymer by ultra-sonication and magnetic stirring. After achieving a uniform dispersion, bulk graphene reinforced UHMWPE nanocomposite and coatings were fabricated and tested at various testing parameters and conditions, such as GNPs amount, contact pressure, sliding speed, temperature, and lubrication. A flow chart illustrating the research methodology can be seen in Figure 1.4

1.5 Research Contribution

Achieving the objectives of this research would pave the way for minimizing the use of additives in lubricants. It is also a means of emission reduction in automobiles through weight reduction by replacing heavy metals with light ones with low wear rate due to UHMWPE/GNPs nanocomposites and coatings. The potential of graphene, an emerging material, in improving the tribological properties of UHMWPE coatings would be demonstrated. Finally, operational limits of mechanical bearings would be increased.

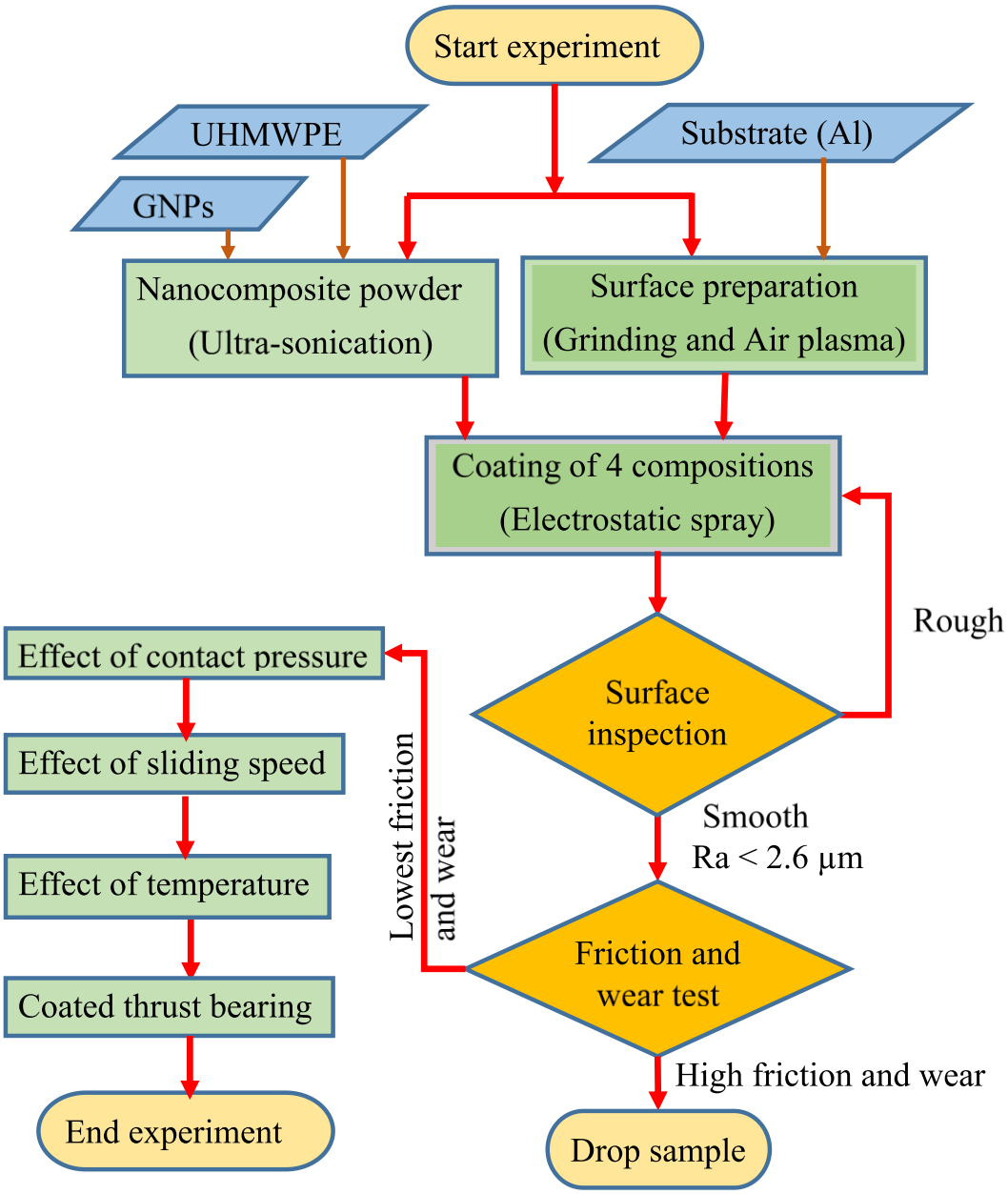

Figure 1.4: Flow chart of the research methodology

The research was carried out in four phases as follow:

I. In this phase, hardness, friction and wear properties of GNPs reinforced UHMWPE bulk nanocomposite were evaluated to understand the possibility of using GNPs effective reinforcement. Bulk UHMWPE nanocomposites were fabricated using hot pressing.

II. After a successful outcome of the bulk nanocomposites testing, UHMWPE coatings on aluminum were deposited using electrostatic spray deposition method. Prior to spraying the nanocomposite powders, a proper surface sample preparation using grinding and air plasma treatment was done. The deposition process was followed by a post heat treatment in an oven using optimized curing parameters to consolidate the powders and obtain a coating with good adhesion. Before any test was done, visual examination and surface roughness of the coatings were measured. Coatings that failed the examinations were discarded. To improve the tribological properties of the coating, it was reinforced with GNPs. The effect of graphene addition was investigated at room temperature. The effect of contact pressure and sliding speed were studied on the composition that gave the best tribological properties. The load-bearing capacity and the pressure and velocity (PV) limit of the coatings were established.

III. Using the maximum contact pressure and sliding speed attained from the previous studies, test temperature was varied to study the thermal capacity of the coatings in order to determine the pressure, velocity and temperature limits of the coatings.

IV. In the fourth part, dry and boundary lubricated wear tests were carried out on pure and GNPs reinforced UHMWPE coated aluminum thrust bearing

CHAPTER 2

LITERATURE REVIEW

2.1 Polymer Tribology

Ceramic and metallic based materials have better mechanical properties and thermal resistance compared to polymers. However, they have higher friction when rubbing against their counterparts. Although ceramics have lower wear rates, the wear rates of metals are higher than polymers as illustrated in Table 2.1. On the other hand, a class of materials known as solid lubricants has very low coefficients of friction (COF). Solid lubricants include Molybdenum disulfide (MoS_2), graphite and hexagonal boron nitride. These materials have layered crystal structure, which explains why they have low friction [18]. However, they are used in powdered form. Polymers, unlike metals and ceramics, have low friction and wear rate. Hence, they can be used as unlubricated bearings over a long period of time. Few polymers, such as polytetrafluoroethylene (PTFE) and UHMWPE have very low friction almost similar to liquid lubricated contact. As such, they are referred to as self-lubricating polymers. Also, polymers are corrosion resistant, light in weight, have reasonable strength, and attractive appearance. This made polymers the right candidate for diverse applications, such as home appliances, biomedical parts, food processing, car engines and aerospace. Taking advantage of these unique properties in automobiles increase operation lifetime, integrity and promote an eco-friendly environment. When polymers are used to reduce friction, it implies that less energy is needed to overcome

friction and in turn less fuel consumption and less emission of harmful gases. This results in low cost and a safer environment.

Table 2.1: The coefficient of friction and wear rate of various material pairs [18]

Material combination	Typical range of coefficient of friction	Typical range of wear coefficient	Comments
Self-mated metals pairs	0.5– > 1 (high)	5×10^{-3} (high)	Undersirable in dry contacts
Dissimilar metals pairs	0.3–0.9 (moderate)	10^{-4}–10^{-3} (moderate)	Easy to fabricate, low cost
Alloy-alloy pairs	0.2–0.6 (moderate)	10^{-6}–10^{-3} (moderate)	
Ceramic-metal pairs	0.25–0.8 (moderate)	10^{-7}–10^{-4} (very low)	For high temperature applications, for lowest wear requirements, self-mated ceramic pairs desirable, good for unlubricated conditions
Ceramic-ceramic pairs	0.25–0.7 (moderate)	10^{-7}–10^{-5} (very low)	
Polymer-hard surface pairs	0.05*–0.6 (low)	10^{-6}–10^{-3} (low)	For corrosive environment and low friction applications, good for low loads, good for unlubricated conditions
Solid lubricant-hard surface pairs	0.05–0.15 (very low)	10^{-4}–10^{-3} (low)	For lowest friction requirement

*PTFE

Several factors, such as polymer hardness, glass transition temperature, surface roughness of the counterface, molecular structure, crystallinity, and chemical electrostatic interactions between the counterface and the polymer determine the COF during sliding. Polymers that have been explored overtime for tribological applications cut across classes of materials, such as rubbers, elastomers, thermosetting and thermoplastic polymers. Of these categories, semicrystalline linear thermoplastics show the lowest coefficient of friction because the nature of its molecular structure enhances easy molecular stretching in the

direction of sliding [32]. Examples of some polymers include polyethylene, PMMA, PTFE, UHMWPE, polyester, polycarbonate, phenolic, nylon, PEEK, ABS, and epoxy [33–35]. PTFE has low friction, high chemical and thermal resistance (Tm=327 °C) making it a potential candidate for applications that require dry lubrication. However, its high wear rate is a major concern. It is therefore used by reinforcing it with various metallic, ceramic or strong fibroid fillers to improve its wear resistance [32]. PTFE is also used as reinforcement in other wear resistant polymers. Polyimide (PI) has high wear resistance but high COF. Fillers like PTFE are added to reduce their friction [36]. It can withstand sliding operation at high temperature and high contact pressure. PEEK unlike soft polymers has high strength, toughness and wear resistance. This polymer can withstand sliding operation at high temperature and high contact pressure and it is resistant to most reagents [37]. However, PEEK has high COF, which results in excessive energy loss during operation. Therefore, nanofillers and low friction polymers like PTFE are added to reduce their friction [36]. The COF of PEEK reduced from about 0.38 to 0.2 when it was reinforced with Carbon nanofiber [22]. Nylon has moderate friction coefficient and low wear rate. It is used for bearings when medium performance is required. However, in the presence of water, wear rate is higher and it has low thermal resistance [37]. Polymethylmethacrylate (PMMA) and Epoxy have high COF and high wear rate as shown in Table 2.2. UHMWPE is widely used for various tribological applications including in the medical field. Example of commercial products includes human joints replacement [38] and mechanical bearings. Its versatility is as a result of its good properties, such as high toughness, and impact strength, low friction and high wear resistance. UHMWPE is more wear resistant than many polymers, such as polyethylene (PE), Epoxy, PEEK,

polyoxymethylene (POM) and polystyrene (PS) [22,32,39,40] as shown in Table 2.2. However, because it has low load-bearing capacity its properties need to be improved by reinforcing it with various fillers. From the several polymers whose properties and applications have been discussed, UHMWPE demonstrates the best combination of properties. Therefore, with the help of appropriate filler and the original excellent properties of UHMWPE, if used as coatings on metallic substrates, such as aluminum, it will provide great tribological advantages.

Table 2.2: The coefficient of friction and wear comparison of some polymers when sliding against a steel disc with roughness, R_a = 1.34 μm [32]

Polymer	Coefficient of Friction	Specific Wear Rate ($\times 10^{-6}$ mm^3 Nm^{-1})	*PV* Value (Pa m s^{-1})
PMMA	0.48	1315.9	145,560
PEEK	0.32	31.7	149,690
UHMWPE	0.19	15.5	187,138
POM	0.32	168.2	149,690
Epoxy	0.45	3506.6	153,997

POM, poly(oxymethylene).

2.2 Coatings

Ranging from applications, such as unlubricated contact motions to liquid lubricated systems with lubrication starvation during starting and stopping period that causes metal-metal contact, friction and wear rate is very high. In order to reduce friction and wear during limited liquid lubrication contact motion, metallic and ceramic surfaces are modified by applying low friction coatings on them. Coatings with a COF equal to or less than 0.2, when sliding against steel, are considered low friction coatings [22]. These coatings are mainly hard coatings. Examples include carbide coatings; ZrC, SiC, TiC, WC, and CrC

[41,42], nitride coatings; TiN, NbN, HfN, and ZrN [41], ternary coatings; CrAlN, and TiAlN [22], oxide coatings TiO_2, and Al_2O_3 [22], diamond-like carbon coating (DLC) [43,44] others Al-Sn, MoS_2/Ti [45,46]. Although these coatings provide low frictions and high wear resistance, they suffer setbacks, such as high cost, poor adhesion to their substrates, harshness to their counterface, non-suitability to liquid lubricant, high thermal stresses, and adverse environmental effect [47–50]. This is why polymeric materials are being explored as an alternative solution to this problem. Polymeric materials have been found to have excellent properties as bulk materials as earlier discussed in the previous section. They have high resistance to corrosion and demonstrate low friction and wear in dry contact motion. As a result, a couple of metallic bearings have been replaced with polymer. However, some bearings cannot be replaced due to the required mechanical and thermal properties being higher than what polymers can withstand. Yet, to take advantage of polymers in this regard, they are applied as coatings on various metallic substrates to improve their tribological and corrosion resistance properties. Polymer coatings are soft coatings, cheaper and have better ease of fabrication as compared to hard coatings mostly fabricated by either CVD or PVD. Some of the existing polymer coatings are polyester, UHMWPE, polycarbonate, PTFE, phenolic, Nylon, PEEK, acrylonitrile butadiene styrene (ABS), and epoxy [33–35,51]. The effect of nanodiamond on the tribological performance of PTFE film was studied by Lee et al. [52]. A low wear rate and reduced friction from 0.21 to 0.16 was reported. The improvement was attributed to the increase in PTFE hardness as a result of uniform dispersion of the diamond. PTFE also demonstrated a self-lubrication effect between the PTFE based coating and the silicon nitride counterface. Also, the reinforcement of PTFE with epoxy enhanced the wear resistance of PTFE twice while

the COF was also reduced [53]. The added epoxy improved the deformation resistance of PTFE, thereby reducing the real area of contact leading to lower friction. The coating of Si with a dual polymer UHMWPE and perfluoropolyether (PFPE) resulted in a COF 6 times lesser than that of Si [54]. An increase in wear resistance, 1000 times compared to Si was also observed. Several polyimide-based coatings were developed on AIS1 440C HT steel substrates by Fusaro et al. [55]. It was observed that the coatings showed reduced friction and wear in vacuum as compared to the environment that contains air. This made the coatings suitable for application in space technology. PEEK reinforced films with different amount of graphene oxide (GO) were fabricated by casting [56]. Wear tests were conducted on the films with a ball on disc configuration. A speed and load of 0.063 m/s and 2.94 N respectively were applied for 20 min. In terms of GO amount, friction and wear decreased with reinforcement up to 0.3 wt. % and afterwards increased. A decrease and then increase in COF as a function of load was observed. A nanocomposite coating made of graphene reinforced Polyphenylene sulfide (PPS) were synthesized by a solution spraying method [57]. GCr15 steel ring was made to slide against the coatings at 0.43 m/s, loads of 100 N. Graphene amounting up to 0.8 wt. % was found to increase the life of the coating, after which the life dropped at 1.5 wt. % graphene. Table 2.3 shows the summary of a couple of researched polymer matrix coatings. Polymer coatings have shown promising potentials for friction and wear reduction, however, care should be taken to avoid fillers or processing methods that can jeopardize the tribological properties. The reinforcement of polyamide (PA11) coatings with dolomite and TiO_2 has led to the increased wear rate of the polymer. However, the addition of short glass fiber to PA 11 composite produced by extrusion and injection molding led to the improvement of both friction and wear significantly.

Table 2.3: Tribological studies of some polymer coatings reinforced with various fillers

S/N	Coatings materials		Substrate	Coating method	Tribological Studies	Ref	Ref No.
	Matrix	Reinforcement					
1	PTFE based	Al_2O_3	Steel	Spin	Wear	Wang et al., 2006	[51]
2	Polyamide 1010	Nano SiO_2	Steel	Flame sprayed	Adhesion fric. & wear	Li et al., 2007	[58]
3	Phenolic	nano Al_2O_3 and PFW	Steel	Spray deposition	Friction and wear	Song et al., 2006	[59]
4	PEEK	Graphite or Nano SiC		Flame spray & painting	Adhesion friction and wear	Zhang et al., 2008	[60]
5	Polycarbonate	Nano SiO_2	Polycarbonate	Spin	Yes	Wang et al., 2010	[61]
6	6FDA-polyimide	MWCNTs*	Al	Direct casting	Friction and wear	Kim et al., 2011	[62]
7	HDPE	SiO_2	……	…….	No	Ma et al., 2013	[63]

The literature search has shown that polymer coatings are promising for providing low friction and wear at limited bearings lubrication condition. However, they have not been fully explored to take advantage of their potentials. The efficient development of polymer coatings with greatly improved friction and wear resistance can pave way for the reduction in the use of liquid lubricants and additives. A reduction in additives will result in a safer environment. The review also showed that although polymer coatings generally have low friction and wear, some of the polymers have even lower friction close to liquid lubricated contact. PTFE is one of these polymers but it has high wear rate. On the other hand,

UHMWPE is a self-lubricating polymer with low wear rate and high impact resistance. Hence it will be good to further explore the tribological properties of UHMWPE with a view to improving them.

2.3 UHMWPE Based Coatings

Although bulk UHMWPE has been identified with outstanding tribological properties, it is challenging to deposit UHMWPE on a substrate due to its high viscosity [8,9]. Also, the load-bearing capacity of UHMWPE is low [5]. Bao et al. [8] synthesized ethylene acrylic acid reinforced UHMWPE coating by flame spray method. It was found that variables, such as particle size of the powder, composition and deposition parameters determine the properties of the coatings. Some difficulties, such as coating non-uniformity, are faced in applying UHMWPE coating by flame spray due to its molecular structure. Electrostatic spray method may yield a coating with better uniformity. In another study, a dip coating method was used to coat UHMWPE on aluminum pins and tested against aluminum disc [64]. The results showed that there was an improvement in both wear resistance properties and friction. With the help of the coating, friction dropped from a range of 0.4 – 1 to a range of 0.02 – 0.2. Also, COF tends to increase with an increase in load or speed. The coating life increased with speed increase but decreased with load [64]. Although this report shows that dip coating can be used to improve the tribological performance of metallic substrates, the process is a chemical based one in which much fumes and gases that can be harmful are generated during the process. This becomes a major concern since one of the aims of this research is to contribute to a safe environment by limiting harmful emissions. Samad and co-authors [65] reported a tribological investigation of UHMWPE/carbon nanotubes (CNTs) coating on steel. A dry wear test was performed

using a silicon nitride ball counterface at a speed and load ranging from 0.1 to 0.25 m/s and 4 N respectively. About 0.16 was obtained as the COF of the coating with 0.2 wt. % CNTs. It was found that CNTs addition up to 2 wt. % increased the life of the coatings. Table 2.4 shows the summary of a couple of researched UHMWPE based coatings. Graphene reinforced UHMWPE nanocomposite was coated on stainless steel using flame spray deposition technique [12]. The coatings were tested against stainless steel using a ball on disc wear test configuration. A normal load and sliding speed of 35 N and 0.01 m/s respectively were applied. About 0.24 was obtained as the COF of pure UHMWPE, while the addition of graphene nanosheet (GNS) lowered the friction to 0.185 [12]. Also, GNS lower the wear rate; however, it was still high in the order of 1.1 X 10^{-3} mm^3/(Nm).

Table 2.4: Tribological studies of UHMWPE coatings reinforced with various fillers

S/N	Coatings materials		Substrate	Coating method	Tribological Studies	Ref	Ref No.
	Matrix	Reinforcement					
1	UHMWPE	Ethylene acrylic acid	steel	Flame sprayed	Wear	Bao et al., 2005	[8]
2	UHMWPE	5 wt. % MWNT	Steel	Electrostatic spraying	Scratch	Bakshi,et al., 2007	[16]
3	UHMWPE	CNTs	Al	Dip coating	Several	Samad and Sinha, 2010	[35]
4	UHMWPE	CNTs	Steel	Dip coating	Several	Samad and Sinha, 2011	[65]
5	UHMWPE	Graphene	Steel	Flame sprayed	Wear	Han et al., 2013	[12]

2.4 UHMWPE and properties

UHMWPE is a polyethylene $–(C_2H_4)_n–$ made of several ethylene monomers (C_2H_4). In the group of polyethylene polymers, it has the highest molecular weight of about 6 million g/mol. A molecular chain contains up to 200,000 ethylene [66]. UHMWPE has gained much popularity due to its use in various industrial applications. Thanks to its good properties, which are stated in Table 2.5. UHMWPE is thermoplastic and inert to chemical attack. It has low COF, high sliding abrasion resistance and high mechanical properties, such as higher toughness and high modulus of rigidity as compared to other polymers.

Table 2.5: The properties of UHMWPE [67]

UHMWPE	
Resin type	GUR 1020
Manufacturer	Ticona
Manufacturing Method	Ram extrusion
Fabricated Form	Annealed
Average molecular wt (molar mass) [g/mol × 10^6]	5.166 to 5.415
Crystallinity; DSC, (20 °C –160 °C) [%]	66 – 71
Density [Kg/m^3]	934
Tensile stress at yield (tensile strength) [MPa]	> 23
Tensile stress at break [ultimate tensile strength [MPa]	> 52
Elongation at break [%]	> 460
Young's modulus [MPa]	> 575
Melting Point DSC, 10K/min [°C]	137.5
Glass Transition Temperature Tg [°C]	-110
Surface and bulk Oxidation Index; material shelf aged 1 year in air (ASTM F2101-01)	0.00

2.5 Carbon-based materials as reinforcement

The term carbon-based materials or carbonaceous materials is used to refer to a couple of allotropes of carbon, which are also called graphitic materials. The advantages of carbon-based materials as reinforcing phase in the development of nanocomposite materials is quite enormous. This has resulted in a lot of technological evolvement wherein new carbon-based materials, such as CNTs and graphene were discovered. Prior to these discoveries, carbon-based materials include diamond, carbon fiber, graphite, and fullerene [68–70]. There has been much of interest on these materials due to their low weight, high strength and Young's modulus, high thermal and electrical conductivity, high surface to volume ratio and ranges of electronic properties that can be manipulated [69,71]. Diamond

and graphite are the first and basic known allotropes of carbon, while diamond carbon atoms are arranged tetrahedrally, those of graphite are arranged hexagonally, layer by layer. Diamond is a 3D material with very high thermal conductivity, hardness, density, and strength. Graphite is a 3D graphitic material from which, a 2D material, such as graphene can be derived by exfoliation. While diamond is a poor lubricant, graphite is a good lubricant due to the ability of their layers to slide over one another. It has lower density and hardness as compared to diamond; however, it is an electrical conductor while diamond is an insulator. Carbon fibers are one dimensional (1D) graphitic materials made of conjugated carbon bonds with sp^2 hybridization. This is why they have high thermal and electrical conductivity and high in-plane strength [72]. They also have layered structures that slide over each other, thereby making the material to have low friction. The structure of this fibers is cup stacked. The material is cheap and has active edges as compared to CNTs. However, it has lower conductivity compared to the other materials in the group, such as CNTs and graphene [72]. Chemical vapor deposition (CVD) is an established method for synthesizing carbon fibers. Carbon fibers have been used to reinforce a couple of polymers for tribological application [73–75]. In most cases, the addition of these fibers leads to the reduction in friction of the polymers during sliding. However, an increase was reported when the fibers were added to polyphenylene [75]. Fullerene is a zero-dimensional (0D), an sp^2 hybridized allotrope of carbon that has a spherical or ellipsoidal shape [76]. Other shapes, such as pentagon and heptagon also exist. Fullerene molecules can be in a couple of forms designated by the number of carbon atom in a molecule, such as C_{20}, C_{24}, C_{36}, C_{50}, C_{60}, and C_{70}. Due to the unique structural, molecular, optical, electrical and mechanical properties of fullerene, it has been used to reinforced various polymers in order

to improve the hardness, optical, electronic and thermal properties [77–81]. The main problem associated with the use of fullerene to reinforce polymer material is their low solubility in organic solvents [82] and narrow UV absorption region [80]. There has to be some form of physical or chemical modification of fullerene to enable their successful reinforcement of polymer for properties improvement. CNTs, one-dimensional materials, were discovered in 1991 by Iijima [83] and since then a lot of research has focused on it. Structure-wise, CNTs have a rolled graphitic structure and is obtained by folding a sheet of carbon atoms into a tube. For instance, the folding of a single graphene sheet results in single wall CNTs. Multi-wall carbon nanotubes comprise several rolled carbon sheets. CNTs have very good physical, mechanical, thermal, and electrical properties [5,68]. However, the main challenge with the use of CNTs to reinforce polymer nanocomposites is the lack of uniform dispersion of CNTs in the matrix due to the entangled nature of the tubes. Various methods such as ultra-sonication, stirring, solution mixing, ball milling, and functionalizing the tubes have been attempted to solve this problem [68]. Another shortcoming of CNTs is their high cost. It is the costliest among the carbonaceous materials. A lot of research work regarding the use of CNTs as polymer reinforcement for friction and wear applications has been reported [5,16,62,84]. Although the addition of CNTs to polymers usually reduce wear rate, it increases COF [65,85]. Among the carbon-based materials discussed so far, graphene is the newest. It has several properties that exceed its counterpart, such as higher elastic modulus, strength, electrical and thermal conductivity [10,11]. This is why it has been chosen as the reinforcement for this research. Hence, detail discussion about graphene, its application, its properties, synthesis and comparison to CNTs is given in the next section.

2.6 Graphene

2.6.1 About Graphene

Graphene is an allotrope of carbon with two-dimension crystal lattice structure formed by sp^2 bonded carbon atoms. Graphite, a 3D structured material contains several sheets of graphene. This is why graphene can be exfoliated from graphite. A single layer of graphene is as thin as the diameter of an atom. Graphene materials exist in several forms, such as graphene monolayer (GML), few layers graphene (FLG), graphene nanoplatelet (GNPs), graphene nanoribbon (GNR), and GO. The crystal structure of graphene and a theoretical structure of GO is shown in Figure 2.1 and Figure 2.2. For the GO structure, He et al. [86] explained that water molecules are present in the interplanar spaces and the hydroxyl groups are normal to the planes.

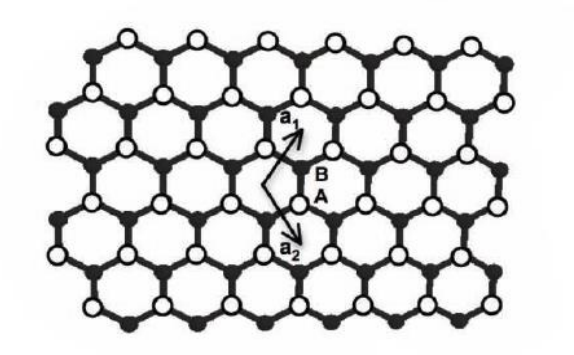

Figure 2.1: Graphene crystal structure [87]

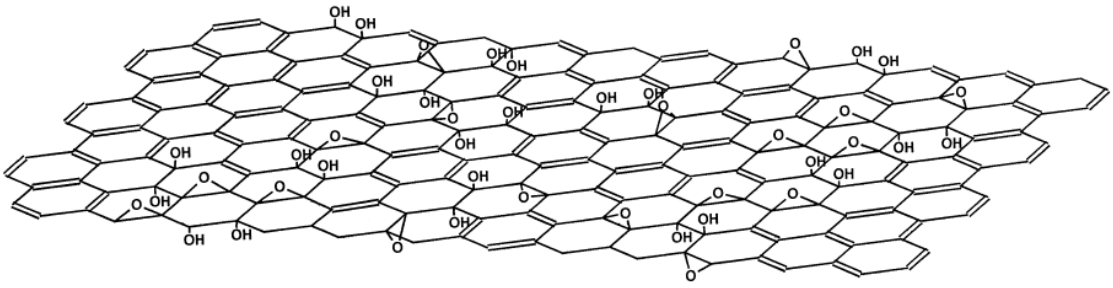

Figure 2.2: A proposed model of graphene oxide structure [86]

2.6.2 Application

Since the discovery of graphene scientists and engineers have explored its application in many ways. These include; transistors, gas detection, conductive films, nanocomposites, coatings, energy storage devices and barrier applications [87–89]. Its application cut across mechanical, tribological, thermal, electrical and optical fields. Even with this, the door is still open for new invention regarding the application of graphene and its related materials. Graphene is currently being explored as reinforcement in polymer coatings to reduce corrosion, friction and wear [12,90,91].

2.6.3 Properties

Graphene has attracted so much attention due to its excellent properties. This excellence cuts across mechanical, tribological, thermal, electrical and optical applications. Despite the fact that the properties of carbon nanotubes (CNTs) are known to be excellent, reports have emerged that graphene can provide better improvement than CNTs when used to reinforce polymer [91]. This is because graphene is 2D and it provides a larger interface with matrices. Lee et al. [92] determined the mechanical properties of graphene experimentally with the aid of analytical and numerical modelling. An intrinsic strength of

42 N/m was obtained for a single layer of graphene. This value was converted to approximately 130 GPa as the strength of bulk graphene. Also, they obtained about 1 TPa as the elastic modulus of two or three layers of graphene and concluded that this will not change for even bulk graphene. Using atomic force microscope (AFM), the friction of a single layer graphene was determined to be 1.0 while that of bulk graphene (number of layers $\geq$ 5) was 0.38. In a different research, a microtribometer was used to measure the COF of monolayer epitaxial graphene [93]. Values ranging from 0.02, initially, to 0.1, after about 100 cycles were obtained. Graphene is hydrophobic and repels oil strongly while GO is hydrophilic [94]. Confocal micro-Raman spectroscopy was used to obtain the thermal conductivity of graphene at room temperature. Values ranging from 4840 to 5300 W/mK was obtained for monolayer graphene [95] while 4100 to 4800 W/mK was obtained for a suspended flake of graphene [96]. 7600 S/m and 2 630 m2/g were reported as the electrical conductivity and specific surface area of graphene respectively [97]. The dispersibility induced by functionalization of graphene to GO is very significant; however, some of its properties depreciate. Unlike graphene, the young modulus of GO is highly influenced by a number of GO layers. With multi-layers, a maximum of 42 GPa was reported [98]. However, the measurement of the modulus of a single GO layer gave a huge difference; an average Young's modulus of 250 GPa was obtained [99]. This value, 250 GPa, is still far less than the elastic modulus of graphene, which is approximately 1 TPa. The intrinsic strength of multi-layer GO was reported to vary from 76 to 293 MPa [98]. Again, this is far less than the strength of graphene, which is approximately 130 GPa. The friction of GO reported is appreciably higher than that of graphene. While 0.1 was obtained for graphene, 0.55 was obtained for GO [100]. Also, the electrical conductivity of GO is poor compared

to graphene. GO is an insulator [101] while the conductivity of graphene is 7600 S/m [97]. Likewise, the thermal conductivity of RGO, ~9 W/mK [102] is very low as compared to that of graphene, which can be as much as 5300 W/mK. A comparison of graphene is made with reference to CNTs, which is a competing carbon with graphene in Table 2.6.

Table 2.6: Properties of graphene compared to CNTs

	CNTs	Graphene
1	High cost	Low cost [10]
2	Lower surface area [10]	Large surface area; greater interface enhancing bonding
3	Lower thermal conductivity 2900 $Wm^{-1} K^{-1}$ [10]	Higher thermal conductivity 5300 $Wm^{-1} K^{-1}$ [10]
4	More difficult to disperse	Easier to disperse than CNTs [11]
5	A lesser degree of lubrication	2D layer provides a higher degree of lubrication [11]
6	Elastic modulus of 1 TPa	Elastic modulus of 1 TPa [10]
7	Specific gravity 0.8 g/cm3	Specific gravity 1.8–2.2 g/cm3 [10]
8	Strength 50–500 GPa	Strength 100–400 GPa [10]

2.6.4 Synthesis

Graphene can be synthesized by either bottom-up or top-down approach [103]. The top-down method involves synthesizing graphene by the exfoliation of graphite. Methods that fall into this category include; mechanical, thermal, liquid-phase, chemical and electrochemical exfoliation [88,103–105]. It has been proposed that in order for exfoliation to happen, a critical temperature of 550 ^{o}C must be attained during thermal exfoliation of

graphite oxide to produce graphene [106]. In the bottom-up method, graphene is synthesized directly from organic compounds [107]. Examples of this method include; epitaxial growth and CVD [88,108]**.** A proposed chart showing the mechanism of growth during the synthesis of graphene by CVD can be found in reference [107]. The mechanism was divided into two, namely carbon precipitation and surface growth. The bottom-up method is preferable because the graphene produced are defect free. However, bulk production is not favored by this method [103]. Hence the top-down approach is easier and more convenient for large scale. Sometimes, to apply a top-down technique, graphite is first oxidized to obtain GO. The GO is then reduced to graphene. Ball milling has found wide use in the mechanical exfoliation of graphite to produce graphene. In some of these research, a mixture of graphite and polymeric material was milled [109–111]. This enhances the intercalation of graphene contributing to the exfoliation process. Also, the graphene becomes functionalized with grafted polymers on its surfaces. In other cases, graphite alone was milled to obtain graphene [112–115]. The exfoliation of graphite to produce graphene by mechanical milling is schematically illustrated in Figure 2.3. The mechanical milling of graphite causes a decrease in crystallinity with an increase in milling time [116].

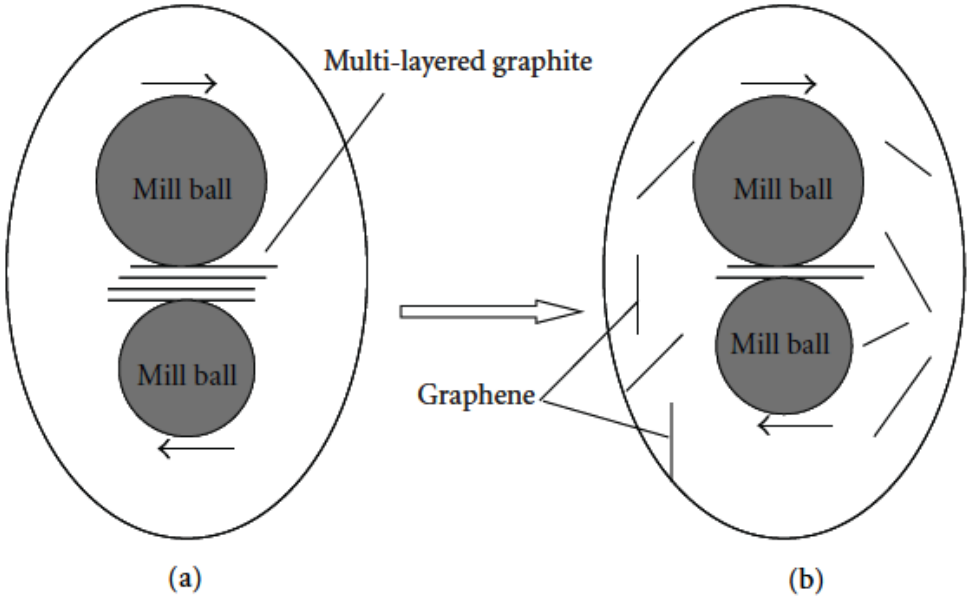

Figure 2.3: Ball milling Schematics (A) initial graphite material with multi-layers (B) graphene platelets exfoliated due to milling [113]

2.7 Polymer Coating Technology

Polymer coatings are very attractive in tribological applications. However, several challenges are being faced in fabricating polymer nanocomposite coatings of desired performance for many evolving applications. Some of these challenges are low load-bearing capacity and low thermal resistance. Therefore, there is the need to review current polymer coating techniques in order to select and improve a technique that can overcome the mentioned problems. This would cater for the continuously emerging applications requirements and mass production adaptability. Prior to choosing a coating method, it is essential to understand its principles and mechanism. This will enable the choice of a good method, the control of process parameters and condition and eventually development of excellent coatings. The features of a potentially good coating method include; quality

coating output; in terms of adhesion and uniform thickness, low cost, adaptability to mass production, ability to coat large surface area and thin film production possibility. Methods that are being used for polymer coatings include; flame spray, solution casting, spin coating, dip coating, and electrostatic spraying [117–119]. These methods can be presented in a classification form as shown in Table 2.7. Main process parameters and conditions include; type of surface pretreatment before coating, spray distance, applied voltage, flow rate, deposition time, powder particle size, powder resistivity, substrate temperature, powder viscosity, curing temperature and time, and type of powder; thermoset or thermoplastic [51,120].

Table 2.7: Classes of coating techniques

Class	Examples
Sol-gel	Dip coating, Spin coating, Spray coating (conventional or electrostatic), electrodeposition [117,118].
Thermal spray	Wire spray, Flame spray, High velocity oxyfuel and plasma spray [118].
Vacuum techniques	Plasma polymerization, Pulsed laser deposition [118,119].
Powder coating	Fluidized bed, Electrostatic spray gun, Electrostatic fluidized bed.
Others (unclassified)	Grafting [119], Painting [118],

Flame spray coating, an example of thermal spray coating process, uses the heat generated from combustion of a fuel gas and oxygen mixture to heat the consumable. The consumable can be a wire or powder material. The heated consumable is then deposited via a gun or

torch [118]. The coating material is sprayed at molten or almost molten state. Thermal degradation is avoided by a careful selection of processing parameters. The spray rate of the process is moderate, the cost is low and the coatings produced by the process are durable [12]. However, the disadvantages of flame spray include; (i) the possibility of the coatings to exhibit a low bond strength, (ii) a high oxide content, (iii) much porosity, (iv) the production of fumes, noise, radiation, and dust during coating process, which are harmful to health [118]. Another method of coatings deposition is solution casting, which has been in existence for over 100 years [121]. A mold is immersed in a polymer (coating material) solution. The polymer solution forms a coat around the mold [121]. The mold is then removed from the solution in a controlled manner. After that, the obtained coating is cured. The process allows application of multi-film with a hybrid of properties and it has widely been applied commercially [122]. With solution casting, high-quality thin films can be produced [123]. However, the process is expensive due to the involvement of some solvents [124]. Some of the solvents are toxic and can be harmful. Organic solvents are normally used while they are incompatible with most plastics [125]. Also, the solvent residue may cause mild or severe defects in the coatings. Casting related methods, such as direct casting are also used to apply coatings on substrates. In direct casting, the coating material solution is poured and spread on the substrate then the solvent is allowed to evaporate. Spin coating is a common and conventional method for coating polymer materials on flat surfaces and dates back decades. An appropriate amount of polymer suspension or resin is dropped on the center of a substrate [126]. The substrate is then spun at a low or high speed depending on the desired coating thickness. Centripetal acceleration causes the coating material to spread over the entire surface of the substrate. The coating

thickness is affected by some parameters, such as time, speed, coating suspension concentration and viscosity [51]. Spin coating is a simple process. The process variables are not coupled so film thickness can easily be adjusted by speed or viscosity variation [127]. It is a cheap process in which film of uniform and desired thickness can easily be achieved. The process is also characterized by short processing time. However, the process is limited to planar substrates [1]. Also, large substrates cannot be spun at a high rate sufficient for the formation of a thin film. Furthermore, there is a significant waste of material because only less than 10 % of the coating solution is actually utilized [128,129]. The process is incompatible with roll-to-roll processing [130] resulting in relatively low yield. In a dip coating process, the substrate is prepared, heated, dipped into coating solution and withdrawn at a specific speed. The solution adheres to the substrate surface while the solvent drains and evaporates to leave behind the coating material. The speed of withdrawal determines the thickness of the film. Dip coating enables prompt and single pass formation of the film [130]. It is also compatible with the roll-to-roll processing enabling mass production. All the sides of the substrate can be coated at a time, unlike vacuum coating processes and spin coating. It can be simply applied to both small and large substrates, unlike the other coating techniques in which large size substrates become more difficult to coat [131]. The disadvantages of dip coating include; non-uniform thickness, internal stress, and difficulty of coating irregular shapes. Another popular technique, used in applying polymer coatings in powder form, is the spray coating. There are two types of spray coating methods. The first one is the non-electrostatic spray coating method that involves the spraying of coating material by a fluid medium. Fluids with various properties can be sprayed. However, it is difficult to obtain a thin film with this method. Also, surface

roughness can be high [132]. The second type of spray coating is the one that operates based on electrostatic mechanism. The coating material is charged before being passed through an electrostatic gun. The gun is faced with a grounded substrate that attracts the coating materials after spraying. This method is unique in that the attractive force allows coating materials just sufficient for the desired thickness of the coating to be sprayed, avoiding waste of coating materials. Also, all the sides of the substrate are coated including those not directly facing the gun. Due to the numerous advantages and fewer disadvantages of this method over the other methods the following section is dedicated to discussing it in details.

2.8 Electrostatic Spray Deposition

The use of electrostatic spray method for coatings date back to 1950s; however, appreciable development in the technology occurred in 1960 [133]. It is suitable for applying polymer coatings. For example, epoxy thermosetting and thermoplastic powders possess electrical properties required for satisfactory electrical charging and spraying [133]. Electrostatic spraying is popularly used for decorative painting, coating of medical devices [134], and fabricating solar cells [135,136]. However, less exploration has been done for tribological applications. The process is either automatic or manual where the sprayed material can be in powder form or atomized liquid. Some research works were reported in which coating materials in solution form were sprayed. The advantages and disadvantages of this method are given below.

2.8.1 Advantages and Disadvantages of Electrostatic Coating

Advantages

- Uniform thickness is obtained due to the even electrostatic attraction between the substrate and the coating material. The particles do not accumulate directly to the portion in front of the gun nozzle.
- It can provide a uniform coating on irregular and complex shaped objects due to electrostatic attraction principle.
- The electrostatic spraying of powder materials has a less negative impact on the environment compared to solvent-based coatings.
- There is no need to preheat the substrate and powder deposition temperature is low due to electrostatic attraction [137].
- The process can be automated [138].
- Electrostatic attraction prevents over-spraying of powder.
- It is easy and environmentally friendly; solvents are not involved.
- There is no substrate size limitation, unlike other coating methods, such as chamber based methods [139].
- It is a fast spray process, unlike dip coating in which coating formation after dipping is slow [139].
- It is a simple, flexible and versatile process compared to other methods.

Disadvantages

- Poor earthing can lead to faulty discharge, which may cause fire [138].
- There is the inability to coat nonconductive substrates without modifications.

- The maximum obtainable thickness is limited by charge saturation.

2.8.2 The procedure, Principle, and Mechanism of Electrostatic coating

The metal substrate is first grounded and polished to yield a good surface finish, which enhances coating adhesion to the substrate. Then the substrate is ultrasonically cleaned in ethanol and wiped in a drying chamber [140]. Next the substrate is held in a sample holder and placed inside the spray booth at a specific distance from the tip of the spray gun [141]. The substrate is electrically grounded, after which feed pressure, auxiliary pressure, voltage, and exposure time are set. Spraying is then carried out after which curing is done to crosslink the polymer by heating the coating in an oven [142]. During curing, after heat is applied the coating may be quenched and then annealed or cooled in different fashions. This can also affect the properties of the developed film due to the possibility of cooling at different rates, annealing at different temperatures for varied amount of time. There are many types of electrostatic coating process and the coating materials may be in powder or liquid form. Powder coating method is environmentally friendly [140,143] since it doesn't involve the use of solvents that can pollute the environment. It is also economical and produces high-quality coatings. The over-sprayed powder can be recycled back into the coating system resulting in less than 5 % material waste [144]. The setup used for spraying liquids is different from the one used for spraying powders. For powder coating, there are also different types of setups and guns. The corona gun and the triboelectric gun are the two most popularly used guns for electrostatic coating. In the triboelectric gun, the powder is charged by friction [133]. The powder is blown through the barrel, and then to the substrate. As for the corona gun, powder particles are charged by electric field resulting from the applied voltage. An additional electric field exists between the gun and the

workpiece. Copious ions, which enhance the charge field, are present in the transport region [133]. Fluidized bed may or may not be used during electrostatic spray coating. The fluidized bed electrostatic coating system consists of a charging system, a powder booth, a delivery system and a recovery system. The main parts include the fluidized bed, also known as the feed hopper, the gun, the booth, the power source and controls, the powder recovery system and the over-sprayed powder collection system. These parts are connected by several cables and hoses. The powder material is initially fluidized by blowing air through a perforated base into the powder in the reservoir [133]. This results in the powder being suspended in air. Fluidized powder is then blown along a feed hose to a charging and dispensing gun where the powder is charged, at high voltage, ranging from 30 to 100kV [133,145], but low current. This is referred to as corona charging. The charged powder is sprayed as a cloud of powder, driven by an electrostatic field and aerodynamic force of air flow, leaving the gun towards the workpiece. The workpiece is dipped in the cloud of the powders, the particles are then attracted to the substrate. The specimen is then heated in the oven, causing it to melt and be cured while the film gets solidified. Fluidized bed method has also been used to refer to a powder coating process in which the powder is not applied by spraying [141]. In this type of fluidized bed coating, the substrate is heated and then dipped into an aerated bed filled with fluidized powder then the powder sticks to the substrate. Substrate temperature assists in melting the power to flow and create a uniform coating. This method is usually used for relatively thick coatings [146]. A simple gun consists of a cylindrical barrel with one or more sharply pointed electrodes maintained at a high negative potential. The intense voltage gradient at around the tip of the electrode sets up a corona discharge through which powder particles pass. Unlike the fluidized bed

system, the simple electrostatic spray set up is composed of a gun (Figure 2.4) and a spray booth. Voltage is applied across a cable that is connected to an electrode located at the tip of the spray gun. This causes current to flow through the circuit creating electric field. Airflow transports powder through the spray gun to the tip and then allow it to be sprayed on a grounded substrate in the spray booth. As the mixture of airflow and powder passes through the gun tip, the powder is charged, as a result of the electrostatic field set by the applied voltage. This makes the powder to be attracted to the substrate as soon as it is ejected from the tip of the gun. The feeding pressure is a function of the amount of powder sprayed per unit time. The auxiliary pressure determines how spread out the powder cloud is when leaving the tip of the gun. Electrostatic and aerodynamic forces ensure a temporary adherence of powder to the substrate before curing [141]. A simple and summarized schematic that describes the electrostatic spray coating process is shown in Figure 2.5.

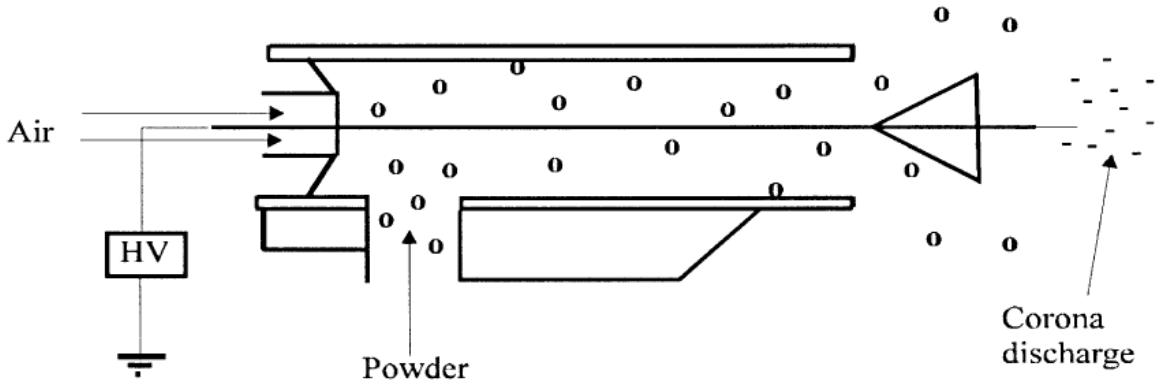

Figure 2.4: A conventional corona gun [133]

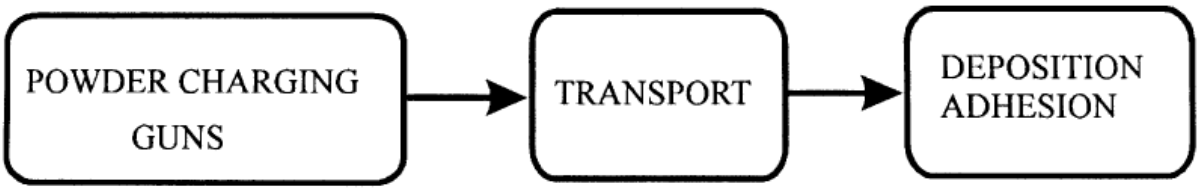

Figure 2.5: A Regions of the powder coating system [133]

The electrostatic spray coating method requires conductive substrates. Nonconductive substrates need to be modified before coating. An example of such modification is the cold spraying of polyamide, a nonconductive substrate, with Cu powder before electrostatically spraying polymer powders on the substrate. Opposite charge between the substrate and the powder allows sufficient adhesion till the coating is cured. The presence of orange peel, pinholes, and micro-dents on coatings may justify corona charge presence [143]. Although the electrostatic coating method has several advantages, it is difficult to fabricate films of small thickness, less than 25 μm [144].

2.8.3 Process Parameters and Their Effect on Coatings Quality

The set of process parameters used during electrostatic spraying can highly influence the coating properties, such as first pass transfer efficiency (FPTE), adhesion strength, coating uniformity [147], coat thickness [148], roughness, friction, and wear. It is desired to obtain adequate cross-linked and gloss film at the minimum possible temperature and/or time. However, it is also important to avoid an incomplete film baking [140]. This is one of the reasons that make it essential to study and optimize the effect of process parameters on coatings quality and properties.

Applied voltage

An increase in applied voltage from 30 to 50 kV increased coating thickness during electrostatic spraying of epoxy–polyester powder [145]. This is due to increase in transfer efficiency when the applied voltage is increased. However, increase in voltage within 70 kV and 90 kV, resulted in a drop in film thickness. This was attributed to the inability of Cu, the conductive interlayer, to ground the whole of the incoming electrical charge, thereby causing some amount of repulsion on the sprayed powder. Also, the polyolefin-based plastic polymer was sprayed on low alloy carbon steel using fluidize bed electrostatic coating method [149]. It was found that coating thickness increased throughout when the applied voltage was varied from 50 to 90 kV.

Feed pressure and Auxiliary pressure

Increase in feed pressure results in coating thickness increase while the increase in auxiliary pressure causes a decrease in coating thickness. The feed pressure determines the powder flow rate ejected at the tip of the gun. It is related to the aerodynamic force of the coating process. The auxiliary pressure determines the spread of the powder cloud; the more the amount of the auxiliary pressure, the more the spread out of the cloud [145]. A different research work also showed that variation in airflow rate from 6 to 12 m^3/h resulted in coating thickness increase [149].

Exposure time

Different observations were reported regarding the effect of exposure time on coating thickness. At constant applied voltage, feed and auxiliary pressure (50 kV, 2.0 bar, and 1.0 bar respectively), the effect of exposure time on roughness, and coating thickness were

studied [145]. Exposure time was varied from 3 to 15 s. Coating thickness increased with exposure time till 9 s before a linear drop in thickness with exposure time was recorded. Roughness was found to decrease with exposure time initially up to 6 s but thereafter increased with time linearly. Another report shows that there was a continuous increase in coating thickness when the exposure time was varied from 3 to 10 s. However, at an applied voltage of 90 kV coating thickness decreased slightly with the increase in exposure time. This implies that an optimum combination of exposure time and voltage is needed to avoid a negative result.

Curing temperature and time

Curing is a very important post-processing step in any coating procedure. It enhances an adequate flow of the coated material on the substrate and promotes adhesion. Hence a proper selection of curing parameters is needed to ensure excellent curing. The outcome of the curing process is affected by the temperature and time at which it is carried out. Barletta et al. [140] demonstrated the effect of these parameters on the coating qualities by curing epoxy based coating at different temperatures and time after electrostatic spraying using fluidized bed coating system. It was found that extent of coating conversion increased with temperature and time. A maximum conversion was observed at 200 ^{o}C, which is the maximum temperature tested. Although the degree of conversion increases with time, the rate of conversion decreases with time making the extent of conversion to approach a limiting amount at a range of curing times. Relatively adequate amount of temperature and time are required to allow sufficient crosslinking during curing. It ensures absolute melting, flowing and leveling of the powders. The curing temperature also affects the roughness of the coating surface. At constant curing time, average roughness decreases with curing

temperature. Higher curing temperature is required to obtain coatings with high adhesive strength. The higher the temperature the higher the adhesion strength at constant curing time. Also, with higher temperature, lower curing time can be adopted to arrive at an equal amount of strength. The adhesive strength is dependent on time in a similar fashion as its dependence on temperature as explained earlier/above. It has also been shown that coatings crosslinked at higher temperature or time resulted in better tribological properties yielding low friction and wear [140].

Amount of reinforcement

In electrostatic spray application of PEEK-PTFE composite coatings on stainless steel, the effect of PTFE amount on tribological properties was studied. The process was carried out at an applied voltage of 90 kV, an applied current of 85 μA while the distance between the nozzle and the substrate was 0.2 m. and a feed pressure of 0.4 MPa was used [150]. The contact angle was found to increase from about 75 to 110 when the amount of the PTFE reinforcement was increased from 0 to 10 wt. % [150]. This is a characteristic evolution from hydrophilic nature to hydrophobic. While COF drops continuously with increase in the amount of PTFE, wear rate increased mainly. Using similar coating method, the increase in the amount of MoS_2, a solid lubricant in polyester was found to decrease both COF and wear [151].

2.9 Thesis objectives

The extensive literature search has shown that although UHMWPE is a promising polymer for friction and wear reduction in mechanical bearings, such as in automotive, only a few studies exist in this regard. Rather UHMWPE has been extensively developed for medical

applications, such as artificial joint replacements in the human body. Although the focus of this work is on friction and wear reduction during boundary lubrication, the bearing will be totally exposed to lubricant during other regimes of lubrication. Hence bearing materials should be compatible with lubricants. The high corrosion resistance of UHMWPE makes it a good candidate for this situation. This characteristic among other properties mentioned earlier has made UHMWPE to be chosen for the current work. The review also showed that graphene reinforced UHMWPE coating is hardly reported. There seems to be only one report that studied UHMWPE/graphene coating [12]. However, the contact type does not accurately simulate plain bearing application, which is the current focus. Therefore, there is a need for a systematic study on the friction and wear behavior of UHMWPE nanocomposites coatings reinforced with graphene in both unlubricated and lubricated state, room and elevated temperature, using a contact configuration that closely simulates the true bearing application.

Therefore, the objectives of this research include:

- To develop a bulk UHMWPE/GNPs nanocomposite in order to assess the feasibility of improvement in tribological properties due to GNPs addition.
- To develop a graphene reinforced polymer nanocomposite coating with improved tribological properties
- To establish the limiting sliding speed, contact pressure and temperature for the coating with an optimum amount of GNPs
- To apply the coating on an aluminum thrust bearing substrate and evaluate its performance under both dry and lubricated test conditions.

CHAPTER 3

MATERIALS AND EXPERIMENTAL DETAILS

The raw materials, equipment, processing techniques and characterizations used for this research are discussed here. Careful selection of materials, equipment, and techniques was made based on the findings from the literature review. This chapter gives detailed information regarding materials, nanocomposite powder preparation, bulk nanocomposite fabrication, development of coatings, and various characterization methods, such as imaging, profilometric, and tribological tests.

3.1 Materials

UHMWPE and GNPs were used as matrix and reinforcement, respectively. The UHMWPE was supplied in powder form by Goodfellow Cambridge Ltd, UK with an average particle size of 90 µm as shown in Figure 3.1A. Its density is 0.94 g/cm^3. GNPs with an average diameter of 10 µm was purchased from Ad-Nano Technologies Private Limited, India. It is made up of several platelets with varying thickness as shown in Figure 3.1B. Each platelet contains several layers of single graphene sheets. The average thickness of the platelets estimated from the SEM image is 180 nm. Acetone was used for the mixing of the powders. The substrates were made from aluminum alloy with composition as shown in Table 3.1. Two shapes of substrates were fabricated. The first is a set of disc samples each 25 mm in diameter and 6 mm in thickness while the second set of substrates, like a thrust bearing, have ring contact surface of inner and outer radius 12.5 and 15 mm respectively (Figure 3.2).

Table 3.1: Composition of the aluminum substrate

Elements	Al	Cu	Pb	Fe	Bi	Si	Cd	Ti	Ni	others
wt. %	95.5	2.85	0.48	0.46	0.42	0.076	0.023	0.023	0.021	0.147

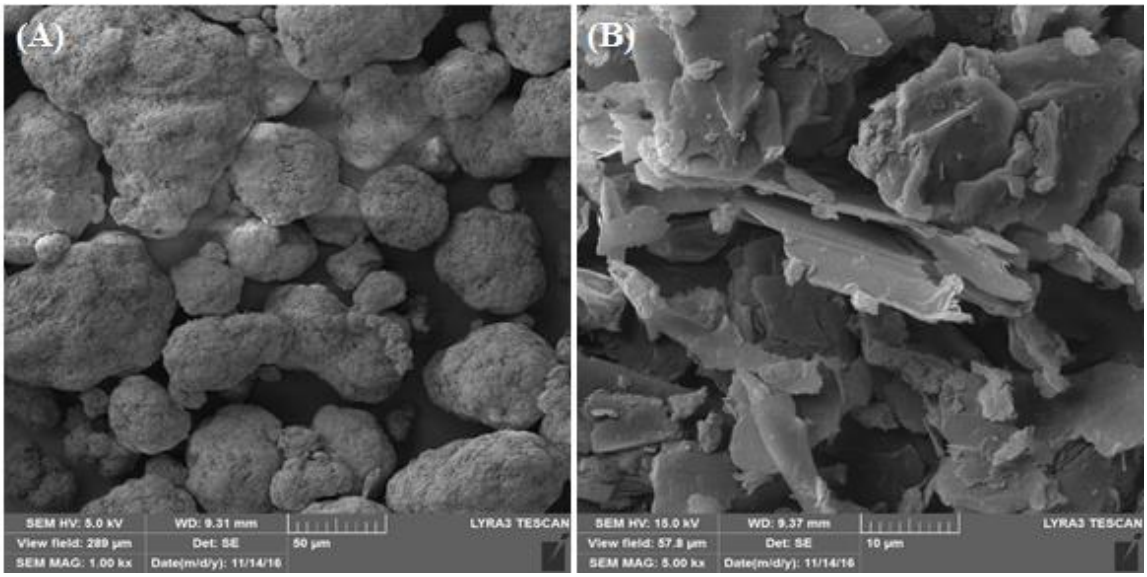

Figure 3.1: As-received (A) UHMWPE and (B) GNPs powders

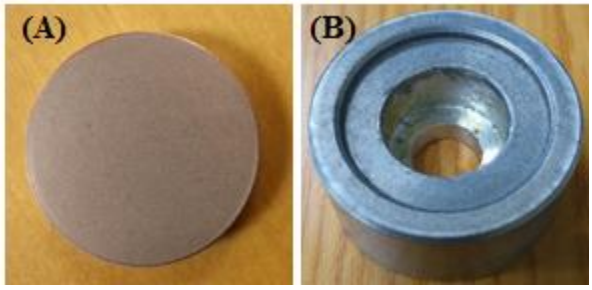

Figure 3.2: Coated (A) disc and (B) thrust bearing substrates

3.2 Raw nanocomposite preparation

It has been established that stirring and/or sonication can yield a uniform dispersion of graphene in UHMWPE [11,152]. Therefore, in this research, a carefully arranged procedure of sonication and stirring was adopted to ensure that the GNPs was uniformly dispersed in the UHMWPE matrix. An appropriate amount, depending on the desired nanocomposite composition, of GNPs was first sonicated in 50 ml of acetone for 10 min using Sonics VCX-130 ultrasound homogenizer with an amplitude of 35 % and an on/off cycle time of 20/5 s followed by stirring for 20 min using magnetic stirrers at 600 rpm. UHMWPE was then slowly added to the mixture such that the total mass was 10 g; an amount that can effectively be ultra-sonicated by the sonicator. The mixture was then ultra-sonicated for 30 min after which it was stirred at 400 rpm and 60 ^{o}C for 1 hr. In the final step, the mixture was drained and dried in an oven at 60 ^{o}C for 24 hr. This process was applied to produce the nanocomposite powders that were used to synthesize both the bulk nanocomposites and the nanocomposite coatings developed in this research. In the case of the bulk nanocomposite, UHMWPE nanocomposite powders with GNPs reinforcement in varying amounts, such as 0.10, 0.25, and 0.5 wt. % were prepared. UHMWPE nanocomposite powders filled with 0.25, 1.0 and 2.0 wt. % GNPs were prepared for the coatings.

3.3 Nanocomposites consolidation

In order to turn the pure and GNPs filled UHMWPE powders into bulk nanocomposites, hot pressing was used. After pouring the powder into the hot press, an initial pressure of 6 MPa was applied at room temperature for 10 min for pre-pressing. This is subsequently followed by an application of a higher pressure, 29 MPa, at 175 ^{o}C for 15 min [153]. Then

the nanocomposite was allowed to cool for 20 min after which the sample with dimensions of 31.6 mm diameter and 4.2 mm thickness were obtained. The surface roughness (Ra) of the nanocomposites were measured to be 0.73 ± 0.080 μm using GTK-A optical profilometer, Bruker Co (Figure 3.7).

3.4 Synthesis of nanocomposite coatings

To fabricate the coatings, an aluminum substrate was first ground using 400 grit SiC paper to a roughness of Ra = 0.314 ± 0.014 μm. The substrate was then sonicated for 5 min for cleaning purpose. Air plasma treatment was then carried out for 5 min using Harrick Plasma Cleaner. This process removes impurities and increases the substrate surface energy [154]. The mechanism of the air plasma treatment is based on ionization of oxygen. It becomes highly energetic and very reactive capable of removing unwanted layers and impurities by chemical reaction or ablation [155]. After the plasma treatment, the samples were placed 44 mm away from the gun nozzle and the spray was immediately applied for 4 sec at a uniform rate by fully pressing the electrostatic gun spray button. Then the coating was cured in a furnace at 180 ^{o}C. The process was controlled to ensure that the surface roughness, Ra, of the coatings is 2.61 ± 0.11 μm using GTK-A optical profilometer, Bruker Co (Figure 3.7).

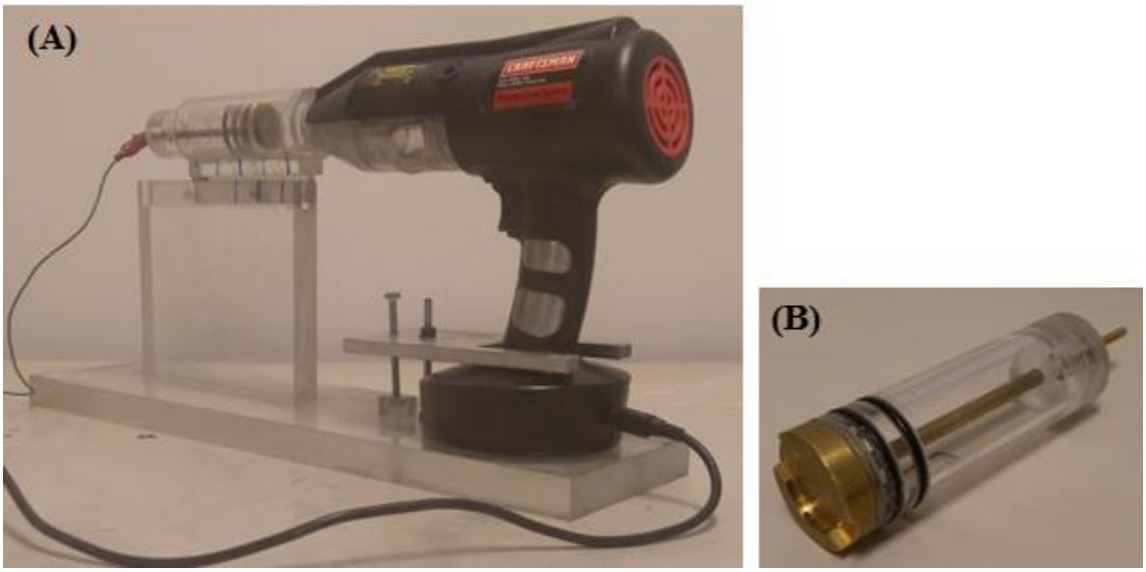

Figure 3.3: Electrostatic spray (A) gun set up (B) sample holder

3.5 Friction and wear tests

3.5.1 Pin on disc (POD) wear tests

Dry POD wear tests were carried out on the consolidated nanocomposite and the nanocomposite coatings using Bruker UMT-3 Tribometer (Figure 3.4A). Pin on disc configuration (Figure 3.4B) was used in order to simulate flat contact, which is a close representation of a plain mechanical bearing application and to ensure that the contact pressure is constant throughout the test. A 100 N sensor with an accuracy of ± 0.5 % of the applied force was used. The counterface is a pin made of hardened tool steel with a surface roughness of Ra = 0.43 ± 0.022 µm, and hardness of 57 ± 1 HRC. While the consolidated samples were tested at room temperature, coatings were tested at both room and elevated temperatures. Every sample was cleaned with ethanol before the test. Three trials were conducted for each sample to ensure that the test is repeatable. Mean and standard deviation

of COF and wear rate for each sample were then computed from the trials. Details on each of the experiments are given below.

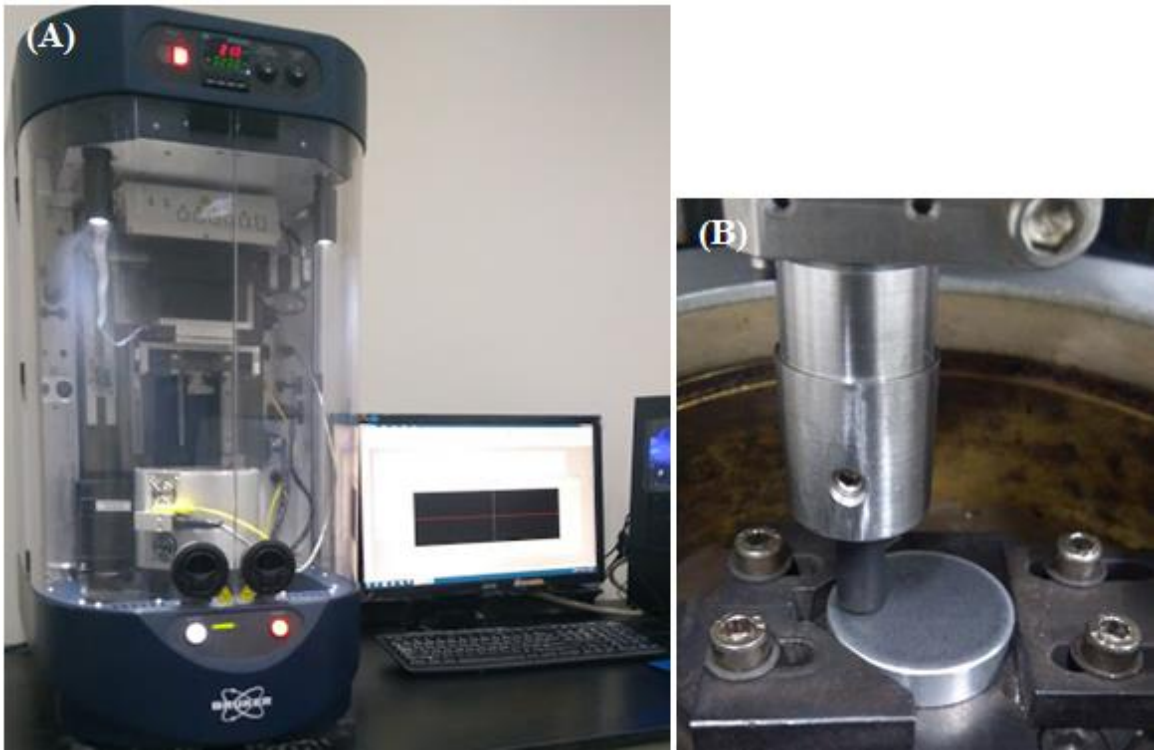

Figure 3.4: (A) Bruker UMT-3 Tribometer and (B) POD configuration

Bulk nanocomposite

The diameter of the counterface pin used was 2.5 mm. A normal load of 39 N (8 MPa) was applied at a linear speed of 0.1 m/s (159 rpm). The radius of the sliding track was maintained at 6 mm throughout the test. A sliding distance of 1 km (26,500 cycles) was covered. The tests were carried out at room temperature, 25 ± 1.3 ^{o}C and a relative humidity between 46 and 54 %. These parameters were maintained constant to initially screen the nanocomposites in terms of composition. After determining the composition that performed best, it was tested at 0.1 m/s and varied contact load; 39 N (8 MPa), 52 N (12 MPa), 69 N (16 MPa) and 86 N (20 MPa), to study the effect of contact load. The effect of

sliding speed on friction and wear rate was also investigated by varying the speed, 0.1 m/s (159rpm), 0.5 m/s (796 rpm), 0.75 m/s (1194 rpm) while keeping other parameters constant. The load was maintained at 55 N (12 MPa).

Nanocomposite coating

A counterface with a surface roughness, Ra = 0.37 ± 0.021 μm, and diameter ~ 3 mm was used for the friction and wear tests of the coatings. A normal load of 14 N (2 MPa) was applied at a linear speed of 0.1 m/s (159 rpm). The radius of the sliding track was maintained at 6 mm throughout the study and the test was carried out for 10,000 cycles resulting in 377 m sliding distance. These parameters were kept constant to first screen the nanocomposites in terms of composition. After determining the composition with the best performance, it was tested at varied load from 14 N (2 MPa) to 64 N (8 MPa) while linear speed was kept constant at 0.1 m/s. The effect of sliding speed on friction and wear rate was then investigated by varying the speed from 0.1 to 1.0 m/s (1592 rpm) at a constant pressure of 4 MPa. Also, the effect of test temperature on the coatings performance was examined by testing the UHMWPE/ 1 wt. % GNPs and pure UHMWPE coatings at elevated temperatures up to 125 ^{o}C.

3.5.2 Ring on disc (ROD) tests

UHMWPE/ 1 wt. % GNPs nanocomposite coating showed excellent tribological performance in previous wear tests using the pin on disc configuration. In order to further explore the capabilities of the coating for mechanical bearing applications, pure and 1 wt. % reinforced UHMWPE were coated on thrust bearing samples made of aluminum alloy. Pure UHMWPE was included to serve as a reference for the performance of the reinforced nanocomposite. The choice of thrust bearing samples is to simulate a true practical

application of a plain sliding bearing. The samples were tested under both dry and boundary lubrication using a tribometer manufactured in the mechanical engineering department, KFUPM with a high speed and high load capacity. The tribometer was connected to a data acquisition device (National instruments, United States) that was then connected to a computer for the display and recording of the frictional force (Figure 3.5). A ROD configuration was used such that the sample is the ring while the counterface is the disc. The sample was mounted on the sample holder before mounting the entity on the upper shaft while the counterface was mounted on the bottom rotating shaft. Figure 3.6 shows the sample before and after coating and the test set up. The disc counterface is made from AISI 4140 with a diameter of 125 mm, a thickness of 20 mm and hardness 51 HRC. The surface was ground to an average Ra value of 0.32 μm. The configuration of the tribometer load cell and the sensor was such that it can measure the friction force in terms of torque. This enabled an accurate measurement of the dynamic friction of a ring on disc test.

Figure 3.5: A tribometer, made in the department of mechanical engineering, KFUPM

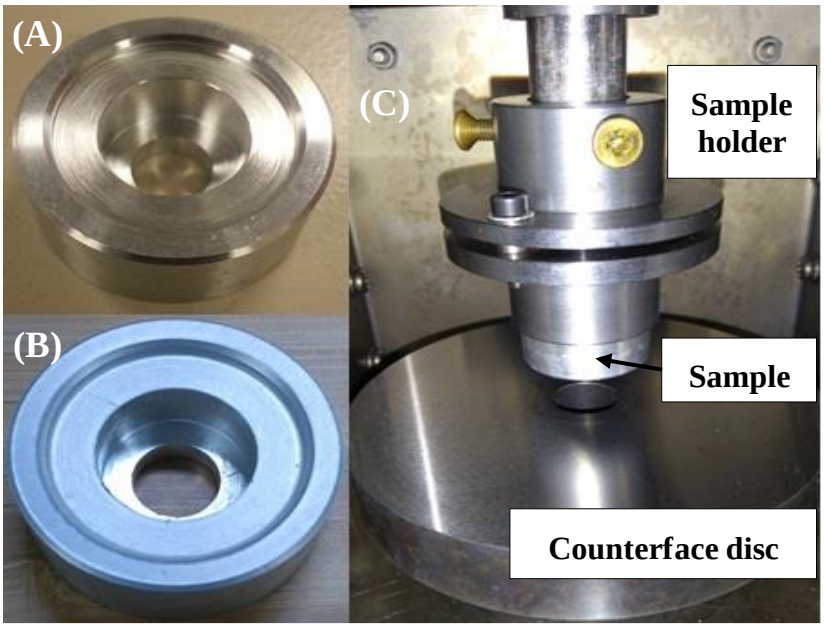

Figure 3.6: Test samples (A) before coating (B) after coating and (C) wear test set up

Dry ROD tests

Un-lubricated friction and wear tests were carried out on an aluminum thrust bearing coated with pure UHMWPE and UHMWPE reinforced with 1 wt. % GNPs. The effect of sliding speed on the performance of UHMWPE/ 1 wt. % GNPs was first studied. Sliding distance and contact pressure were maintained at 0.75 km and 0.5 MPa respectively while the sliding speed was varied from 1 to 2 m/s. Subsequently, the effect of contact pressure on the performance of pure and 1 wt. % reinforced UHMWPE was investigated by keeping the speed constant at 2 m/s while the contact pressure was varied from 0.1 to 1 MPa. Each test was repeated three times to evaluate repeatability.

Boundary lubricated ROD tests

Boundary lubrication friction and wear tests were carried out on the aluminum thrust bearing coated with pure UHMWPE and UHMWPE reinforced with 1 wt. % GNPs. Before conducting the tests, the sample and the counterface were cleaned using ethanol. Then an uncoated ring was dipped slightly into the lubricating oil and brought out. Majority of the oil was allowed to drain away. Then the ring was placed on the counterface to transfer a thin film of oil on it. After that, the sample to be tested was mounted on the sample holder on the top shaft. Then the required load was applied and the test started. The effect of sliding speed on the performance of UHMWPE/ 1 wt. % GNPs was first studied in base oil boundary lubrication. Sliding distance and contact pressure were maintained at 1 km and 1 MPa respectively while the sliding speed was varied from 1 to 2 m/s. Subsequently, the effect of contact pressure on the performance of pure and 1 wt. % reinforced UHMWPE was investigated by keeping the speed constant at 1.5 m/s while the contact pressure was varied from 0.5 to 1.5 MPa. Each test was repeated three times to ensure repeatability. The mean and standard deviation of each sample were then obtained. The maximum wear testing parameters (1.5 m/s and 1.5 MPa) were then used to evaluate the UHMWPE/ 1 wt. % GNPs coating under Mobil1 0W-40 and Sunflower vegetable oil in comparison with SN-150. The specifications of the lubricants are given in the result section.

3.6 Characterizations

3.6.1 Dispersion, Crystallinity, and Phase analysis

Wide angle X-ray diffraction (XRD) measurements were carried out on the nanocomposite powders using a high-resolution X-ray diffractometer, Bruker D8, Madison, WI, USA with a wavelength, λ, of 1.5418 A°. Each scan ranged from 5° to 50° with a step of 0.02°. The

spectrum produced by XRD is unique with respect to each crystalline material. As such it is convenient to determine the crystallinity and the phases present in each sample. Raman spectroscopy was also done to study the phases of the nanocomposite powders. A spectrometer operating with a 455 nm laser source was used. Each sample was scanned from 1000 cm^{-1} to 3000 cm^{-1}. Scanning Electron Microscope (SEM) was used to view the morphology of the nanocomposite powder after sonication to evaluate the level of dispersion. Differential scanning calorimeter (DSC) was also used to determine the crystallinity and melting temperature of the powders. Each sample was tested at a temperature range from 40 to 180 ^{o}C.

3.6.2 Measure of consolidation

The density of the consolidated UHMWPE nanocomposites was measured using density measurement kit model AG285 purchased from METTLER TOLEDO GmbH & weighing Technologies, Switzerland. The precision of the weighing balance in dynamic measuring mode is ± 0.037g. Each sample was weighed in the air and in ethanol. Eq. (1) is then used to calculate the density of the sample.

$$\rho_o = \frac{A}{A-B} * (\rho_e - \rho_a) + \rho_a \quad (1)$$

Where $\boldsymbol{A}$ and $\boldsymbol{B}$ are weights of the sample in air and ethanol respectively, $\boldsymbol{\rho_e}$ and $\boldsymbol{\rho_a}$ are densities of ethanol and air respectively. The reported densities of GNPs and UHMWPE are 1.8 and 0.94 g/cm^3 respectively. Hence the expected density of composites ρ_c can be obtained using Eq. (2).

$$\rho_c = \rho_m V_m + \rho_r V_r \quad (2)$$

Where $\boldsymbol{\rho_m}$ and $\boldsymbol{\rho_r}$ are the densities of matrix and reinforcement respectively, $\boldsymbol{V_m}$ and $\boldsymbol{V_r}$ are the volume fractions of matrix and reinforcement, respectively. After obtaining the densities of the samples, relative density was calculated using Eq. (3).

$$\text{Densfification} = (\rho_c/\rho_{theoretical}) * 100 \quad (3)$$

3.6.3 Hardness

After hot pressing, the microhardness of the bulk nanocomposites was measured using CSM MicroCombi micro-indentation machine. A load of 0.2 N was applied on the indenter. Hardness value was measured at five different locations on each sample surface after which the average of the results was computed. As for the nanocomposite coatings, a load of 0.1 N was applied on the indenter to ensure that Buckle criterion [156] is met; the depth of indenter penetration should be less than 10 % of the coating thickness.

3.6.4 Wear rate measurement

After the POD wear test, GTK-A optical profilometer, Bruker Co. (Figure 3.7), with an accuracy of ± 0.63 % of measured value, was used to measure the wear track depth and area. 2D and 3D profile plots were recorded. To determine the specific wear rate, the crossectional area of the wear track as given by the optical profilometer is multiplied by the average circumference of the entire track to get the wear volume. The obtained value alongside other parameters is substituted into Eq. (4) to obtain the specific wear rate.

$$w = \frac{V}{F * D} \quad (4)$$

Where ***w*** is the wear rate in $mm^3(Nm)^{-1}$, ***V*** is the wear volume**,** ***F*** is the normal force and ***D*** is the linear sliding distance traveled.

For the ROD tests, the mass of each sample was measured before and after the test in order to obtain the weight loss. The wear volume was then calculated from the weight loss using the samples' density. Wear rate in terms of depth per kilometer was then calculated according to Eq. (5).

$$d = \frac{m}{\rho * A * D} \quad (5)$$

Where ***d*** is the wear rate in µm/km, ***m*** is weight loss, ***ρ*** is the density of the nanocomposite, ***A*** is the contact area and ***D*** is the linear sliding distance traveled.

Figure 3.7: Optical profilometer

3.6.5 Imaging

Optical microscope, Meiji Co., Japan was used to record the image of the counterface before and after every wear test and also after cleaning the pin at the end of the test. This is to enable the determination of the precise characteristics of the transfer film. The wear tracks of the samples were studied with scanning electron microscope (SEM) shown in Figure 3.8 to determine the underlying wear mechanisms. Since UHMWPE is nonconductive, a gold coating was applied to the samples prior to SEM characterization.

The results obtained in both imaging aided the analysis of the transfer film, wear debris and ultimately the wear mechanism.

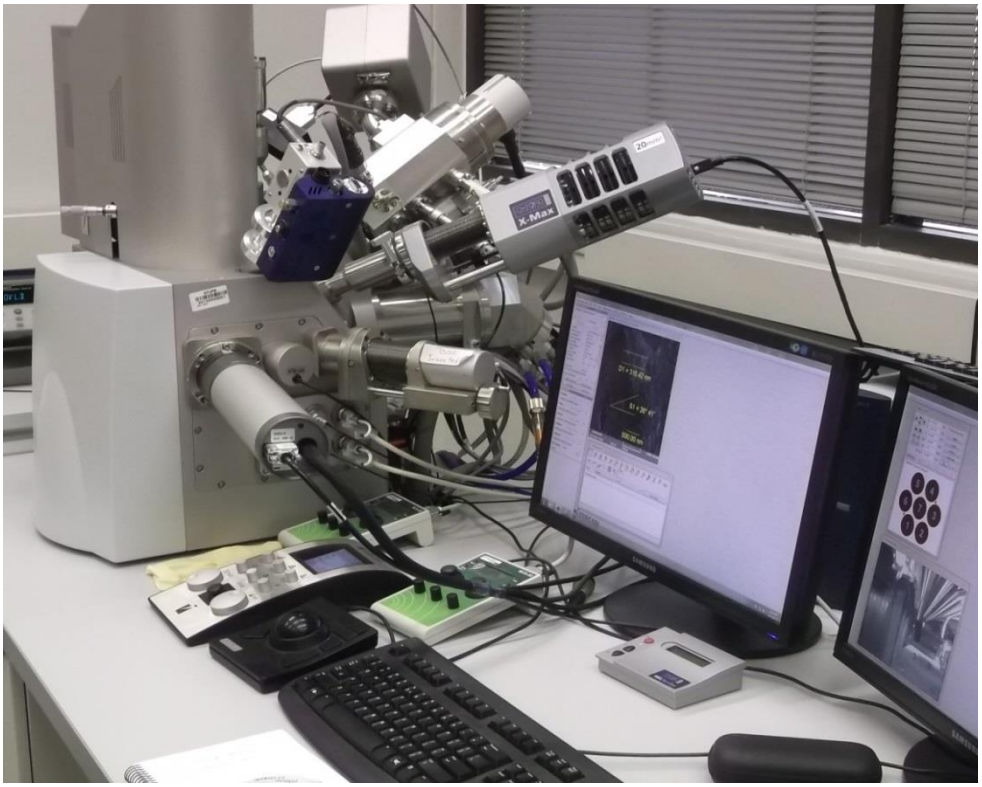

Figure 3.8: Field emission scanning electron microscope

CHAPTER 4

RESULTS AND DISCUSSION

TRIBOLOGICAL PERFORMANCE OF UHMWPE/GNPs BULK NANOCOMPOSITE

4.1 Phase analysis

The XRD spectrum of as-received GNPs powder is shown in Figure 4.1. The spectrum has a peak at a diffraction angle of 26.38° indicating a highly crystalline GNP with few defects. Graphene related materials are known to produce an XRD peak at about 26.38° [157,158]. The (002) plane is responsible for this reflection. Using Bragg's law, the separation between any two adjacent (002) planes was obtained as 0.34 nm. Figure 4.1 shows the XRD spectra for pure and ultra-sonicated GNPs reinforced UHMWPE nanocomposite powders. All the spectra show the two characteristic peaks of UHMWPE planes (110) and (200) at 22.2° and 24.2°, respectively [12,159] that implies that the UHMWPE remain as a single phase orthorhombic crystalline material [160]. The XRD spectra did not contain any foreign peaks. This suggests that the addition of GNPs did not cause any phase change to UHMWPE.

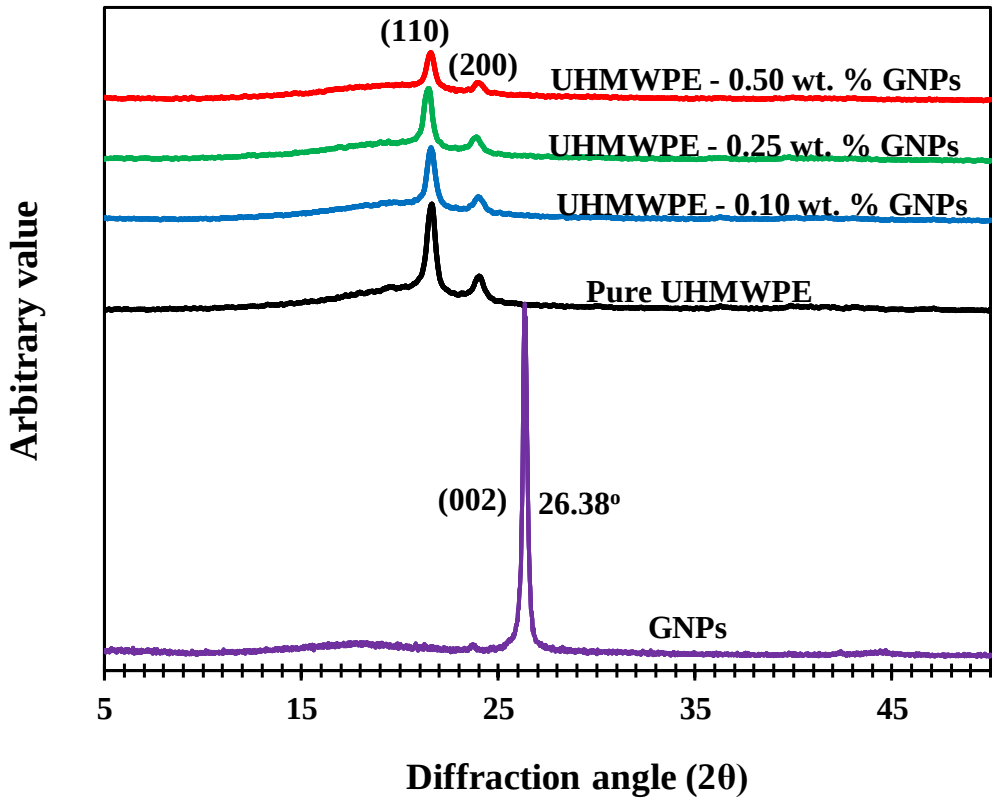

Figure 4.1: XRD pattern of as-received GNPs, pure and GNPs reinforced UHMWPE

The Raman spectrum for the GNPs powder in Figure 4.2 shows the presence of three bands typical of graphene materials; D band at 1376cm^{-1}, G band at 1577 cm^{-1} and 2D band at 2751 cm^{-1} [161,162]. The D band is excited by defects, while G band results from the vibration of sp2 hybridized carbon atoms and the 2D band is a second order peak of D produced by zone boundary photons [161,163]. The intensity ratio, I_{2D}/I_G of the 2D and G bands, is a unique parameter used to determine the number of layers of graphene. It can be used to differentiate graphene, GNPs, and graphite from each other. The I_{2D}/I_G, of the GNPs powder used in this research, as obtained from Figure 4.2, is 0.22, confirming that the powder is made up of several layers of graphene. This agrees with the outcome of a recent

research [162] in which the I_{2D}/I_G ratio of produced GNPs ranged from 0.12 to 0.42. The Raman spectra of the GNPs reinforced UHMWPE bulk nanocomposites are also shown in Figure 4.2. The bands seen are all from the polymer material except in the case of UHMWPE/0.5 wt. % GNPs. These include; the asymmetric stretching vibration of the C-C bonds (1062 cm^{-1}), the symmetric stretching vibration of the C-C bonds (1130 cm^{-1}), twisting vibration of the CH_2 groups (1294 cm^{-1}) and bending vibration of the CH_2 group (1426 and 1442 cm^{-1}) [164]. An equal number of peaks are seen at similar Raman shifts (Figure 4.2) in all the nanocomposites except in UHMWPE/ 0.5 wt. % GNPs where the peaks belonging to GNPs became clearly visible. As such, it can be concluded that there was an efficient dispersion of GNPs in UHMWPE when 0.1 and 0.25 wt. % GNPs were added to UHMWPE. However, once a higher amount of GNPs, such as 0.5 wt. % was added, there was an indication of GNPs agglomeration.

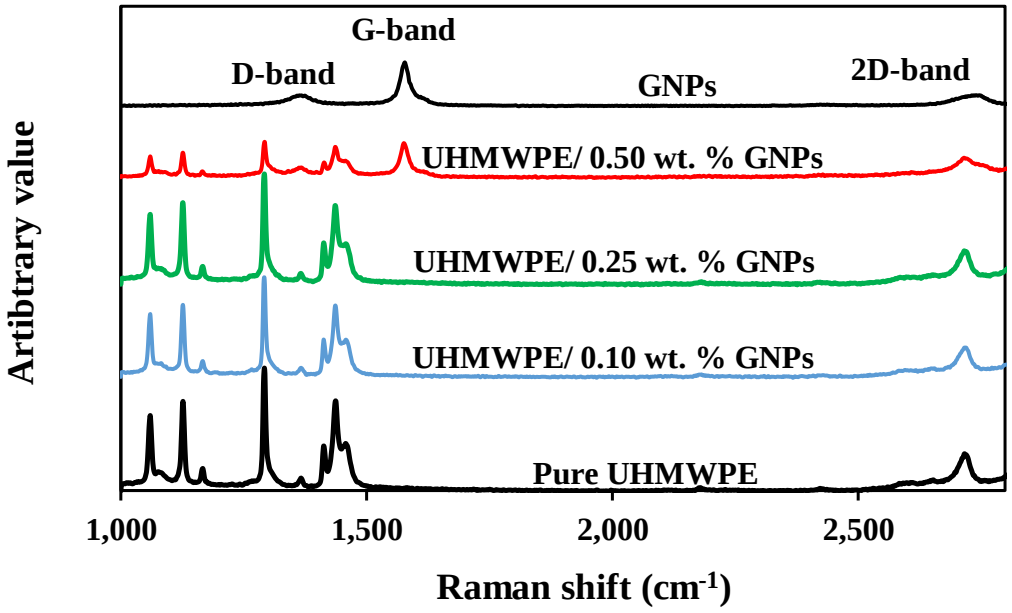

Figure 4.2: Raman spectrum of as-received GNPs and consolidated pure and GNPs reinforced UHMWPE

As-received GNPs, Pure, and GNPs reinforced UHMWPE nanocomposite powders were analyzed using DSC. The obtained DSC curves are shown in Figure 4.3. Using the software connected to the machine, the crystallinity and peak temperatures were evaluated for each sample and presented in Table 4.1. The crystallinity of UHMWPE reduced when the amount of GNPs was increased. It dropped from 65, for pure UHMWPE to 58.6 for UHMWPE/ 2 wt. % GNPs.

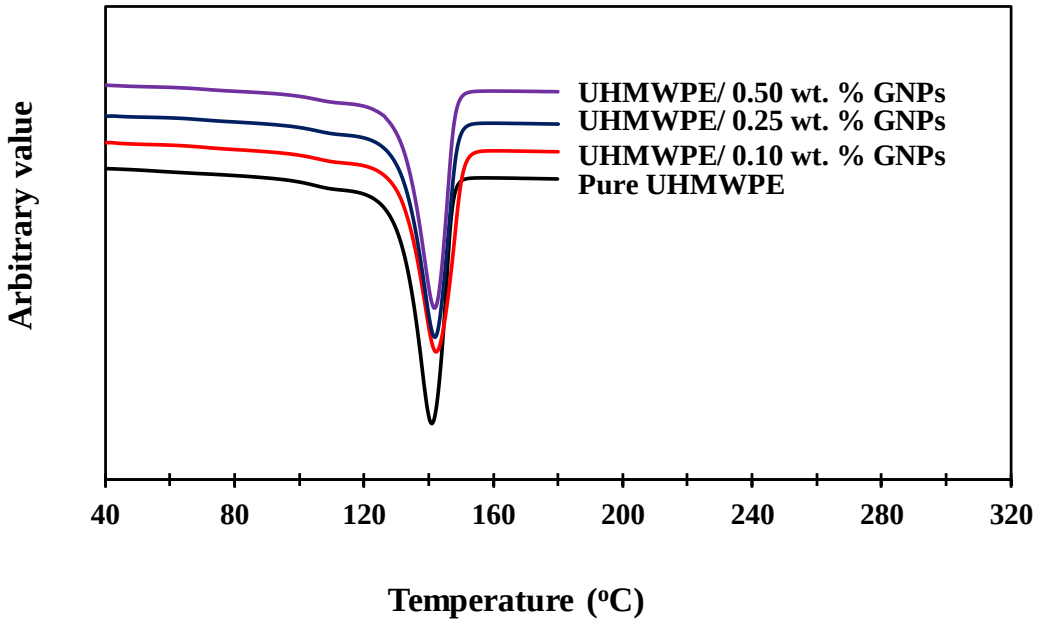

Figure 4.3: DSC spectra of GNPs, pure and GNPs reinforced UHMWPE powders

Table 4.1: Crystallinity and Peak temperatures of prepared powder nanocomposites

Sample	Peak temperature (°C)	Crystallinity (%)
Pure UHMWPE	141.0	65.2
UHMWPE/ 0.10 wt. % GNPs	142.3	62.0
UHMWPE/ 0.25 wt. % GNPs	141.9	59.4
UHMWPE/ 0.50 wt. % GNPs	141.8	58.6

4.2 Consolidation and hardness

The hot-pressing procedure together with the set of process parameters used for fabricating the nanocomposites ensured adequate consolidation as shown in Table 4.2. The densification of all the nanocomposites was observed to be greater than 99 %.

Table 4.2: Densification of hot pressed pure UHMWPE and UHMWPE nanocomposites

Material	Measured Density (g/cm3)	Densification (%)
UHMWPE	0.934	99.4
UHMWPE/ 0.10 wt. % GNPs	0.935	99.4
UHMWPE/ 0.25 wt. % GNPs	0.935	99.3
UHMWPE/ 0.50 wt. % GNPs	0.934	99.3

The Shore D hardness of the consolidated pure UHMWPE is 60.7 ± 0.56, close to the result of a similar technique [165]. When GNPs were added as reinforcement, the hardness of the nanocomposite did not increase significantly as shown in Figure 4.4. This might be due to the low amount of GNPs reinforcement in the UHMWPE matrix.

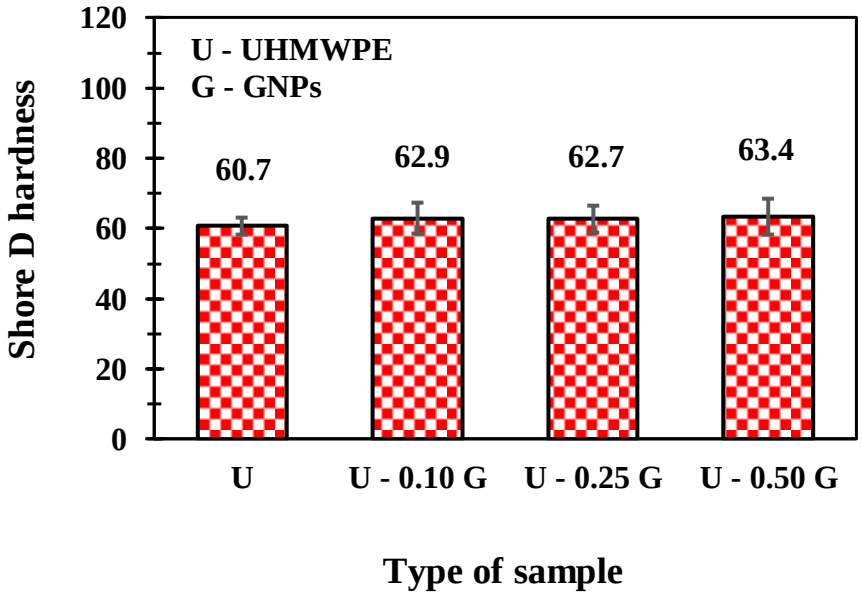

Figure 4.4: Shore D hardness of bulk UHMWPE with 0 to 0.5 wt. % GNPs reinforcement

4.3 Friction and wear behavior of GNPs reinforced nanocomposites

The friction response of the four nanocomposites tested at 0.1 m/s and 8 MPa is shown in Figure 4.5. Sliding speed of 0.1 m/s was selected to test the load-bearing capability of the nanocomposites while 8 MPa was selected because from initial trials it was found that it was the minimum pressure that could cause a measurable wear. It can be observed from Figure 4.5 that the brake-in is less than 70 m for all the samples. The steady-state dynamic COF of pure UHMWPE is observed to be 0.15. COF increased with the addition of GNPs up to 0.24. (Figure 4.6). This can be attributed to the anchoring of the UHMWPE chains by GNPs preventing them from sliding over each other. A similar observation was noted in previous references when UHMWPE was reinforced with GO [14,166] and CNTs [35,85].

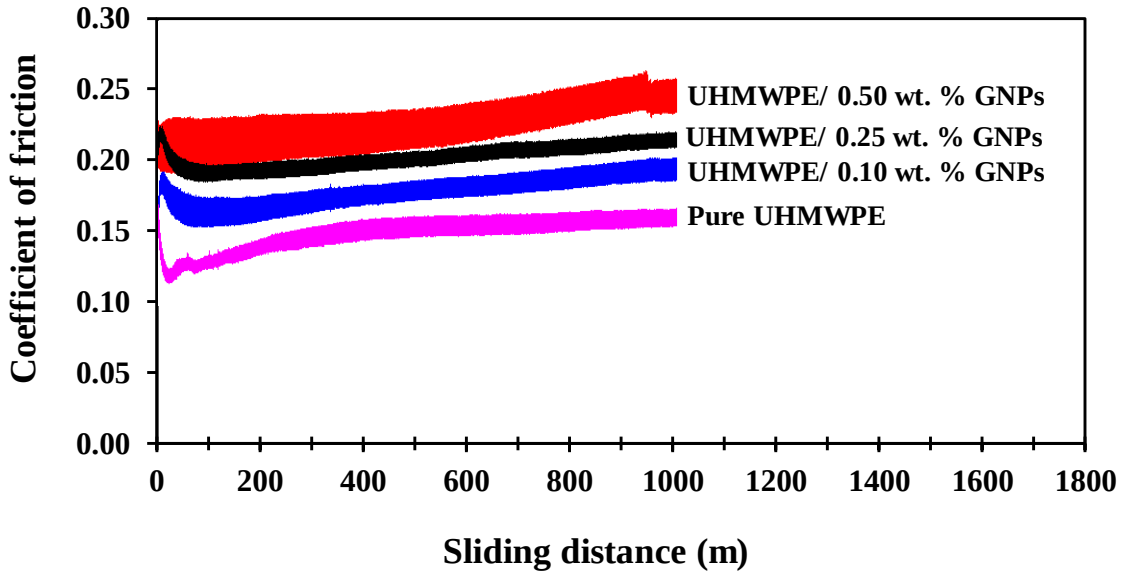

Figure 4.5: Typical Friction plots of pure UHMWPE and UHMWPE nanocomposites reinforced with 0.1, 0.25 and 0.5 wt. % of GNPs tested at 0.1 m/s and 8 MPa

In general, the wear rate of the nanocomposites is lower as compared to that of pure UHMWPE as shown in Figure 4.6. The wear depths in the 2D optical images in Figure 4.7A were used to obtain the wear rates in Figure 4.6. Corresponding 3D optical profilometric images are shown in Figure 4.7B illustrating a consistent comparative degree of wear rate with the results in Figure 4.6. The reduction in wear rate can be due to enhanced mechanical strength and thermal conductivity as a result of GNPs addition [10,11,152]. Moreover, the high aspect ratio and large surface area of GNPs enhance the interaction between the polymer and the reinforcement [14], resulting in an effective load transfer from the matrix to the reinforcement. However, it is to be observed that the optimum amount of GNPs that resulted in the maximum wear resistance is 0.25 wt. %. A further increment of GNPs concentration reduced wear resistance. This can be attributed to the agglomeration of GNPs when the reinforcement amount was increased to 0.5 wt. %

as observed in Figure 4.2. The optical microscope images of the counterface after the wear tests are shown in Figure 4.7C. There was little or no polymer transfer film. This is an indication that the wear mechanism in all the samples is not adhesive. Also, there were no scar marks on the counterface implying that the nanocomposite did not damage the counterface. Figure 4.7D shows the SEM wear track morphology of all the samples. Parallel lays along the sliding direction can be seen in all the compositions. This is an indication of purely abrasive wear due to plastic deformation. The nanocomposite reinforced with 0.1 and 0.25 wt. % of GNPs showed smoother wear track as compared to the wear tracks of pure UHMWPE and UHMWPE/0.5 wt. % GNPs wherein the wear track looks rougher in nature. Also, the degree of plastic deformation in UHMWPE and UHMWPE/0.5 wt. % GNPs are higher than those in UHMPWE reinforced with 0.1 and 0.25 wt. % of GNPs.

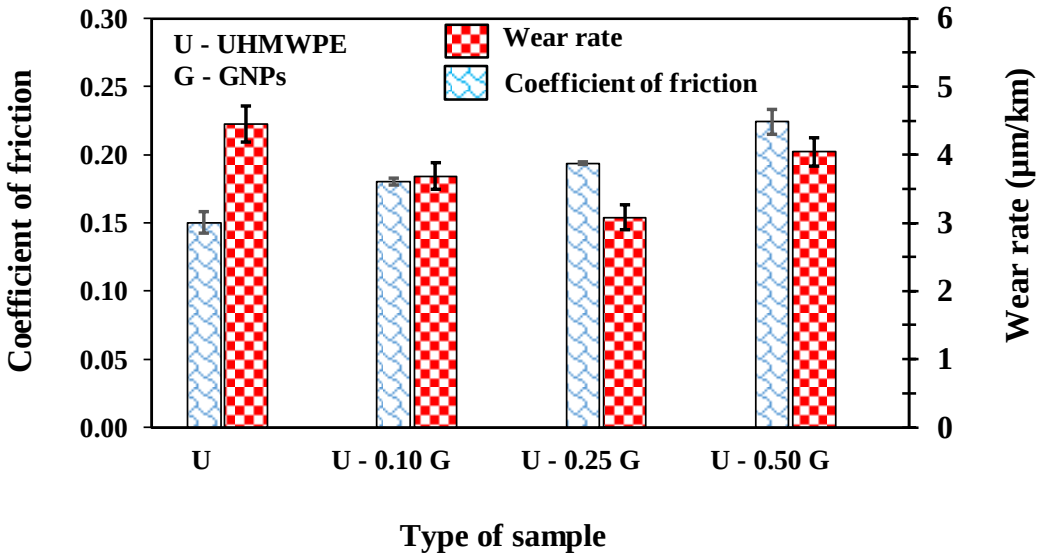

Figure 4.6: COF and wear rate of UHMWPE nanocomposite reinforced with 0 to 0.5 wt. % GNPs tested at 0.1 m/s and 8 MPa

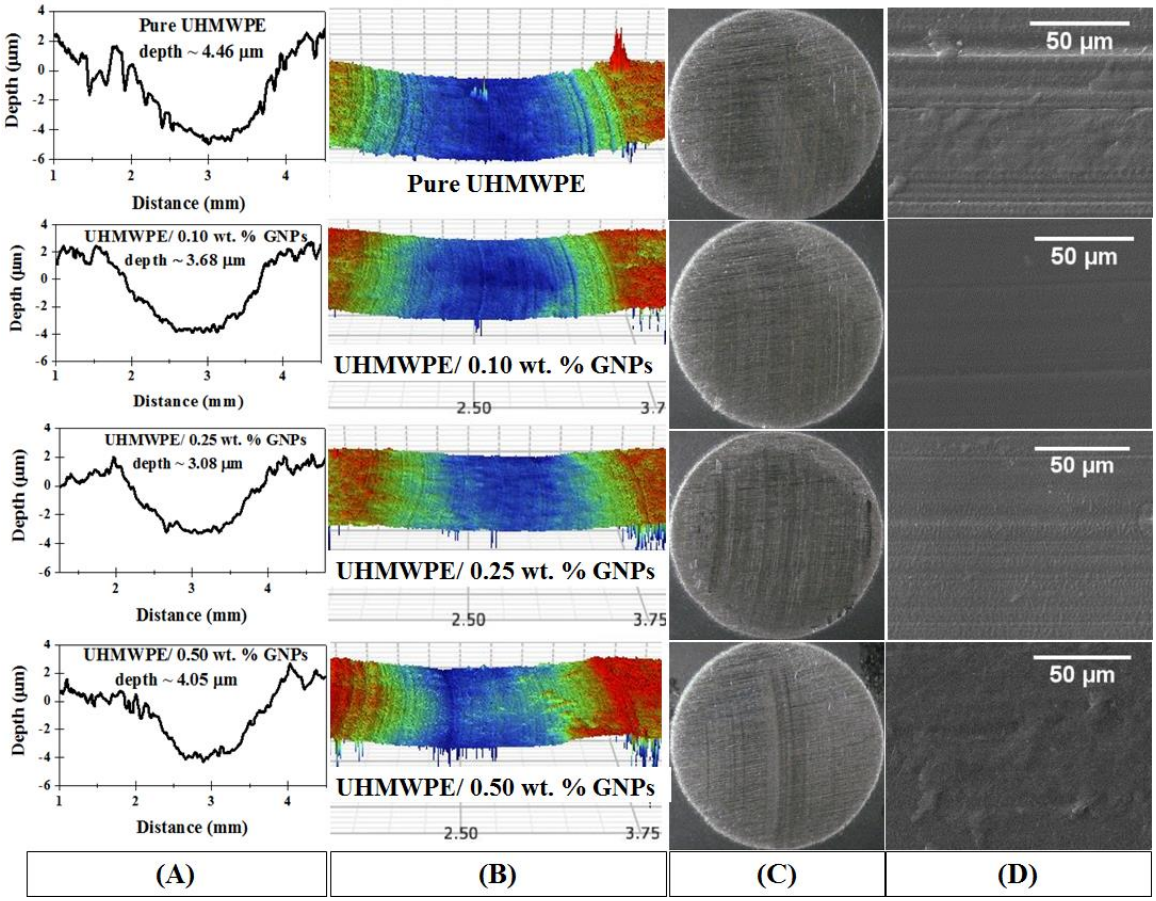

Figure 4.7: Wear tracks (A) 2D and (B) 3D profilometric images, (C) optical microscope image of the counterface steel pin after the wear test and (D) SEM images of the wear tracks of pure UHMWPE and UHMWPE reinforced with 0, 0.1, 0.25, and 0.5 wt. % GNPs after the wear test at 0.1 m/s and 8 MPa

4.4 Effect of normal load on the friction and wear behavior of UHMWPE reinforced with 0.25 wt. % GNPs

UHMWPE/0.25 wt. % GNPs being the most wear resistant was selected for further tribological analysis. In order to explore the effect of normal load on friction and wear behavior of this nanocomposite, contact pressure was varied from 8 to 20 MPa at a speed of 0.1 m/s. The typical friction plots at various contact pressures are shown in Figure 4.8. Steady dynamic COF was attained at about 100 to 200 m into the test. This is less than 20 % of the total sliding distance. There wasn't a significant decrease in the average COF with the increase in contact pressure as shown in Figure 4.9. Figure 4.11A shows that there wasn't much transfer film on the counterface after the wear tests at all the contact pressures used.

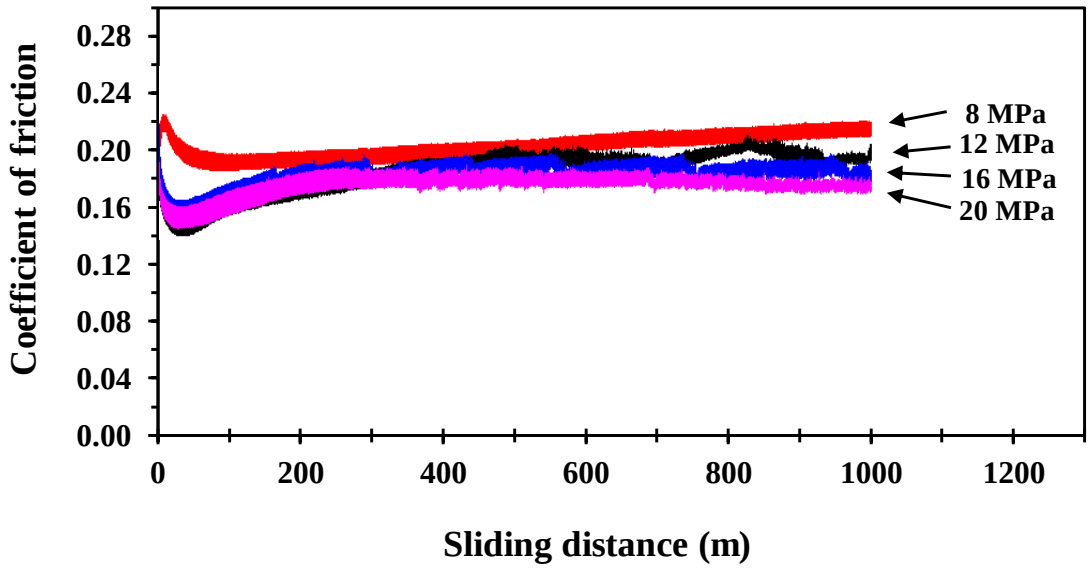

Figure 4.8: Friction plot of UHMWPE/0.25 wt. % GNPs with varied load and constant sliding speed, 0.1 m/s

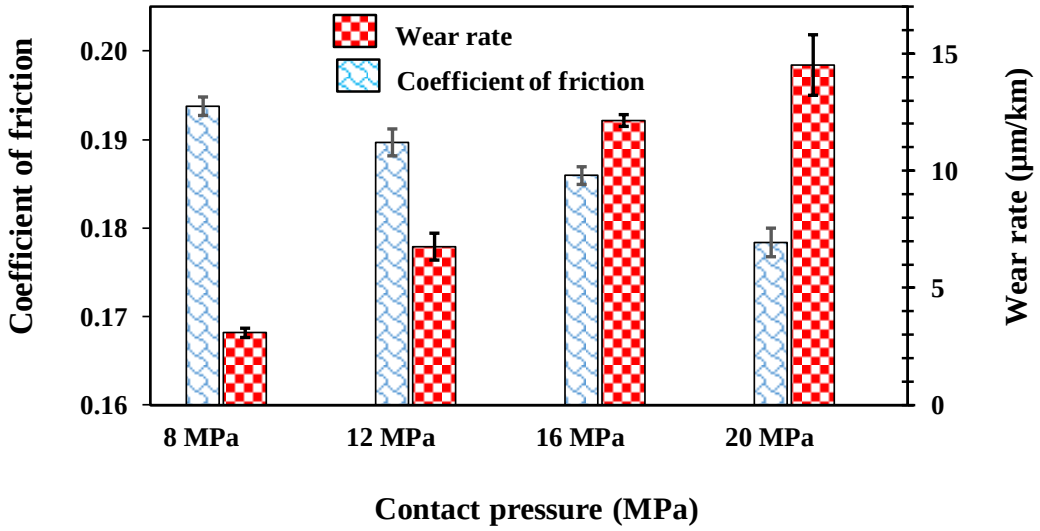

Figure 4.9: Average steady-state COF and wear rate of UHMWPE/ 0.25 wt. % GNPs under varied load and constant sliding speed, 0.1 m/s

The increase in contact pressure resulted in a linear increase in wear rate (Figure 4.9). The wear rates were determined using optical profilometric images shown in Figure 4.10. The corresponding 3D profilometric images are also shown in Figure 4.11B. It is to be noted that, the higher the contact pressure, the more the penetration of counterface asperities (Ra = 0.43 ± 0.022 µm) into the sample surface, resulting in a deeper abrasion per cycle of contact. This explains the increase in the wear rate as a function of normal load. In addition, higher load enhances plastic deformation hence more material removal. Despite the increase in wear rate with load, there was no observation of severe wear at contact pressure up to 20 MPa corresponding to a PV of 2 MPa.m/s as shown in Figure 4.11C. The wear track morphology of UHMWPE /0.25 wt. % GNPs tested at contact pressures ranging from 8 to 20 MPa can be seen in Figure 4.11C. Parallel plowing lines along the sliding direction can be seen in all the samples indicating that the predominant wear mechanism is abrasive

wear by plastic deformation. The image also shows that the severity of the plastic deformation increases with contact pressure increase.

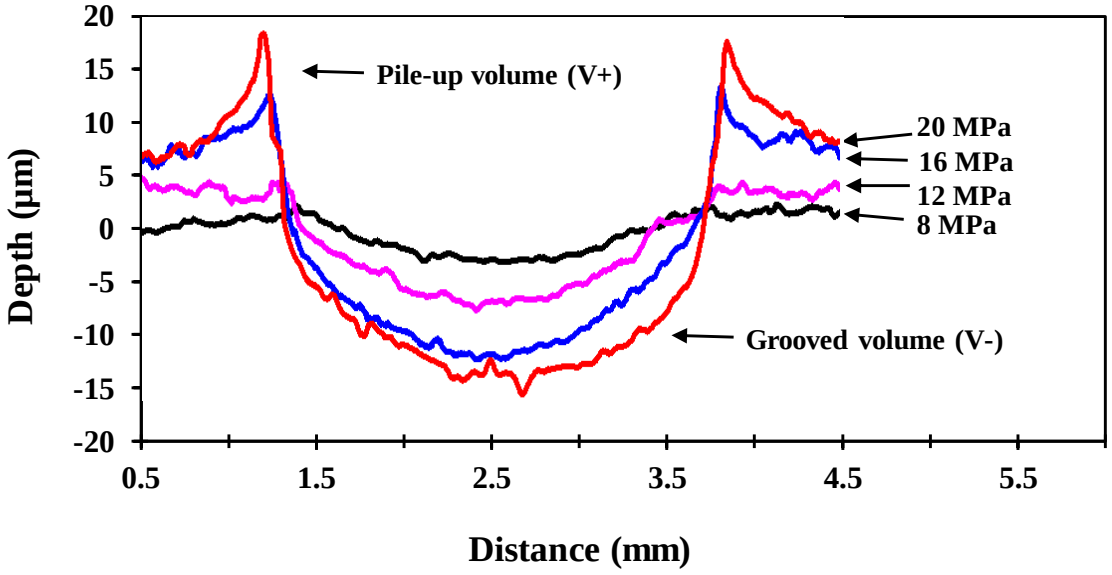

Figure 4.10: 2D wear track of UHMWPE/0.25 wt. % GNPs tested at various load and constant linear speed, 0.1 m/s

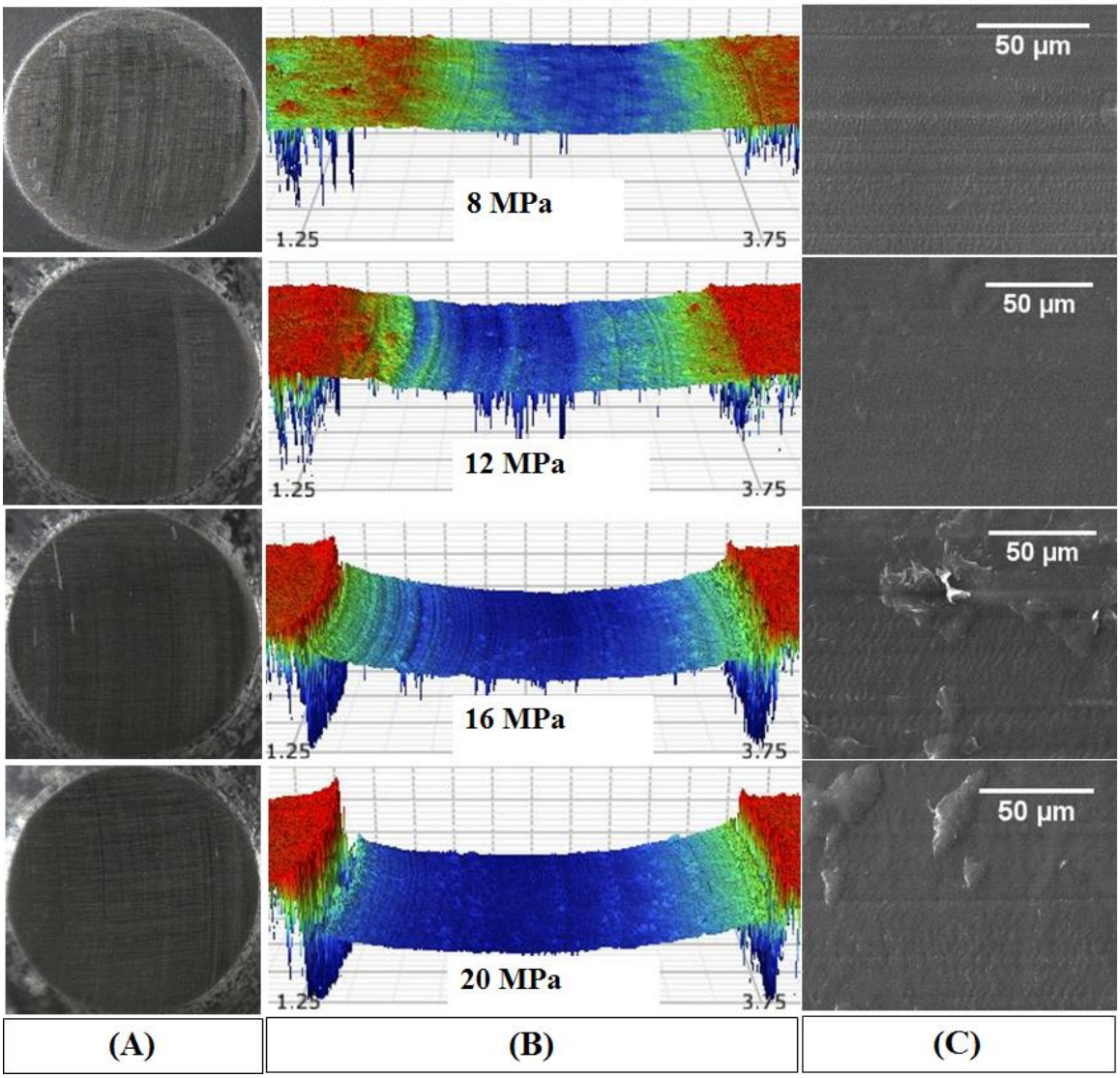

Figure 4.11: (A) optical microscope image of the counterface steel pin after the wear test and wear tracks (B) 3D profilometric images (C) SEM images of UHMWPE/0.25 wt. % GNPs at normal load of (a) 8 MPa, (b) 12 MPa, (c) 16 MPa and (d) 20 MPa and constant linear speed, 0.1 m/s

4.5 Effect of varying sliding speed on the Friction and wear behavior of the UHMWPE reinforced with 0.25 wt. % of GNPs

To further assess the capabilities of UHMWPE/0.25 wt. % GNPs, sliding speed was varied from 0.1 m/s to 0.75 m/s to see its effect on friction and wear properties at a constant contact pressure of 12 MPa. It can be seen from Figure 4.12 that the curve of dynamic COF against distance is steady after an initial break-in period. The steady-state is attained after a range of 10 to 150 m. This implies that the lower the sliding speed, the shorter the length of sliding distance to accomplish break-in. The average COF decreased gradually from 0.2 to 0.17 with an increase in sliding speed up to 0.75 m/s as shown in Figure 4.13. A similar occurrence was noted in reference [167]. This could be attributed to the lesser shear resistance at the contact surface caused by polymer surface softening due to the local surface heating at higher sliding speeds. Hence, the higher the sliding speed, the higher the contact temperature and the softer the contact surface and eventually the lower the friction.

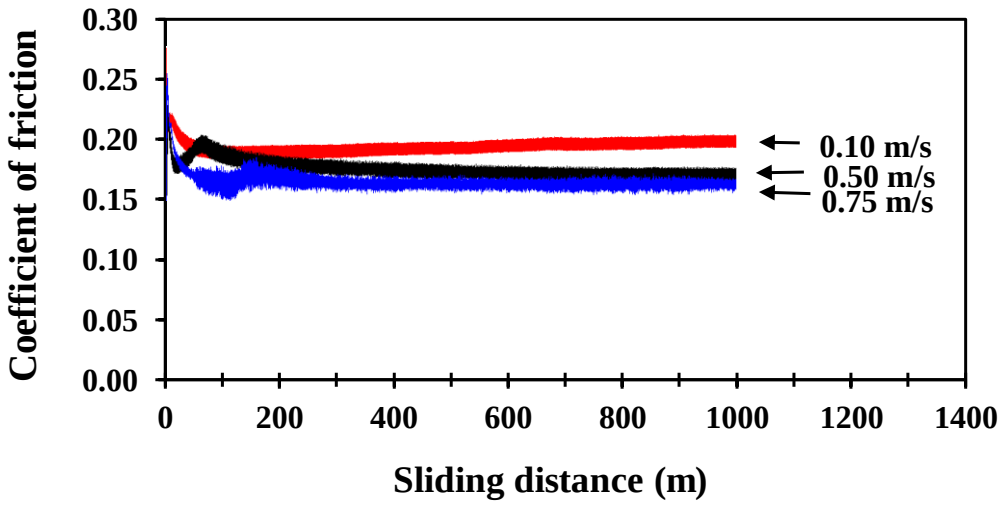

Figure 4.12: Friction plot of UHMWPE/0.25 wt. % GNPs with varied linear sliding speed and constant contact pressure, 12 MPa.

The wear rate of the nanocomposite increased with increase in linear sliding speed (Figure 4.13). The higher the speed, the higher the contact temperature and subsequently the softer the polymer nanocomposite at the surface. This leads to a reduction in mechanical strength at the surface resulting in more material loss.

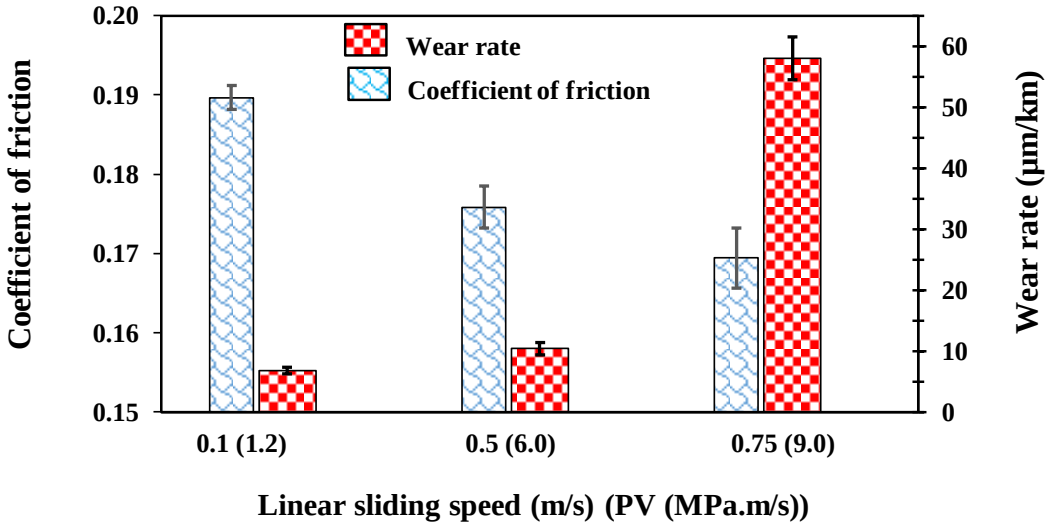

Figure 4.13: Average COF and wear rate of UHMWPE/0.25 wt. % GNPs with varied sliding speed at constant contact pressure, 12 MPa

The wear track surface morphology of the samples tested at the three different sliding speeds shows an obvious difference. At 0.1 m/s the wear track surface is smooth (Figure 4.15B) Speed effect up to 0.5 m/s can be regarded mild as the wear rate is not severe as can be seen from the wear depth in Figure 4.14 and the wear track morphology in Figure 4.15B. Sparsely distributed ridges or protrusions are seen, a sign of surface heating. Despite this morphological difference as compared to samples tested at 0.1 m/s, the polymer can still sustain the sliding speed. At a sliding speed of 0.75 m/s, the wear rate became excessive as evident in Figure 4.14. The rate of wear increased by 757 % against an initial

54 % increase when sliding speed was varied from 0.1 to 0.5 m/s. This is an indication of a change in wear mechanism and that the sample cannot withstand a speed of 0.75 m/s. This is due to excessive contact heat at high speed. Moreover, polymers have poor thermal conductivity. Hence accumulated heat causes softening and enhances the loss of material to sliding. Also, the wear track surface is very rough as can be seen from Figure 4.15B confirming that the sample has failed. Hence the PV limit of the polymer is determined as 0.5 * 12 = 6 MPa.m/s. Figure 4.15A shows the optical images of the counterface after the test at each sliding speed. A slight amount of transfer film was formed on the counterface. The samples are mild to the counterface since they did not cause significant scratches on it.

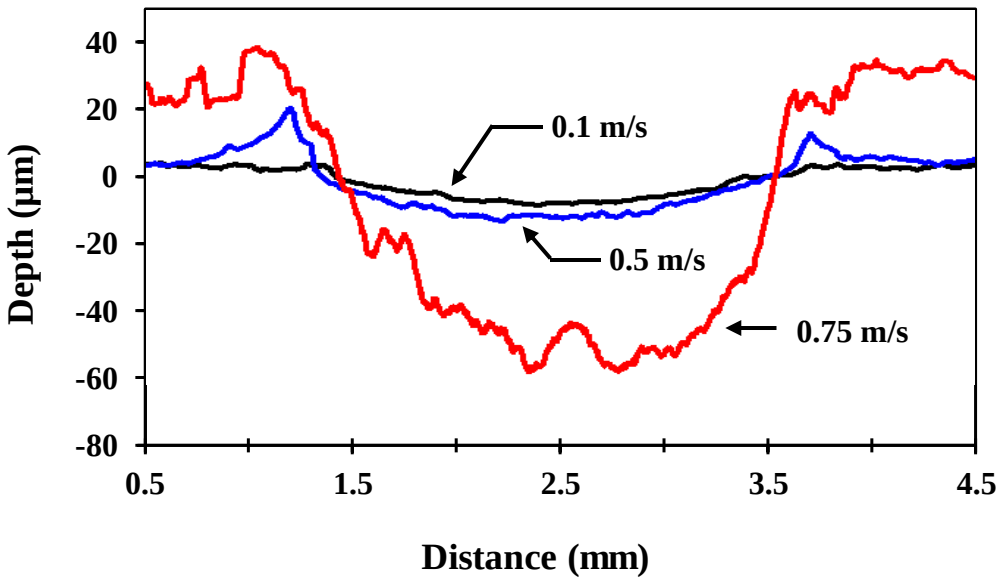

Figure 4.14: 2D wear track of UHMWPE/0.25 wt. % GNPs tested at sliding speed of 0.1, 0.5 and 0.75 m/s while maintaining contact pressure constant, 12 MPa

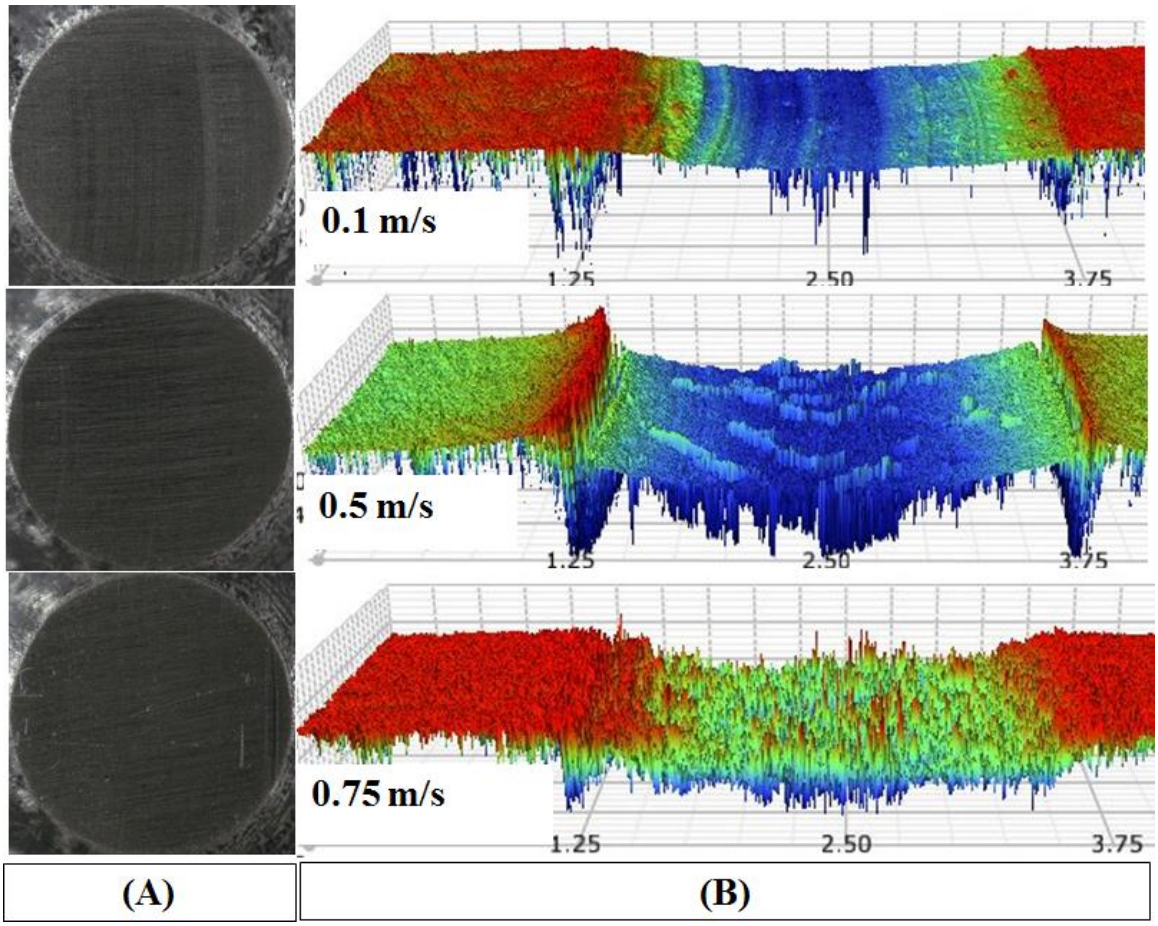

Figure 4.15: (A) Optical microscope image of counterface pin after wear test and (B) 3D wear track of UHMWPE 0.25 wt. % GNPs tested at sliding speeds of 0.1, 0.5 and 0.75 m/s and constant contact pressure, 12 MPa

4.6 Conclusions

GNPs reinforced UHMWPE nanocomposites were successfully fabricated and tested in terms of friction and wear resistance.

UHMWPE/0.25 wt. % GNPs nanocomposites showed the optimum wear resistance with a wear rate reduction of 31 % as compared to the pure UHMWPE.

The wear rate increased as the contact pressure increased from 8 to 20 MPa. The nanocomposite sustained the maximum contact pressure.

A further investigation of tribological properties, as a function of sliding speed at a constant contact pressure (12 MPa), showed a reduction of friction coefficient to 0.17 with a gradual increase in wear rate up to a sliding speed of 0.5 m/s. Once the sliding speed was increased to 0.75 m/s, a severe increase in wear rate by 757 % was observed. Hence the PV limit for this nanocomposite is determined to be 6 MPa.m/s.

CHAPTER 5

RESULTS AND DISCUSSION

TRIBOLOGICAL PERFORMANCE OF UHMWPE/GNPs NANOCOMPOSITE COATINGS

5.1 Dispersion and phase analysis

The XRD spectra of as-received raw powders and ultra-sonicated powers are shown in Figure 5.1. The GNPs reinforced UHMWPE powders show two peaks from planes (110) and (200) are produced at 22.2^{o} and 24.2^{o} respectively. These peaks imply that the UHMWPE remain a single phase orthorhombic crystalline material [160] after the dispersion process. Peaks belonging to GNPs did not appear in the spectra except at 2 wt. % GNPs. This is an indication that the GNPs are adequately dispersed in the UHMWPE matrix [159] when reinforced with GNPs up to 1 wt. %. No foreign peak was seen in the XRD spectra. This suggests that the addition of GNPs to UHMWPE did not cause any phase change. Figure 5.2 shows the Raman spectra of the as-received GNPs along with samples of pure and GNPs reinforced UHMWPE coatings. All the samples produced peaks at the typical Raman shifts respectively. The GNPs reinforced coatings did not show the peak of GNPs due to uniform dispersion. However, once the amount of GNPs reached 2 wt. %, an obvious peak belonging to GNPs was seen. This signifies that 2 wt. % GNPs is

too much to be uniformly dispersed in the UHMWPE after the powder preparation and coating deposition process.

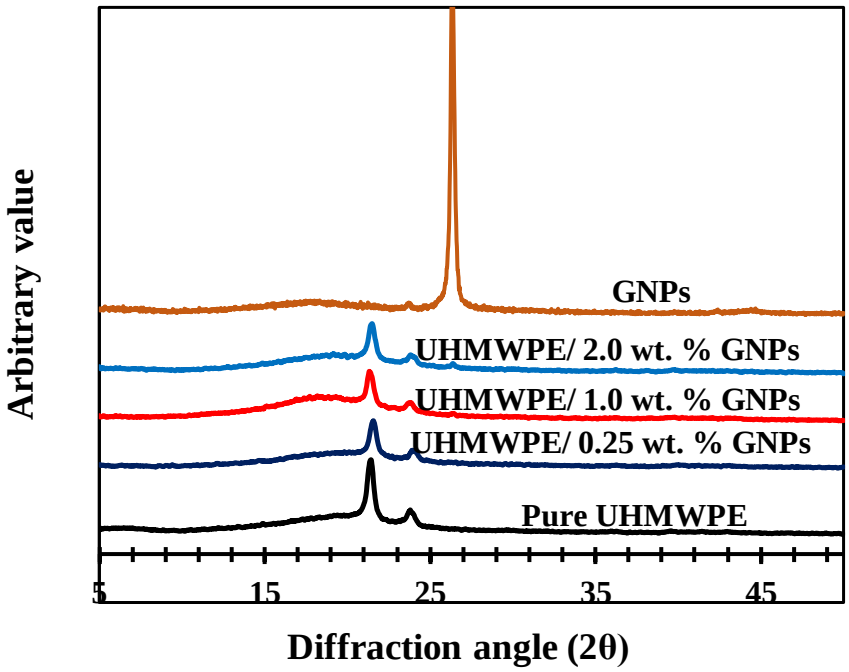

Figure 5.1: XRD pattern of UHMWPE/GNPs nanocomposite powders

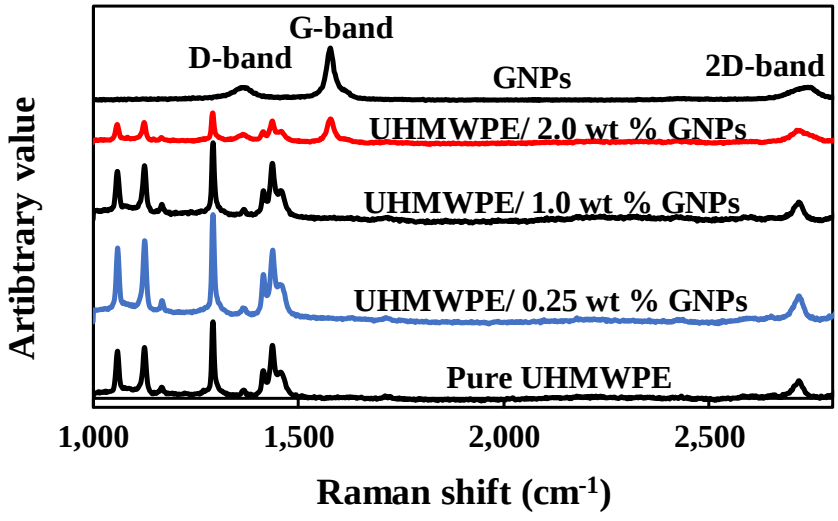

Figure 5.2: Raman spectra of UHMWPE/GNPs nanocomposite coatings

The SEM images of UHMWPE powder reinforced with 1 and 2 wt. % GNPs respectively are shown in Figure 5.3. For UHMWPE reinforced with 1 wt. % GNPs, single platelets of graphene can be seen attached to the surface of the polymer matrix particles at various points thus indicating a uniform distribution. It is believed that the morphology is similar throughout the material. This agrees with evidence of uniform distribution seen in Raman spectra. However, at 2 wt. % GNPs reinforcement, cluster of GNPs are seen close to one another (Figure 5.3B) justifying the agglomeration of GNPs.

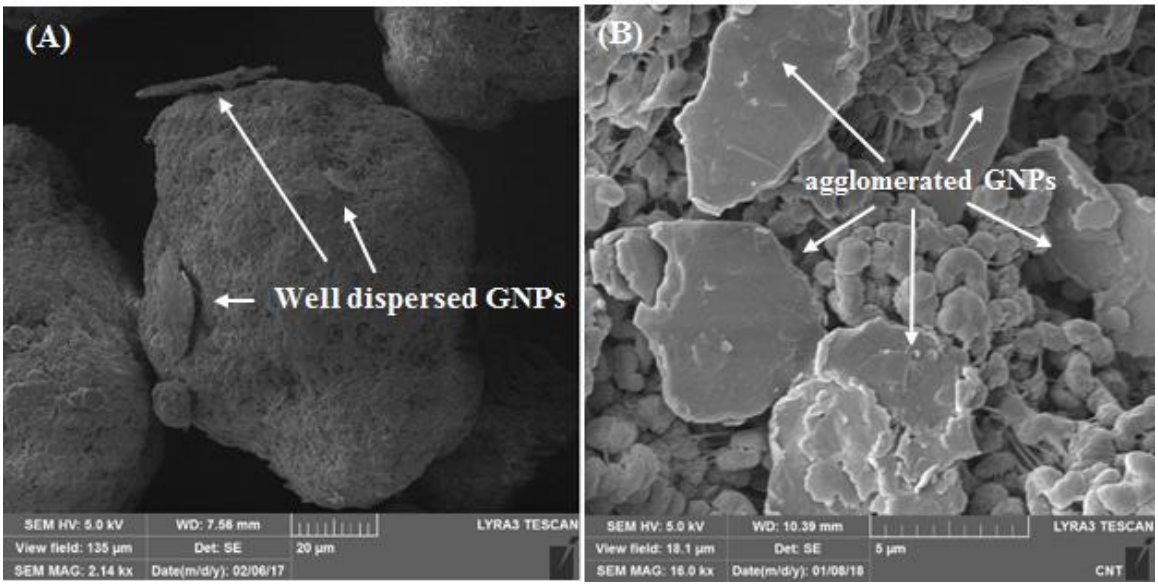

Figure 5.3: SEM image of (A) UHMPWE/1 wt. % GNPs and (B) UHMPWE/2 wt. % GNPs nanocomposite powder

5.2 Coating thickness

The SEM image of a typical coating cross-section is shown in Figure 5.4. The figure shows that the thickness of the coatings is uniform. Measurements were taken from five different locations resulting in an average thickness of 96 ± 4.7 µm. Using the values of coating

thickness from pure and GNPs reinforced UHMWPE coatings, it was observed that the addition of GNPs did not cause any difference in the thickness of the coatings.

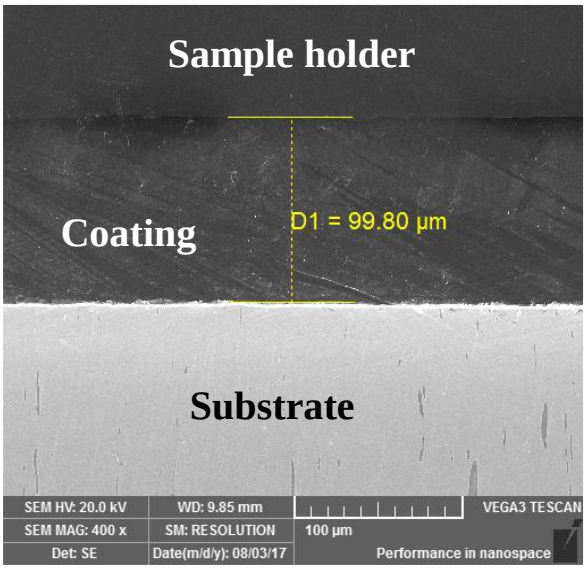

Figure 5.4: SEM image of UHMWPE/1 wt. % GNPs coating on the substrate

5.3 Microhardness

The microhardness of pure and reinforced UHMWPE coatings is shown in Figure 5.5. The hardness of the pure coating is as high as 10.02 HV. In reference [12], reinforced coatings had a maximum hardness of 6.4 to 7.3 HV based on the amount of GNS. This is an indication that the electrostatic spray method and the curing approach used was efficient enough to yield coatings with high hardness. When the coatings were reinforced with different amount of GNPs, the hardness increased from 10.02 to 13.02 HV, a 30 % increase, as can be seen in Figure 5.5. This means that GNPs are effective in improving the hardness of UHMWPE coatings by creating an efficient load transfer mechanism. There is no significant increase in the microhardness between the reinforcement 1 and 2 wt. % GNPs indicating a limiting effect and 1 wt. % GNPs as the optimum amount. The current result

shows the manifestation of GNPs' physical and mechanical properties that were mentioned earlier. The 2D structure is helpful in promoting efficient load transfer mechanism via increased interfacial strength between the reinforcement and the matrix.

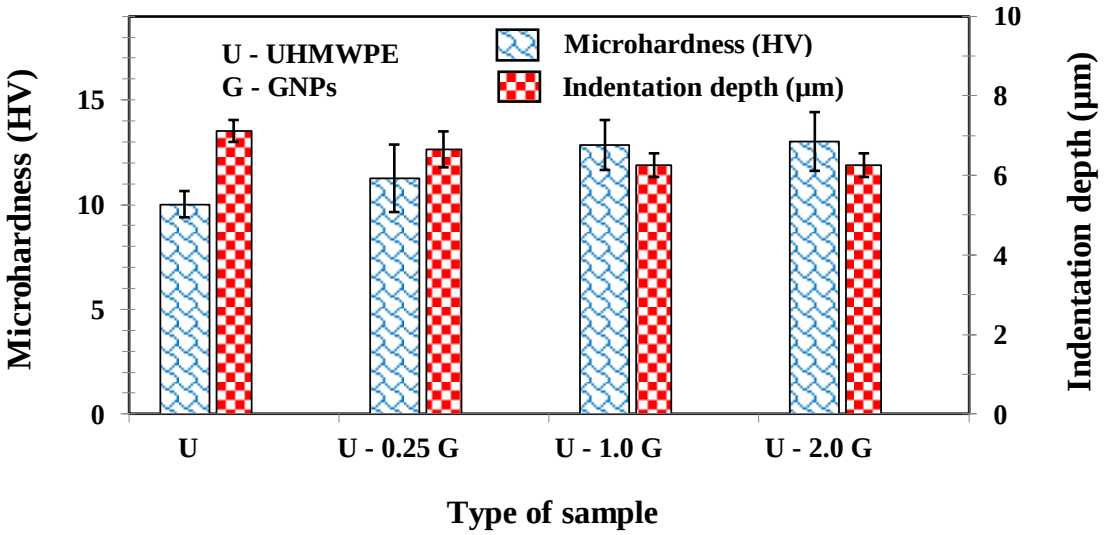

Figure 5.5: Microhardness of UHMWPE coatings with 0 to 2 wt. % GNPs reinforcement

5.4 Friction and wear behavior of GNPs reinforced nanocomposites coatings.

Dry sliding wear tests were carried out on pure and reinforced (0.25, 1 and 2 wt. % GNPs). UHMWPE nanocomposite coatings. A hardened tool steel pin with hardness, diameter and roughness of 57 HRC, 3.2 mm and 0.37 ± 0.021 µm respectively was used as the counterface. The contact pressure was set to 2 MPa. The sliding radius, 6 mm was kept constant for all the tests. Rotational speed was set to 159 rpm that corresponds to a linear speed of 0.1 m/s. All tests were carried out for a total sliding distance of 377 m. Figure 5.6 shows the friction response of the four nanocomposites. Steady-state was attained at just 10 m of sliding distance for all the reinforced nanocomposite coatings while the steady-

state was attained at about 25 m for the pure UHMWPE coatings. This is an indication that with GNPs, the dynamic friction of the coatings can easily attain a steady-state. Moreover, the COF curves were steady throughout the test. The COF of the pure UHMWPE coating is 0.33. The addition of GNPs to the UHMWPE did not cause a significant change in the dynamic COF of the coatings as the average COF of UHMWPE/2 wt. % GNPs is 0.31 as shown in Figure 5.6B. In a different study, a COF of 0.4, higher than the one observed in the current study, was reported [168]. Bulk UHMWPE pin was slid against a steel disc at a pressure and velocity (PV) value, 0.09 MPa.m/s. The higher COF value could be attributed to lower pressure and velocity (PV) value as compared to 0.2 MPa.m/s of the current study.

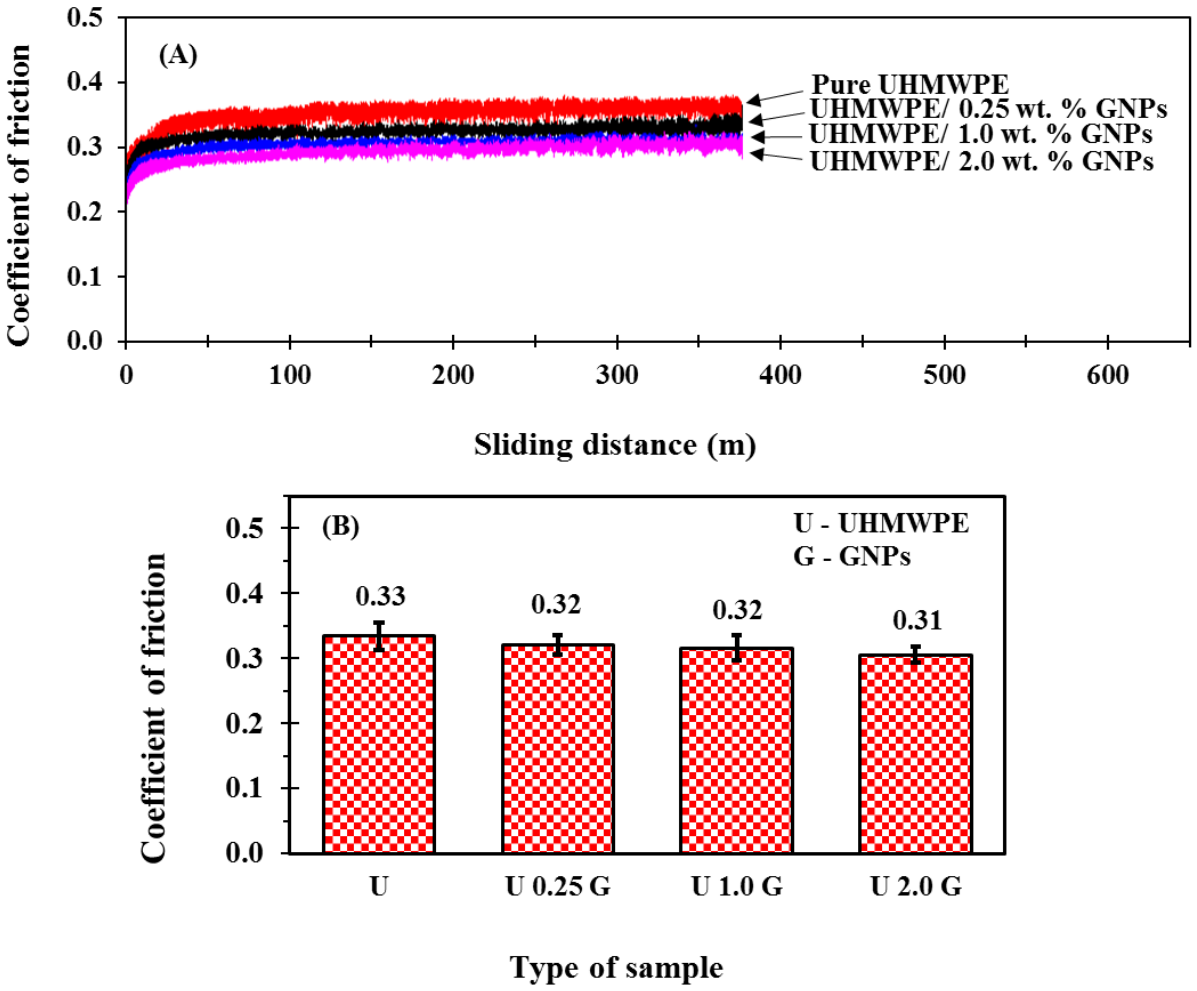

Figure 5.6: (A) typical Friction plots and (B) average COF of Pure, 0.25, 1 and 2 wt. % GNPs reinforced UHMWPE nanocomposite coatings tested at 2 MPa and 0.1 m/s

The wear depth of the tested specimens was obtained from 2D optical profilometric images shown in Figure 5.7A. The wear depth was then used to compute the wear rate for all the compositions as given in Figure 5.7B. The wear resistance of the nanocomposite coatings increased appreciably when reinforced with GNPs. UHMWPE/1 wt. % GNPs attained the highest wear resistance having an average wear rate of 18.2 µm/km, a 51 % reduction in wear rate. There was a slight drop (16 %) in the wear resistance of the coating when reinforced with 2 wt. % GNPs. This can be attributed to agglomeration of the nanoplatelets

in the UHMWPE matrix that reduced the toughness and strength of the nanocomposite coating. This is evident in Figure 5.2 where a peak belonging to GNPs became apparent in the Raman spectra of UHMWPE/2 wt. % GNPs coating. Also, SEM images in Figure 5.3 shows that GNPs are uniformly dispersed in UHMWPE/ 1 wt. % GNPs nanocomposite powder while agglomerates of unexfoliated GNPs can be seen in that of UHMWPE/ 2 wt. % GNPs. Although the wear rate varies, none of the coatings failed in any of the tests as shown by EDS in Figure 5.8 where aluminum peak is absent. This is an indication that the surface preparation and coating fabrication method led to a high strength of adhesion between the coating and the substrate. In the SEM images shown in Figure 5.8, a pull out of material and some plowing lines can be seen in the pure UHMWPE coating. This is an indication of a mixed adhesive and abrasive wear mechanism mode. However, only abrasive wear occurred in the reinforced coatings since plowing lines only are seen. Thus, improved heat transfer and friction coefficient of the nanocomposite due to the GNPs reduced contact temperature and prevented softening of the matrix. Hence the reinforcement of UHMWPE with GNPs can lead to a change in mechanism from mixed to purely abrasive wear that in turn resulted in lower wear magnitude for the reinforced coatings. Irrespective of the GNPs amount, the wear rate of the nanocomposite coatings fabricated in this study is much lower than the wear rate of similar composite coatings in literature. The specific wear rate ranged from $1.36 * 10^{-4}$ to $2.09 * 10^{-4}$ $mm^3/(Nm)$. In a previous study, the wear rate obtained for UHMWPE/1 wt. % GNS is $1.1 * 10^{-3}$ $mm^3/(Nm)$ [12]. This is almost 6 times the wear rate achieved in the current research despite the fact that the applied load is only 2.5 times greater than the load used in the current tests (35 N compared to 14 N) while the speed is ten times less (0.01 m/s compared to 0.1 m/s). The

increase in wear resistance displayed by the reinforced coatings in the current research could be due to uniform dispersion and enhanced hardness and toughness. The high aspect ratio and large surface area of GNPs result in an efficient load transfer from the matrix to the reinforcement. It was also suggested that GNPs can enhance the mechanical strength and thermal conductivity of polymer matrix [10,11,152]. There are two thermal mechanisms, which could explain the wear rate reduction in these coatings. First, the thermal conductivity of the polymeric material might have been enhanced by GNPs, preventing the accumulation of local friction heat during sliding. Also, the aluminum substrate has high thermal conductivity. It further dissipates friction heat away from the coatings. From the overall results, UHMWPE reinforced with 1 wt. % GNPs was selected as the best coating. The coating was then subjected to further tests at various contact pressures and sliding speeds.

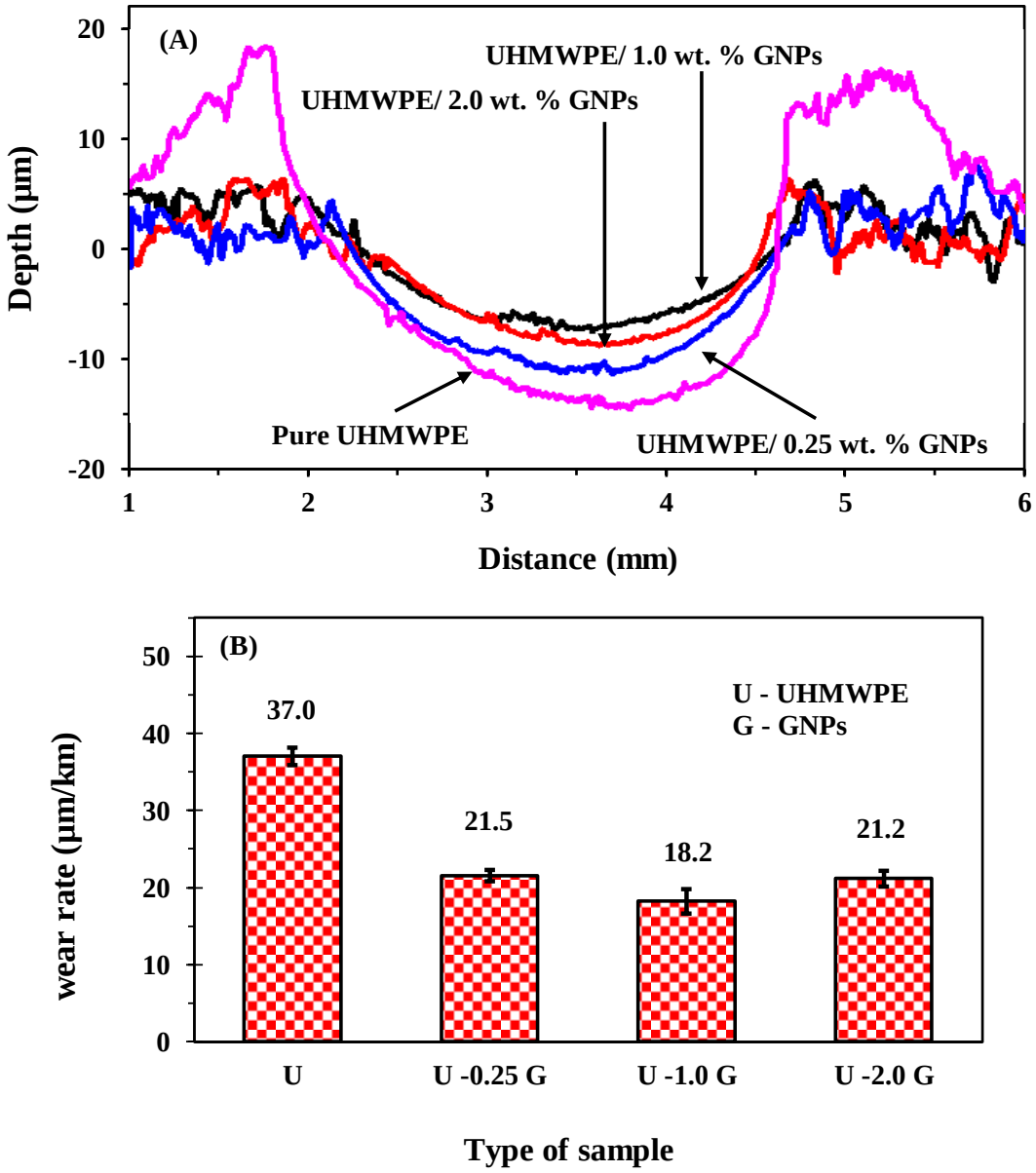

Figure 5.7: (A) 2D wear tracks profilometric images and (B) wear rate of pure, 0.5, 1, and 2 wt. % GNPs reinforced UHMWPE coatings tested at 2 MPa and 0.1 m/s

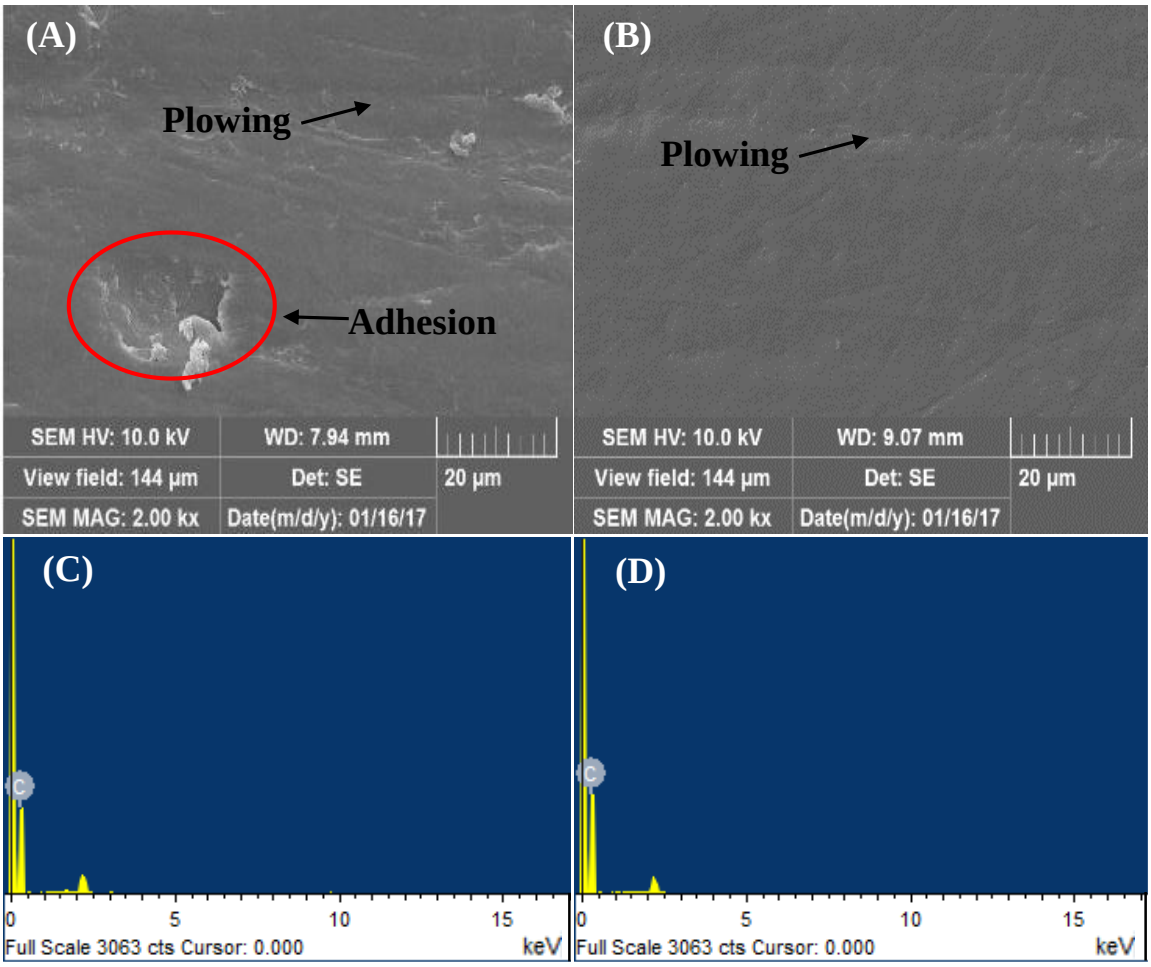

Figure 5.8: Wear tracks SEM images for (A) pure UHMWPE (B) UHMWPE/1 wt. % GNPs and EDS (C) pure UHMPWE (D) UHMWPE/1 wt. % GNPs coatings tested at 2 MPa and 0.1 m/s

5.5 Friction and wear behavior under varied contact pressure

In order to study the friction and wear behavior of the selected nanocomposite coating, UHMWPE/1 wt. % GNPs under varying contact pressure, wear tests were conducted at four different contact pressures (2, 4, 6 and 8 MPa) and constant sliding speed, 0.1 m/s. The friction results of the tests (Figure 5.9) showed that increase in contact pressure caused a progressive decrease in COF from 0.32 to 0.20. The coating sustained all the applied pressure until 8 MPa where it failed as shown in the friction curve (Figure 5.9A). The

decrease in friction as a function of load increase could be attributed to the surface softening of the polymer resulting from localized heating from a higher PV factor due to contact pressure increase. Figure 5.12A – D shows the optical images of the counterface pin after wear test. Some amount of the polymer film can be seen to have transferred on to the counterface due to softening of the polymer. The amount of the transferred material increased with increasing load. A similar observation was reported in previous research [169,170].

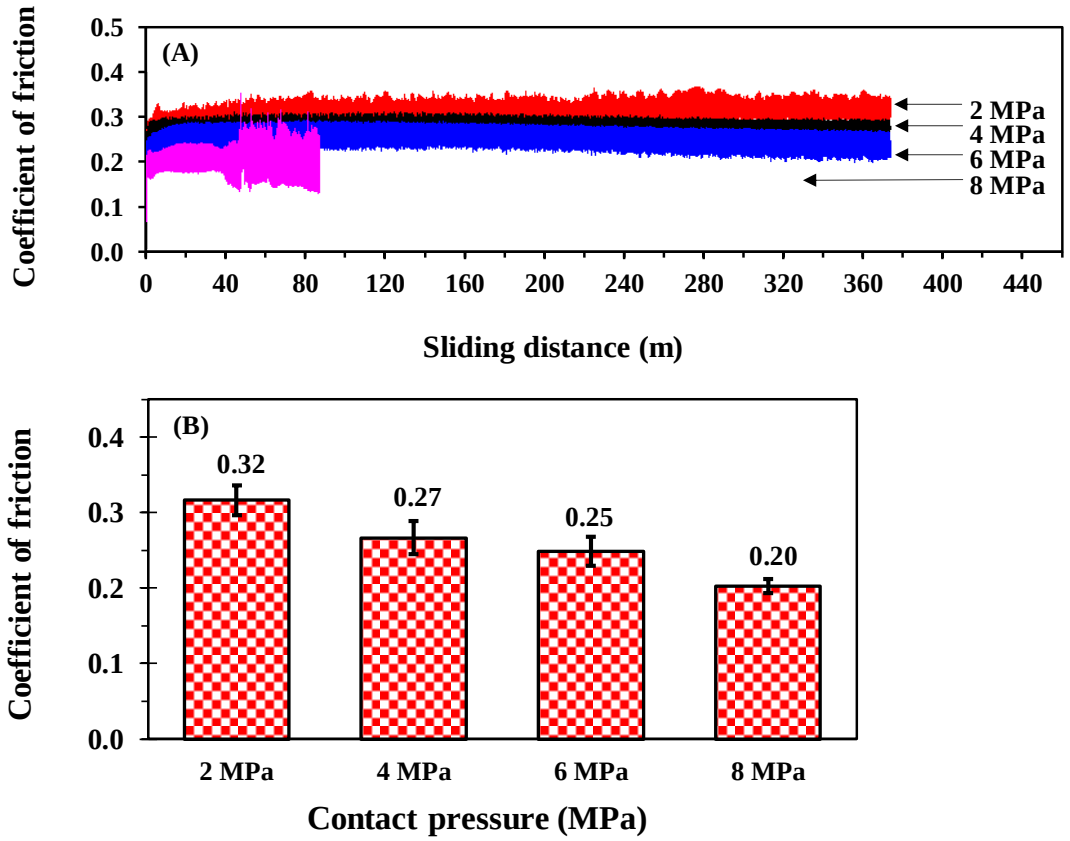

Figure 5.9: (A) Typical friction plot and (B) average COF of UHMWPE nanocomposites coating reinforced with 1 wt. % of GNPs tested at varied pressure and constant linear speed, 0.1 m/s

The wear rate increased with increase in contact pressure as shown in Figure 5.10. A sudden increase was observed as the pressure was increased from 6 to 8 MPa. This is an indication that the coating failed at 8 MPa in addition to the fact that the coating was totally removed from the substrate (Figure 5.11).

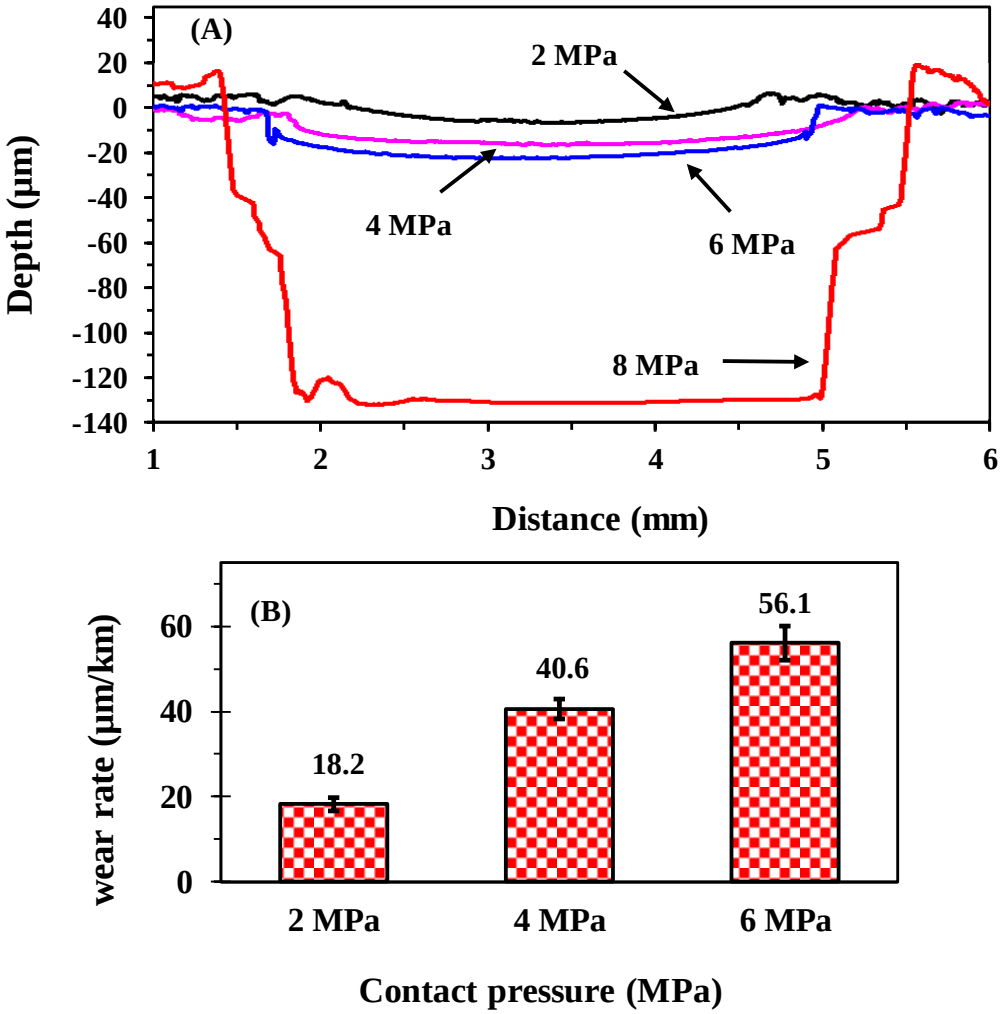

Figure 5.10: (A) 2D wear track (B) and average wear rate of UHMWPE/1 wt. % GNPs coating tested at varied pressure and constant linear speed, 0.1 m/s

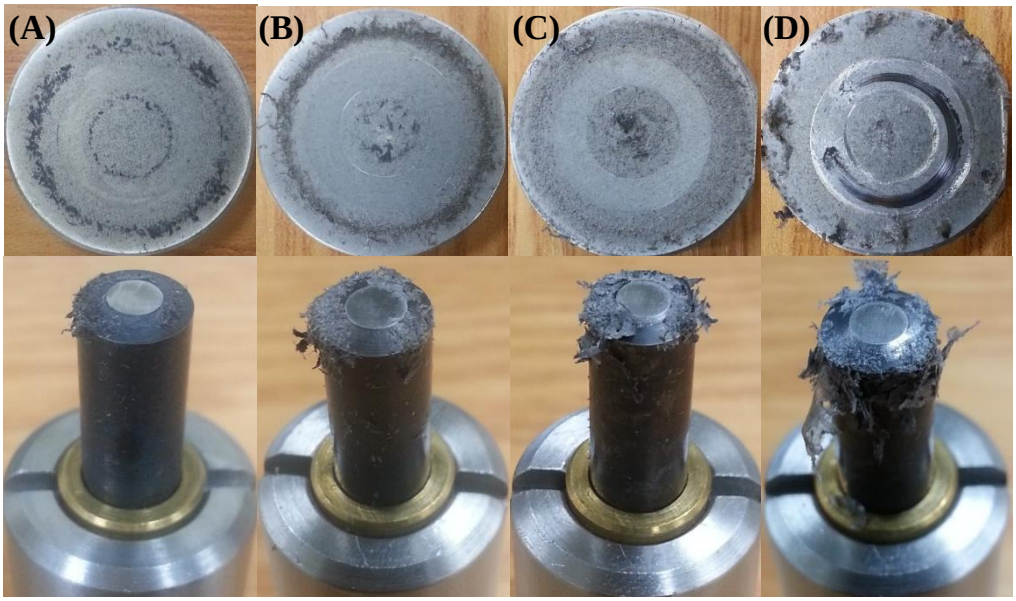

Figure 5.11: Test samples and pin counterface immediately after wear test at (A) 2 MPa, (B) 4 MPa, (C) 6 MPa and (D) 8 MPa and 0.1 m/s

The 3D profilometric images are shown in Figure 5.12E – H. Higher pressure increased plastic deformation resulting in more material removal. The sample tested at 8 MPa has a totally flat bottom, an indication that the coating has been totally removed and the substrate has been reached. Since the coatings cannot sustain 8 MPa, It can be concluded that the load-bearing capacity of the polymer nanocomposite coating reinforced with 1 wt. % of GNPs is up 47 N (6 MPa) corresponding to a PV limit of 0.6 MPa.m/s. Also, no visible significant scar lines could be seen on the counterface. This is an indication that the coating is mild to the counterface.

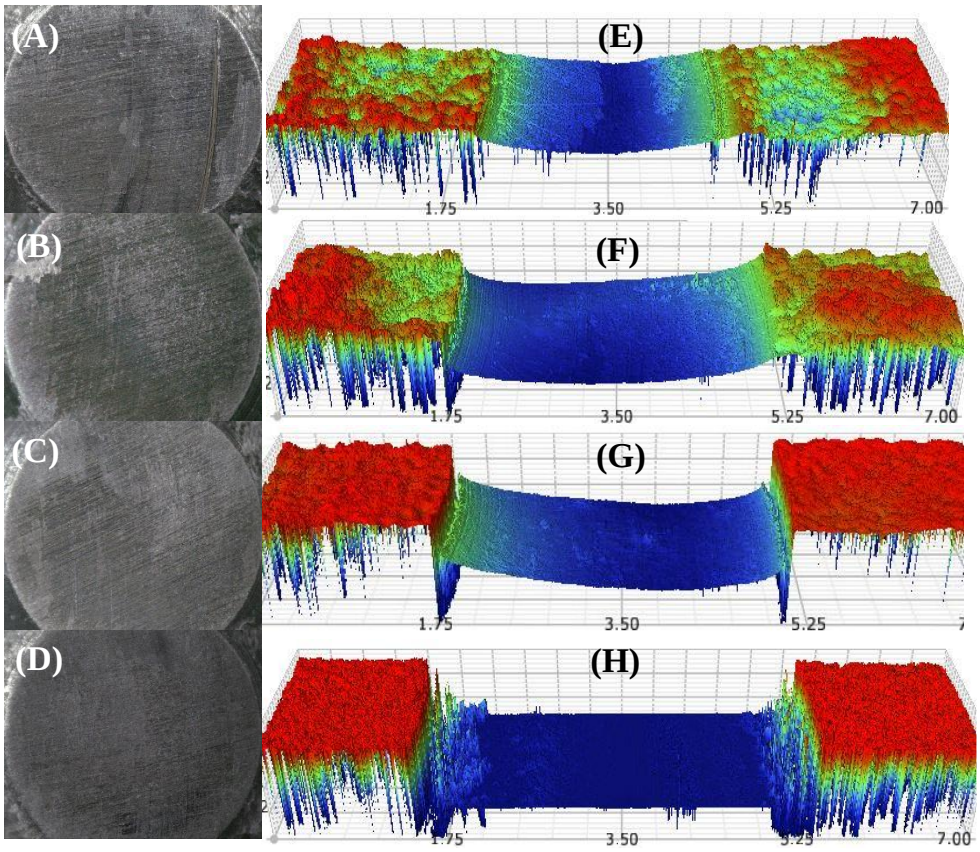

Figure 5.12: Optical microscope images of counterface after wear test of UHMWPE/1 wt. % GNPs nanocomposite coatings at (A) 2 MPa, (B) 4 MPa, (C) 6 MPa and (D) 8 MPa and 3D profilometric images at (E) 2 MPa, (F) 4 MPa, (G) 6 MPa and (H) 8 MPa

Figure 5.13 shows the SEM images and the EDS of the wear track for the sample that failed at 8 MPa. At the left side of the wear track, a small amount of the coating is still left but the substrate is about to be reached. The wear mechanism of the coating changes from abrasive to adhesive and excessive plastic deformation. The exposed part at the left side of the track shows the lay created on the surface of the substrate during surface preparation by grinding. It implies that the counterface has not yet started to wear the substrate in those regions. Once the counterface starts to wear the substrate (wear track center), several large plowing lines are seen parallel to the direction of sliding. This signifies severe abrasive

wear of the metallic substrate due to metal-to-metal contact. The polymeric material has been removed totally indicating that the coating has failed. Comparing the EDS of the wear track to that of the unworn surface, it is totally clear that the sample has failed by the presence of substantial amount of Al and Cu.

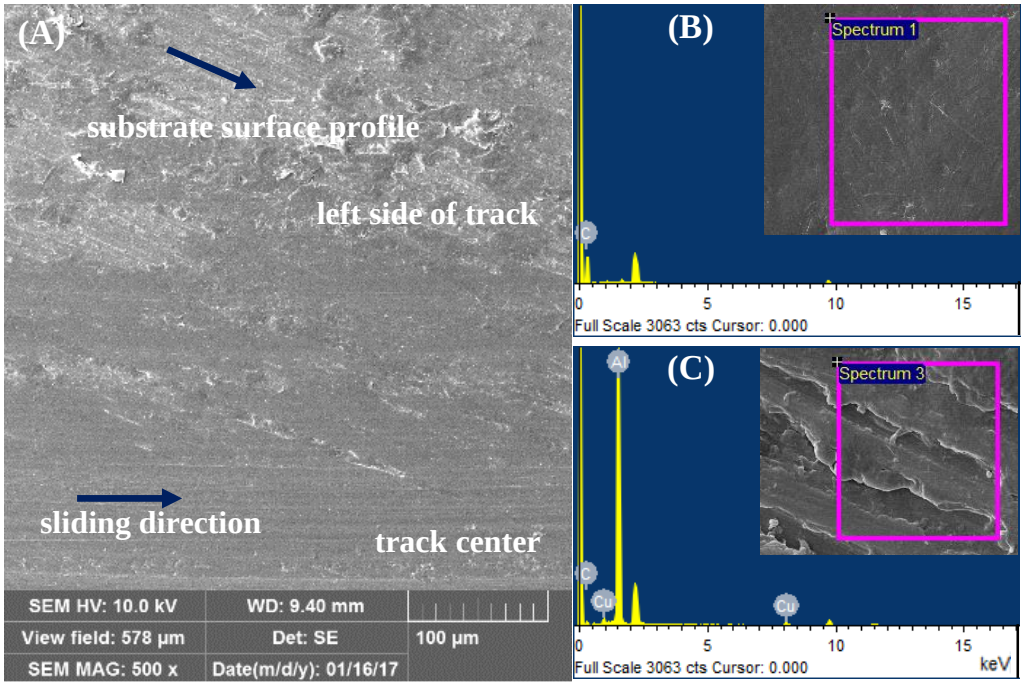

Figure 5.13: UHMWPE/1 wt. % GNPs coating tested at 8 MPa and 0.1 m/s (A) SEM image of the worn track, EDS of (B) unworn surface and (C) worn track

5.6 Friction and wear behavior under varied linear speed

In order to assess the effect of linear speed on friction and wear of UHMWPE/1 wt. % GNPs coating, a set of wear tests was conducted at varied speed (0.1, 0.5 and 1 m/s) while pressure was kept constant at 4 MPa. Figure 5.14A shows the typical plot of dynamic friction. Steady-state was attained immediately after the tests were started for all the three speeds with no significant break-in period. The average dynamic COF was computed and plotted in Figure 5.14B. It can be seen that the COF decreased with speed increase. A

similar observation was made in [169] where the COF of UHMWPE decreased with increased linear speed. It is believed that at higher speed, friction heating increases. This heat causes the relative softening of the polymer coatings resulting in lesser shear resistance at the contact surface. Also, by observing the optical microscope images of the counterface in Figure 5.17A – C, it is clear that the amount of the transfer film at high speed is greater, uniform and intact. The transfer film coatings formed at a sliding speed of 1m/s is the most adhesive to the counterface; it has to be cleaned several times before the film could be removed. The film helped to prevent metal-to-metal contact leading to lower friction.

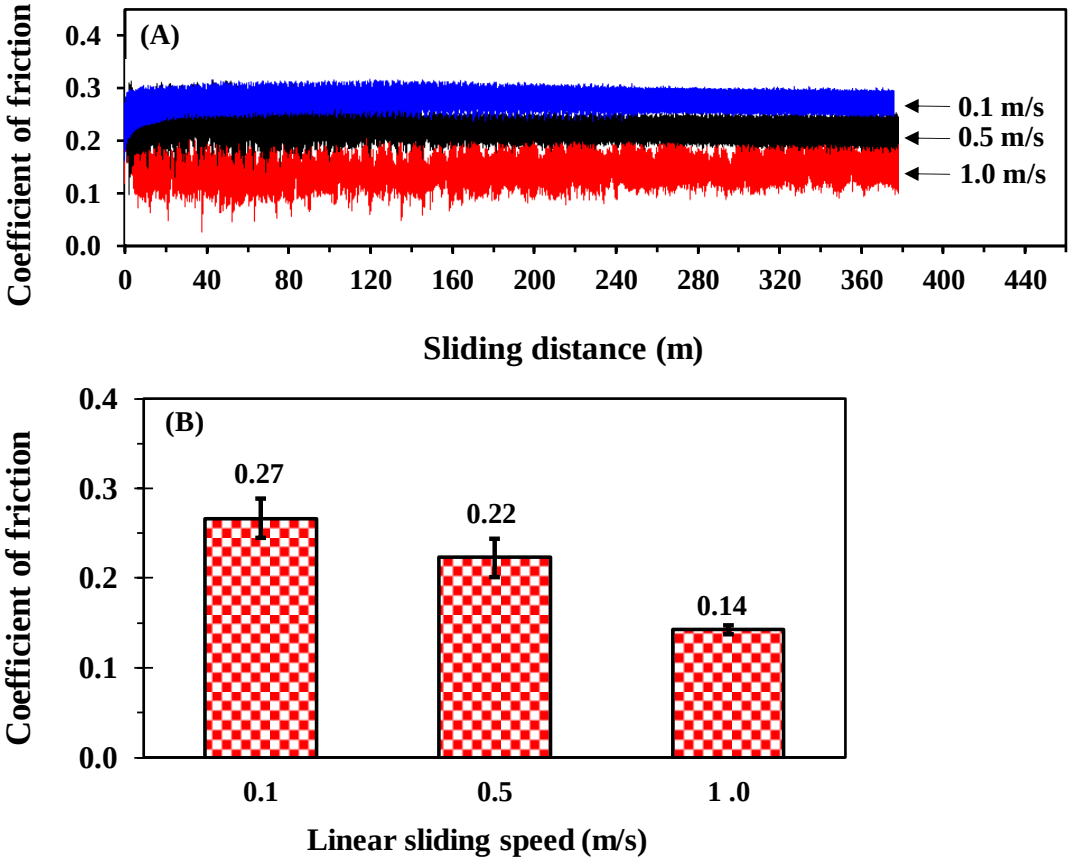

Figure 5.14: (A) Typical friction plot and (B) average COF of UHMWPE nanocomposites coating reinforced with 1 wt. % of GNPs tested at varied linear speed and 4 MPa.

As for the effect of sliding speed on wear severity, the increase in speed resulted in increased wear rate (Figure 5.15). An increased velocity amounts to increased heat energy at the contacts. This causes surface softening making material removal by sliding much easier. Hence more material was removed.

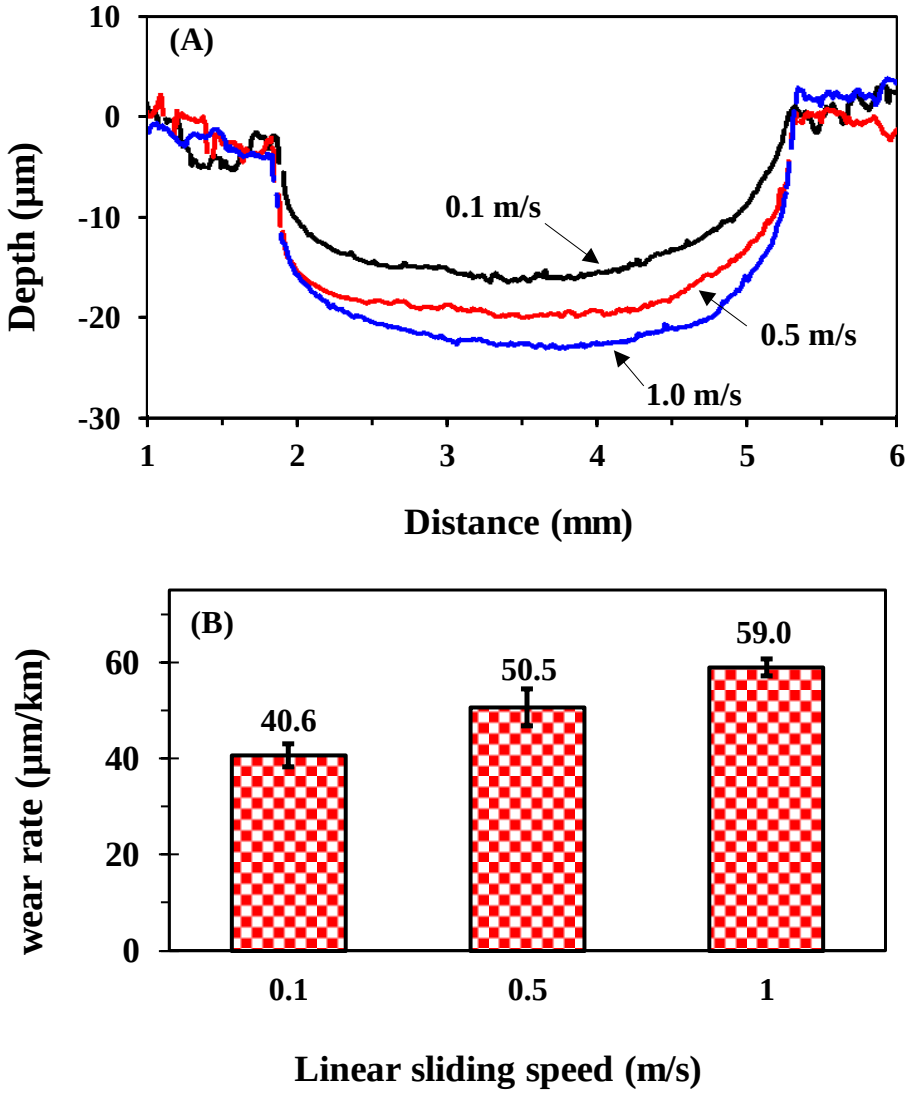

Figure 5.15: (A) 2D wear track (B) and average wear rate of UHMWPE/1 wt. % GNPs coating tested at speeds of 0.1, 0.5 and 1.0 m/s and 4 MPa

At 1 m/s the transfer film is more intact and uniform covering almost all the surface of the counterface as shown in Figure 5.17C. This could have helped minimize the effect of velocity increase on wear. This trend indicates that although wear rate increased moderately with increased speed, the current coating is wear resistant at high sliding speed. The SEM images (Figure 5.16A and D) of UHMWPE/1 wt. % GNPs tested at 0.1 m/s and 1 m/s respectively, indicates that the wear mechanism remains abrasive irrespective of the sliding speed. However, a higher magnification (Figure 5.16B and E) into the plowed valley shows some difference. At low speed (0.1 m/s), the plowing indicated plastic deformation; however, at high speed (1 m/s), cracks were observed perpendicular to the sliding direction. This can be attributed to the high wear rate at higher speed.

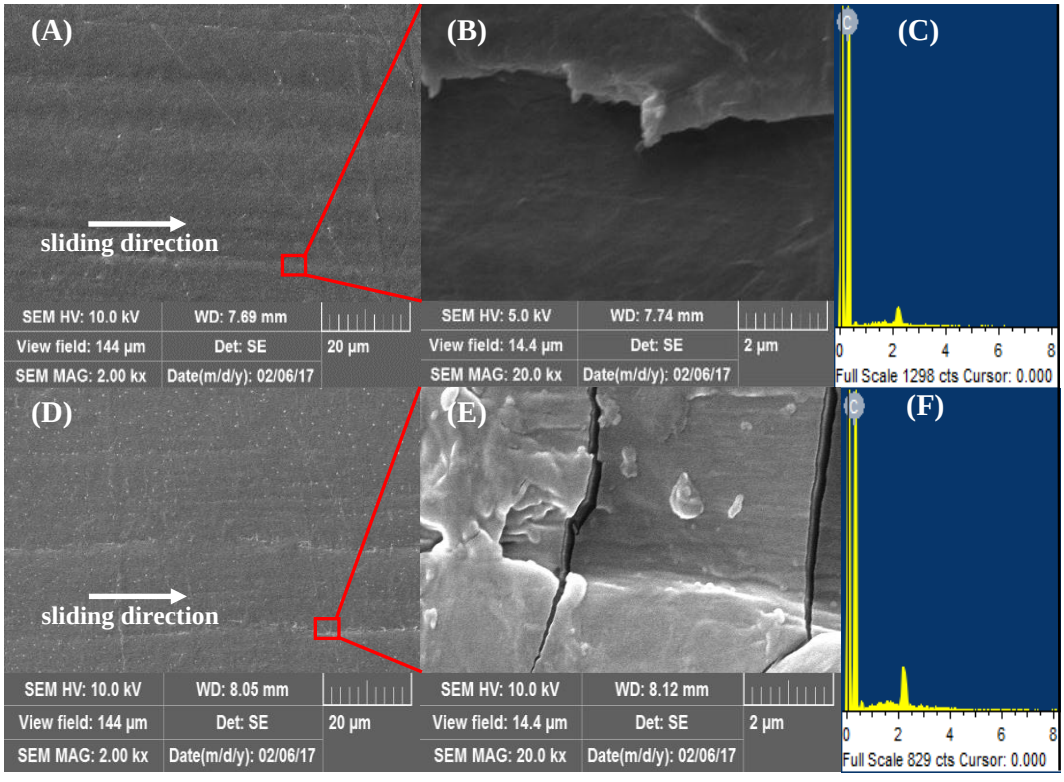

Figure 5.16: SEM images of UHMWPE/1 wt. % GNPs coating at sliding speed of 0.1 m/s (A) wear track, (B) within plowing line (C) EDS and 1 m/s (D) wear track, (E) within plowing line (F) EDS

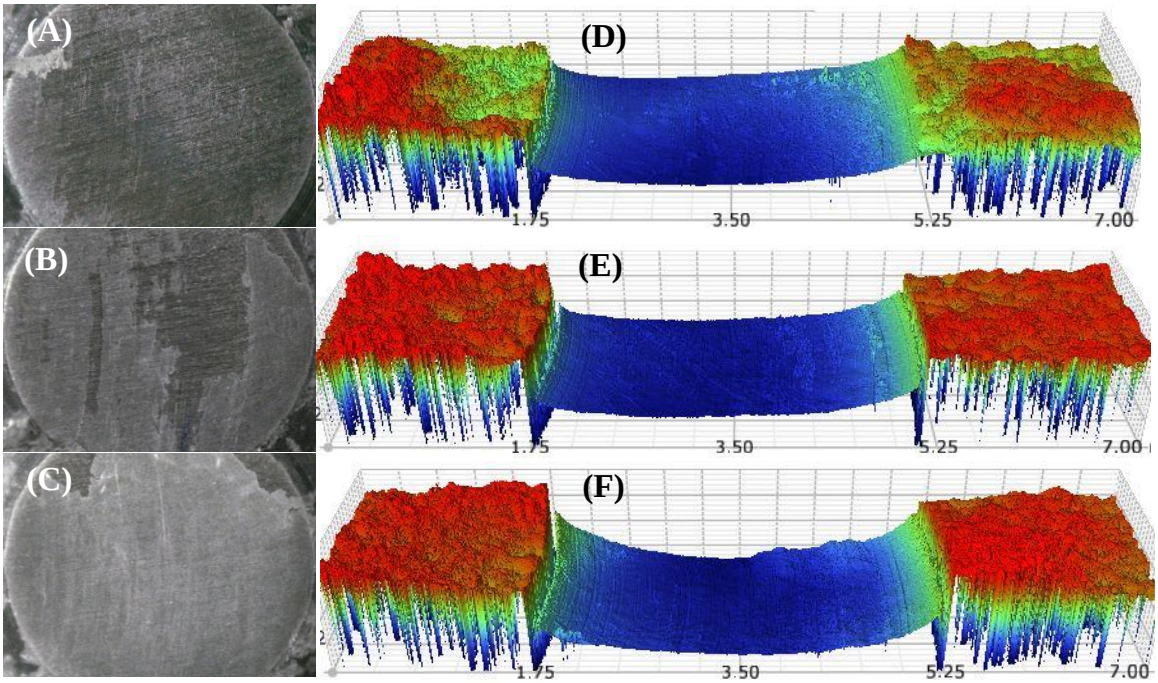

Figure 5.17: Optical microscope images of counterface after wear test of UHMWPE/1 wt. % GNPs nanocomposite coatings at (A) 0.1 m/s, (B) 0.5 m/s, and (C) 1 m/s and 3D profilometric images at (E) 0.1 m/s, (F) 0.5 m/s, and (G) 1 m/s

The 3d profilometric images of the coatings at various sliding speed are shown in Figure 5.17B. It shows that the wear level is progressively increasing with speed. The coating sustained a PV of 4 MPa.m/s. This value is quite higher than the PV limit (0.35 MPa.m/s) for Avalon® 37; a commercial product made from UHMWPE by a leading bearing company [171]. The thermal conductivity of the Aluminum alloy substrate (157 W/m-K) might have contributed to the high PV limit attained by the coating. Heat generated during sliding is conducted away by the substrate making the effect of heat on the coating less significant.

5.7 Conclusions

UHMWPE/GNPs nanocomposite coatings were successfully fabricated on an aluminum alloy. The pure UHMWPE coating demonstrated a microhardness of 10.02. But GNPs addition increased the hardness continuously to 13.03 at a reinforcement amount of 2 wt. %. The friction study showed that pure UHMWPE had a dynamic COF of 0.33 while the addition of GNPs did not cause a significant change in the COF of the UHMWPE coating. Although the effect of GNPs addition on friction is not significant, it appreciably reduced the wear rate. The UHMWPE nanocomposite coating reinforced with 1 wt. % GNPs performed best. Its COF was low and it had the lowest wear rate (18.2 μm/km) equivalent to 51 % reduction in wear rate.

The COF of UHMWPE/1 wt. % GNPs coating decreased from 0.32 to 0.2 with contact pressure increase. The wear rate increased linearly with contact pressure increase from 2 to 6 MPa. Coating failure was then observed at 8 MPa. The load-bearing capacity of the coating is therefore 47 N (6 MPa). This corresponds to a PV limit of 0.6 MPa.m/s.

On the investigation of the tribological properties of UHMWPE/1 wt. % GNPs coating with respect to sliding speed (0.1 to 1 m/s), it was found that the COF decreased from 0.27 to 0.14. Wear rate increased linearly with increasing speed but none of the coatings failed at the maximum tested speed (1 m/s). Testing at 4 MPa and 1 m/s resulted in the formation of a thin, uniform and durable transfer film on the counterface. The current PV capability is therefore 4 MPa.m/s.

The polymer coating is a good mating pair because it did not leave scratches on the counterface in most of the testing condition.

CHAPTER 6

RESULTS AND DISCUSSION

TRIBOLOGICAL PERFORMANCE OF UHMWPE/GNPs COATING AT ELEVATED TEMPERATURE

In order to assess the high-temperature applicability of the developed coating, dry wear tests, at temperatures varying from 25 ^{o}C to 125 ^{o}C, were carried out on pure and 1 wt. % GNPs reinforced UHMWPE coatings. Pure UHMWPE coating was included in the test to serve as a reference. In was reported in chapter 5 that UHMWPE/ 1 wt. GNPs survived wear tests at pressures up to 6 MPa and sliding speed up to 1 m/s (1592 rpm). Therefore, these values were used as contact pressure and sliding speed respectively. The sliding distance was maintained at 377 (10,000 cycles) for all the tests.

6.1 The effect of test temperature on the friction of pure and 1 wt. % reinforced UHMWPE

The dynamic COF is plotted against sliding distance as shown in Figure 6.1. The plots indicate that the break-in period for pure and reinforced UHMWPE at all tested temperatures is short, about 20 m. Also, the friction plot is steady over the entire test period. While UHMWPE/ 1 wt. % GNPs survived the test up to 115 ^{o}C, pure UHMWPE failed at 75 ^{o}C. The plots also show that the samples that did not survive the test at temperatures indicated in the figure failed at about 310 m into the test. The average dynamic COF of all

the tests are summarized in Table 6.1 and plotted in Figure 6.2. COF decreased linearly with increase in temperature. At lower temperatures, the COF of the GNPs reinforced coating is barely less than that of the pure coating based on the indications from the error bars of the plots. However, at higher temperatures, the pure polymer coating had already failed while the GNPs reinforced coating continue to maintain a reduction in friction as a function of temperature. This is a further decrease in friction to those achieved when contact pressure and sliding speed were increased in chapter 5. The decrease in friction is as a result of polymer coating surface softening due to contact heating. The higher the heat, the softer the polymer material at contact region resulting in lower shear stress, lower resistance to sliding and lower friction.

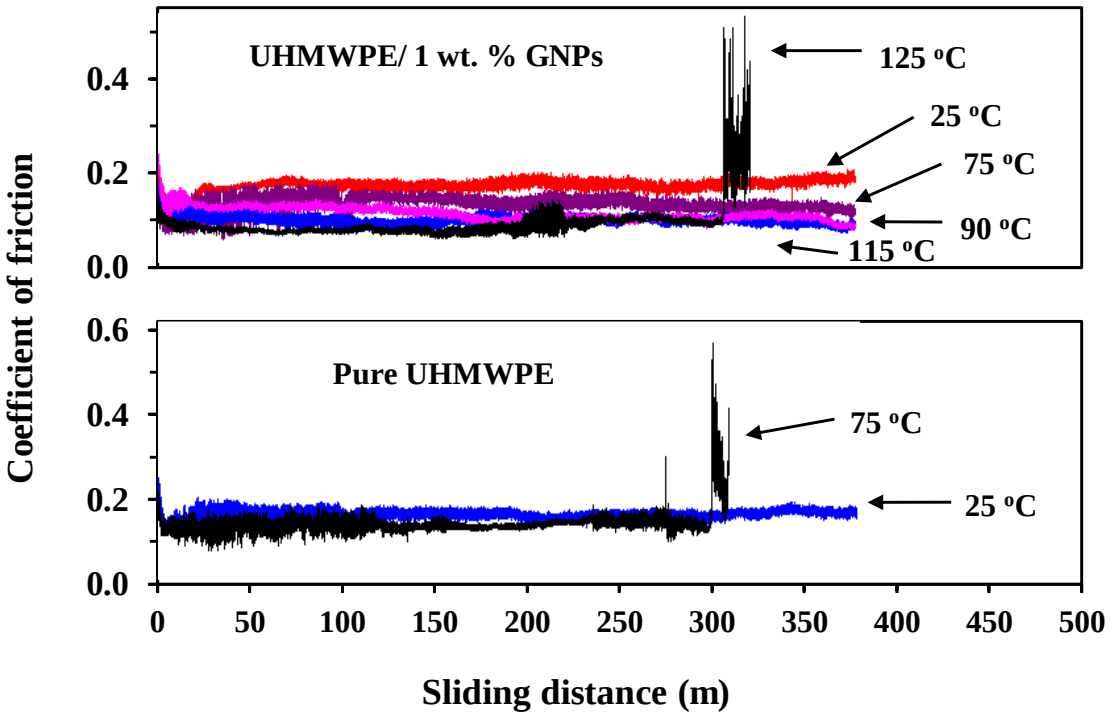

Figure 6.1: Typical Friction plots of pure UHMWPE and UHMWPE/1wt. % GNPs samples tested at 6 MPa and 1 m/s while test temperature was varied from 25 to 125 °C

Table 6.1: Dynamic coefficient of friction of UHMWPE and UHMWPE/1wt. % GNPs samples tested at 6 MPa and 1 m/s

Temperature (°C)	Pure UHMWPE	Standard Deviation	UHMWPE/ 1 wt. % GNPs	Standard Deviation
25	0.140	0.0217	0.134	0.0124
75	0.134	0.0083	0.123	0.0069
90			0.104	0.0084
115			0.096	0.0024
125			0.086	0.0030

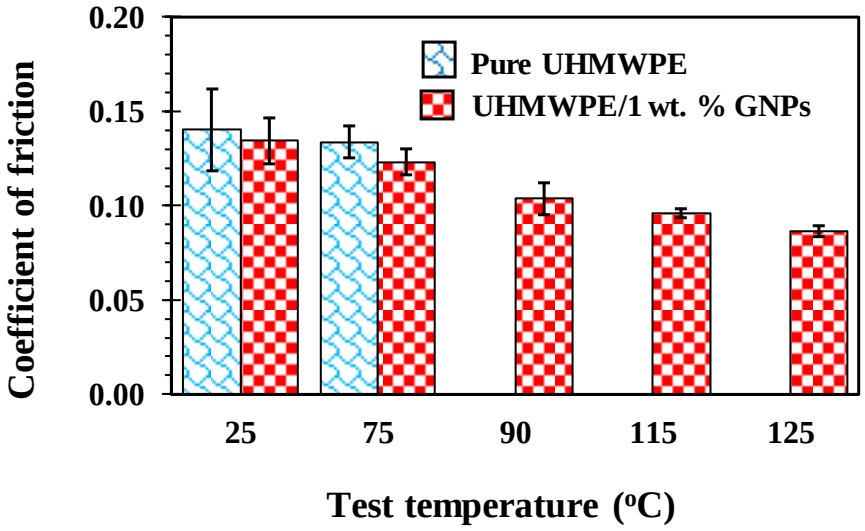

Figure 6.2: Average dynamic coefficient of friction chart for UHMWPE and UHMWPE/1wt. % GNPs samples tested at 6 MPa and 1 m/s and varied temperature

6.2 The effect of test temperature on the wear rate of pure and 1 wt. % reinforced UHMWPE

Generally, the wear rate increased with temperature for both the pure and the GNPs reinforced coating as shown in Figure 6.3 and Figure 6.4. While the pure UHMWPE coatings failed at 75 °C, the 1 wt. % GNPs reinforced coating sustained a much higher temperature. The change in temperature did not result in a significant increase in wear rate

until 115 ^{o}C. Although the effect of temperature started to become pronounced at 115 ^{o}C, the coating successfully withstood the wear test. The coating was still intact on the substrate and the wear rate was relatively less. The coating failed only when the temperature was further raised to 125 ^{o}C. It can, therefore, be concluded that the critical temperature of the coating is 115 ^{o}C and the PV limit at this temperature is 6 MPa.m/s. This is a significant improvement in the wear resistance of the UHMWPE nanocomposite coating at elevated temperature. This improvement can be attributed to the reinforcement of the coating with GNPs that increased the mechanical strength of the coating at elevated temperature. The reinforcement was able to anchor the chains of the polymer at elevated temperature to avoid failure. Since the tribometer reads the chamber temperature it is expected that the temperature at the contact has already exceeded the test temperature. For instance, the softening temperature of pure UHMWPE is 80 ^{o}C [172]. Hence for the pure UHMWPE coating to fail at 75 ^{o}C, its softening point had already been exceeded. This implies that for the 1 wt. % GNPs reinforced coating, which survived the test at 115 ^{o}C, its softening temperature has been improved from 80 ^{o}C to a value above 115 ^{o}C depending on the actual temperature rise due to frictional heating. UHMWPE deflection temperature was said to have been improved to 125 ^{o}C by an unspecified reinforcement [173]. The current research has led to a tremendous improvement in the thermal tribological properties of the UHMWPE polymer coating by increasing the operating temperature range of UHMWPE coating. This gives the current polymer a potential to be used as coatings for automotive bearings where oil temperature can be as high as 110 ^{o}C [174]. This will be impossible with pure UHMWPE coatings that failed at 75 ^{o}C. Since the UHMWPE/1wt. % GNPs coating survived the critical temperature 115 ^{o}C test at 6 MPa, a life test was done using

these set of parameters and further at 4 and 2 MPa. Figure 6.5 shows the life attained at varied contact pressure. At 6 MPa, the coating sustained the test for a sliding distance of 0.5 km. However, at 4 MPa, the sliding distance before failure increased to 1.5 km while it increased to 4.1 km at 2 MPa. The maximum sliding distance of the nanocomposite coating at 115 ^{o}C can be modeled as a function of applied pressure (Eq. (6))

$$L = 11.22e^{-0.507P} \tag{6}$$

Where ***P*** is the applied pressure in MPa and ***L*** is the maximum sliding distance in km.

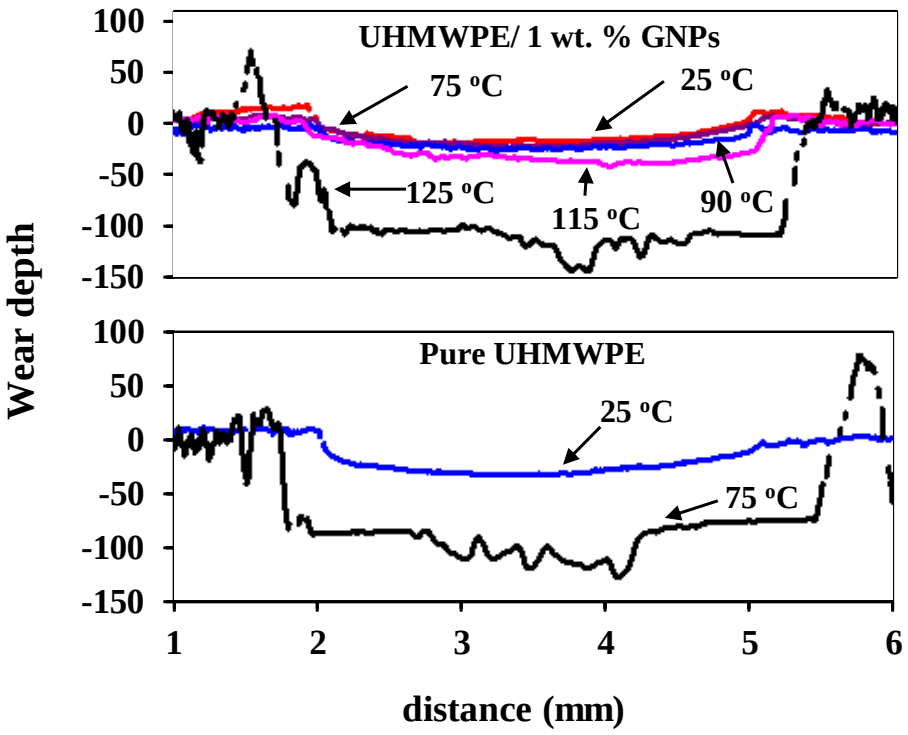

Figure 6.3: 2D wear tracks profilometric images of pure UHMWPE and UHMWPE/1wt. % GNPs samples tested at 6 MPa and 1 m/s while test temperature was varied from 25 to 125 ^{o}C

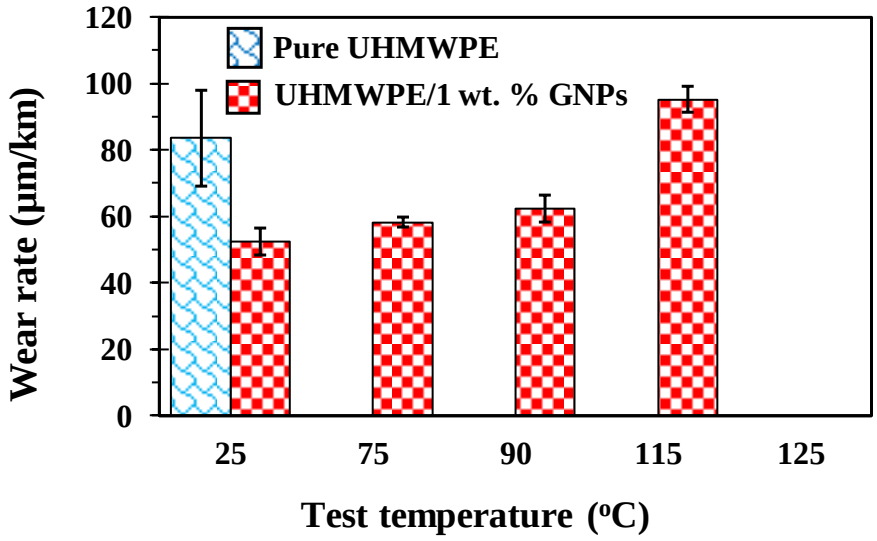

Figure 6.4: Average wear rate of pure UHMWPE and UHMWPE/1wt. % GNPs samples tested at 6 MPa and 1 m/s while test temperature was varied from 25 to 125 °C

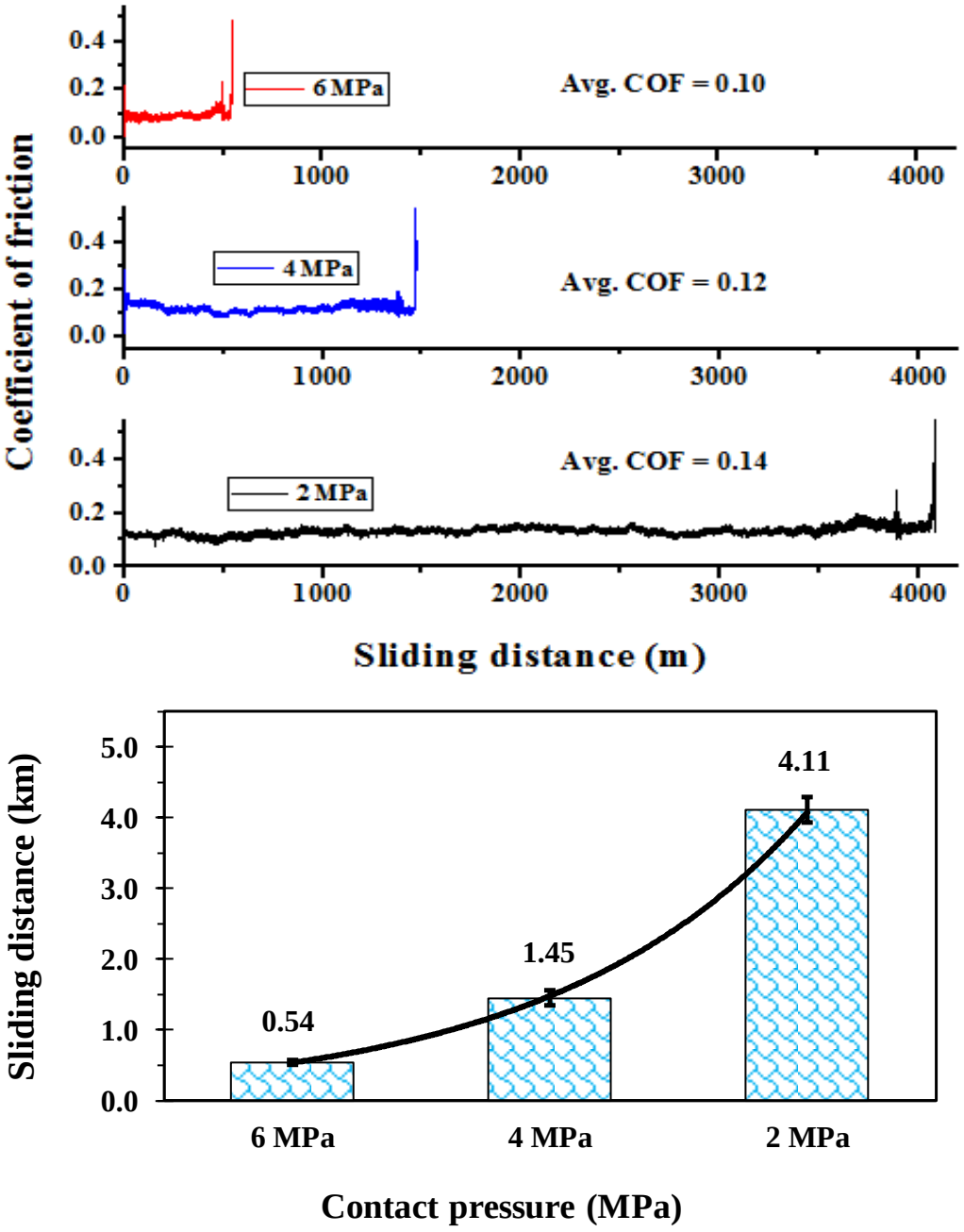

Figure 6.5: Maximum sliding distance of UHMWPE/1wt. % GNPs samples tested at 1 m/s, 115 ^{o}C, and varied contact pressure

6.3 Microscopic and profilometric analyses

Prior to every wear test, the optical microscopic image of the counterface is taken. The same is done after the wear test. This is to enable analysis of the transfer film and sample effects on the counterface. The optical images of the counterface after the wear tests are shown in Figure 6.6A to E. The images show varying amounts of polymer transfer film after the test. The film is intact and transparent suggesting that they are thin films. The counterface after the test of the GNPs reinforced coating showed a higher amount of transfer film as compared to the pure coating at equal testing temperature. This justifies why it had a lower COF. Another observation from comparing the images is the visibility of deep scratch lines and aluminum debris on the counterface of the pure and GNPs reinforced UHMPWE coatings that failed at 75 ^{o}C and 115 ^{o}C respectively (Figure 6.6B and F). The 3D wear track optical profilometric images of few selected samples are shown in Figure 6.6G to J. The figures represent pure and 1 wt. % GNPs reinforced UHMWPE coatings both at room temperature and individual failure temperatures, 75 and 125 ^{o}C respectively. Large plowing lines are visible, on the surface of the substrate, at the center of the track of samples that failed. In comparison, the tracks of the samples that did not fail are smooth throughout. Also, the sizes of their tracks are smaller than those of failed samples in support of previously reported results.

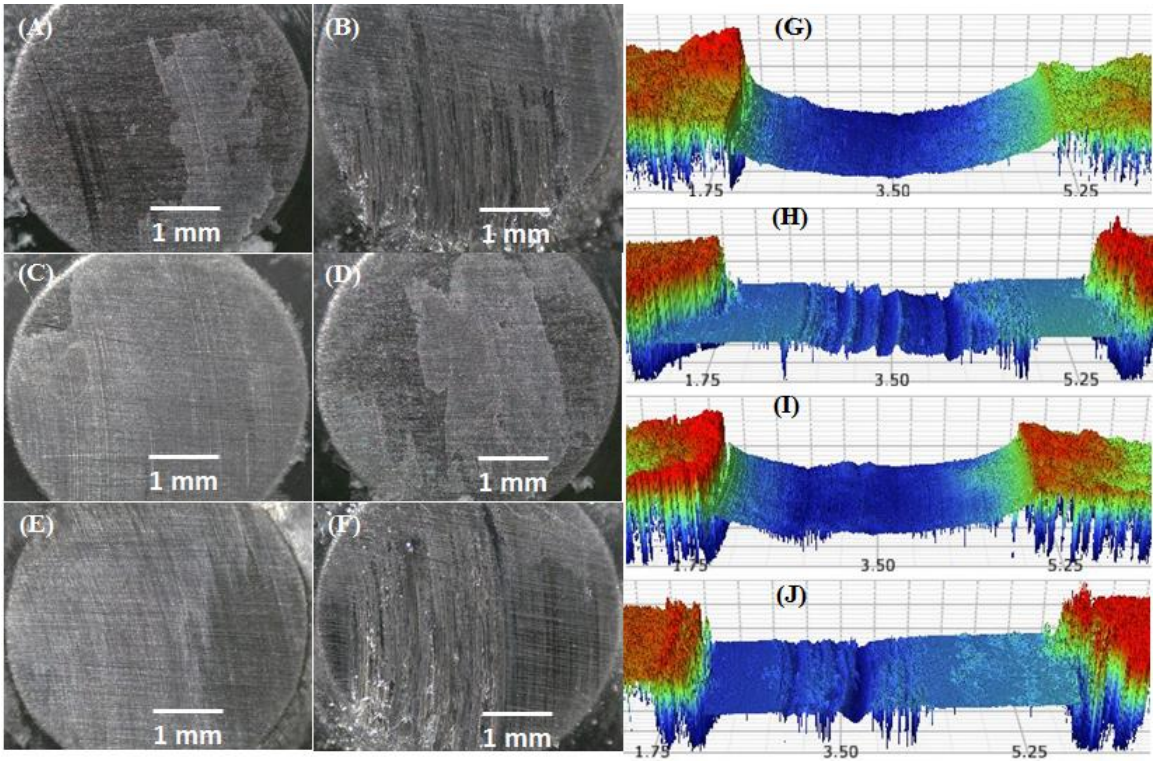

Figure 6.6: Optical microscope images of counterface after wear test of pure UHMWPE at (A) 25 ^{o}C, (B) 75 ^{o}C and UHMWPE/1wt. % GNPs (C) 25 ^{o}C, (D) 75 ^{o}C, (E) 115 ^{o}C, (F) 125 ^{o}C and 3D profilometric images of pure UHMWPE wear track at (G) 25 ^{o}C, (H) 75 ^{o}C and UHMWPE/1wt. % GNPs at (I) 25 ^{o}C, (J) 125 ^{o}C

Figure 6.7 is a set of wear track SEM images of pure and 1 wt. % GNPs reinforced UHMWPE. For each of the mentioned materials, two samples were analyzed; a sample that survived the wear test at a given temperature and a sample that failed the test at 75 ^{o}C in the case of pure UHMWPE and 125 ^{o}C in the case of UHMWPE/ 1 wt. % GNPs. For those samples that survived the test, a wear mechanism that involves surface softening and material flow were observed (Figure 6.7A and C). The inset image of Figure 6.7C shows a clearer picture of the materials softening and the flow. The EDS results confirm the failure of pure UHMWPE at 75 ^{o}C and that of UHMWPE/1wt. % GNPs at 125 ^{o}C showing high peaks of Al.

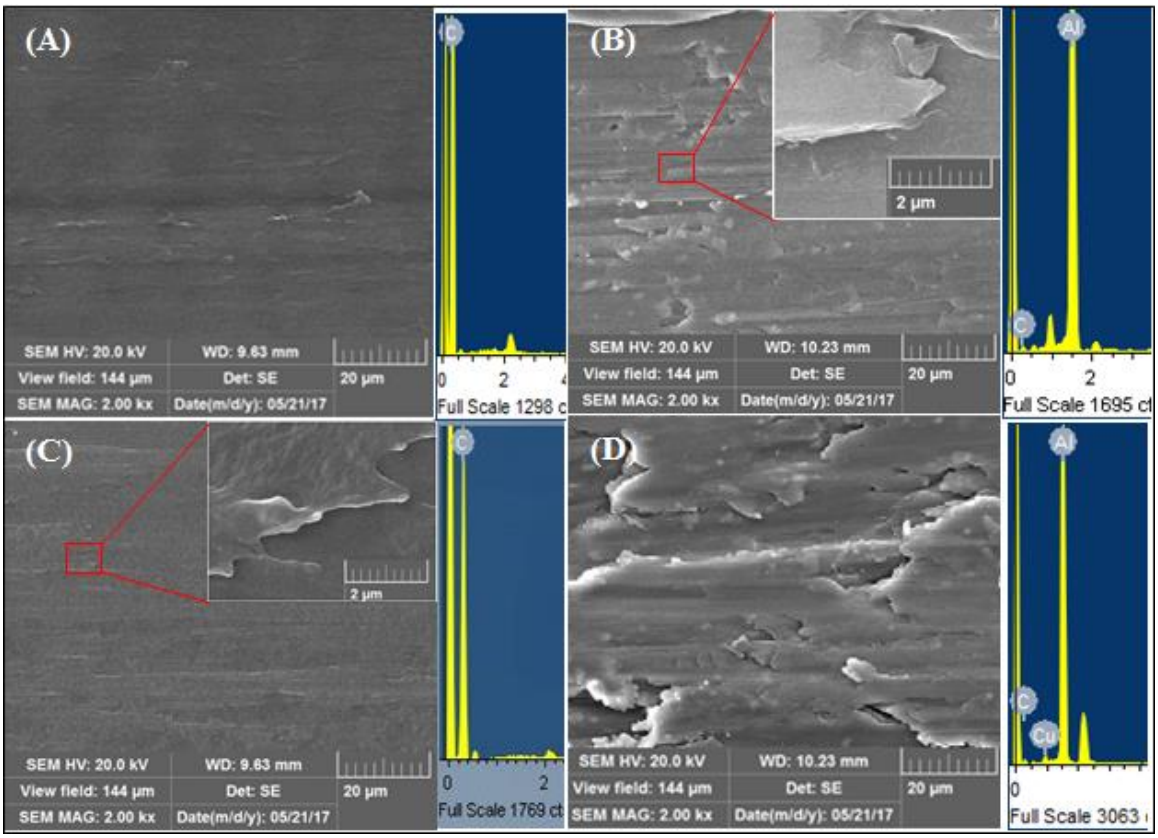

Figure 6.7: Wear tracks SEM images and corresponding EDS of pure UHMWPE tested at (A) 25 ºC (B) 75 ºC and UHMWPE/1 wt. % GNPs tested at (C) 75 ºC and (D) 125 ºC. Each inset is a 20k magnification

6.4 Conclusions

Pure and 1 wt. % GNPs reinforced UHMWPE coatings were successfully synthesized and tested at elevated temperatures up to 125 ^{o}C. The critical operating temperature of the coatings was established.

The COF of UHMWPE/ 1 wt. % GNPs, 0.13, reduced with temperature by about 28 % at 115 ^{o}C. On the other hand, Pure UHMWPE had slightly higher COF than UHMWPE/ 1 wt. % GNPs.

The wear rate of the coatings increased with increase in the test temperature. UHMWPE/ 1 wt. % GNPs showed outstanding performance by passing the wear test at temperatures up to 115 ^{o}C. This was termed the critical temperature for operating the coating. The coating eventually failed at 125 ^{o}C. Pure UHMWPE failed at a much lower temperature, 75 ^{o}C.

A life test was conducted on UHMWPE/1wt. % GNPs at 115 ^{o}C. The coating life decreased with increase in contact pressure, following an exponential relation. A maximum life of 4.1 km sliding distance was attained at 2 MPa.

CHAPTER 7

RESULTS AND DISCUSSION

FRICTION AND WEAR OF COATED THRUST BEARING

UHMWPE/ 1 wt. % GNPs nanocomposite coating had shown improved tribological performance under a pin on disc wear tests compared to pure UHMWPE and UHMWPE reinforced with 0.25 and 2 wt. % GNPs. The coatings sustained severe testing conditions under different normal load, sliding speed and elevated temperature. In order to further explore the capabilities of the coatings for mechanical bearing applications, it was deposited on a thrust bearing made of aluminum alloy. This is to simulate a true practical application of a plain sliding bearing. The sample was tested under both dry and boundary lubrication.

7.1 Dry sliding tribological performance of the coated thrust bearing

Dry ROD tests were carried out on pure and 1 wt. % GNPs reinforced UHMWPE coated aluminum thrust bearing. In the first set of tests, the tribological behavior of UHMWPE/ 1 wt. % GNPs under varied speed at a constant contact pressure of 0.5 MPa was assessed. The maximum sustained speed, 2 m/s, was then used to test both the pure and 1 wt. % GNPs reinforced coatings at varied contact pressure.

7.1.1 The effect of sliding speed on friction and wear of UHMWPE/ 1 wt. % GNPs coating

The typical plot of the dynamic COF is shown in Figure 7.1. The break-in period is quite short at all sliding speeds. The dynamic COF is also steady throughout the sliding distance. Since none of the coatings failed, a sudden change in friction was not observed. Figure 7.1 shows the average COF of the samples. The average COF decreased with increase in sliding speed from 0.42 to 0.33. However, the COF at 1.5 m/s and 2 m/s are almost equal. The decrease in friction at increased sliding speed can be attributed to surface softening due to frictional heating. Less shear force is required to slide over a softer surface, thereby resulting in lower friction.

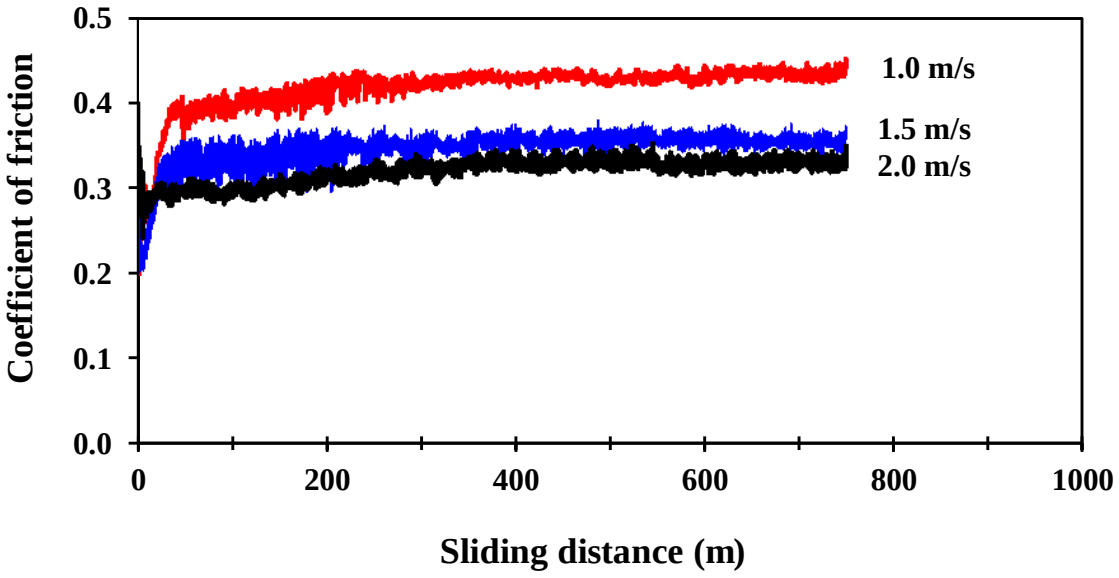

Figure 7.1: Typical COF of UHMWPE/1 wt. % GNPs coating tested at 0.5 MPa and varied sliding speed under dry sliding condition

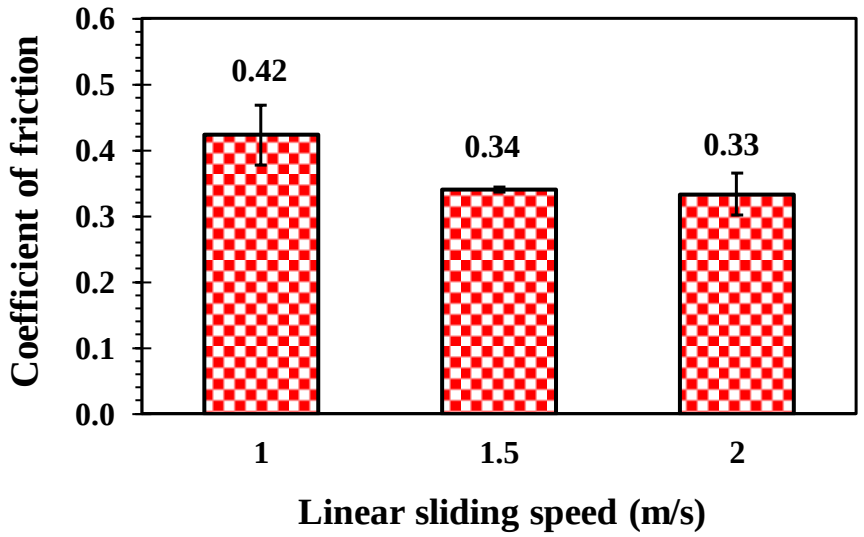

Figure 7.2: Average COF of UHMWPE/1 wt. % GNPs coating tested at 0.5 MPa, varied speed under dry sliding condition

The wear rate of the coatings increased with speed increase from 8.7 to 13.4 µm/km as shown in Figure 7.3. This can be attributed to friction heating and surface softening. However, the coating survived the test at all the sliding speeds.

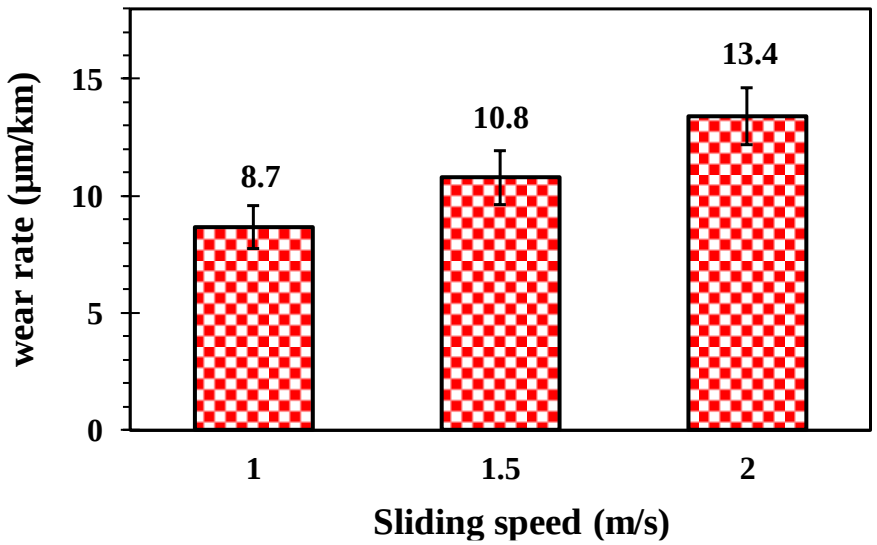

Figure 7.3: Average wear rate of 1 wt. % GNPs reinforced UHMWPE coating tested at 0.5 MPa and varied speed under dry sliding condition

7.1.2 The effect of contact pressure on friction and wear of pure and 1 wt. % GNPs reinforced UHMWPE coatings

The dynamic COF plot of pure and 1 wt. % GNPs reinforced UHMWPE is shown in Figure 7.4. At a maximum of 10 m sliding distance, the dynamic COF has reached a steady-state. The COF curves were also steady throughout the tests except for samples that failed. As the contact pressure was increased for the pure and reinforced coatings, the average COF decreased as shown in Figure 7.5. The decrease was more significant in the case of pure UHMWPE. However, the COF of the GNPs reinforced coating is lower than that of the pure coating by 31 % when tested at a similar condition, at 0.1 MPa. The GNPs is believed to play a friction reduction role by a mechanism of adjacent graphene sheets sliding easily over one another.

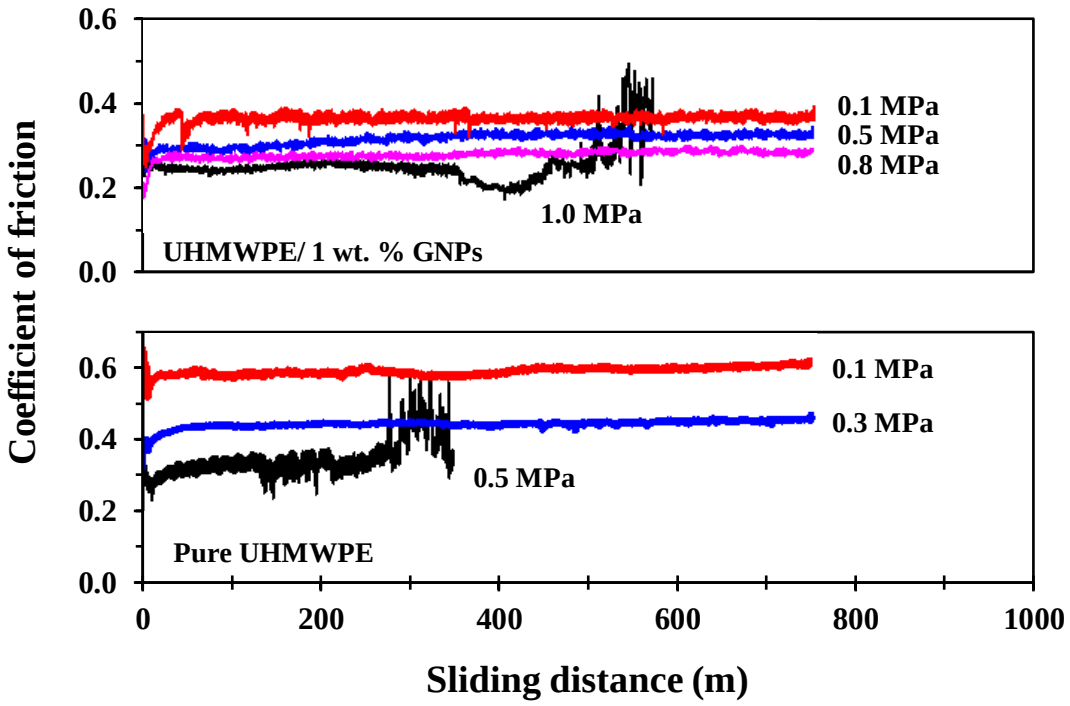

Figure 7.4: Typical COF plot of UHMWPE/1 wt. % GNPs and pure UHMWPE coatings at 2 m/s and varied contact pressure under dry sliding condition

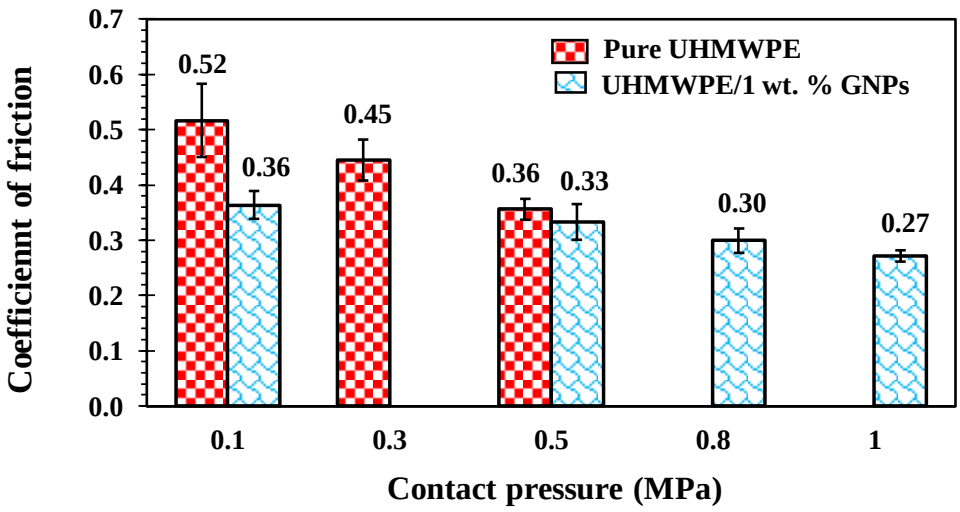

Figure 7.5: Average COF of pure and 1 wt. % GNPs reinforced UHMWPE coatings tested at 2 m/s and varied contact pressure under dry sliding condition

The wear rate of both the pure and reinforced coatings increased as the contact pressure was increased (Figure 7.6). Increase in contact pressure results in the increase in the PV that manifests in the form of heat energy. This energy softens the coatings and increases the wear rate. Also, increased pressure increases the adhesion between the coated bearing and the counterface leading to an increase in adhesion wear. However, the wear rate of the reinforced coating is lower than the pure UHMWPE coating at similar test condition, 0.1 MPa. Also, UHMWPE/ 1 wt. % GNPs survived the test up to 0.8 MPa but failed at 1 MPa. This amounts to a PV limit of 1.6 MPa.m/s. Hence the critical contact pressure for UHMWPE/ 1 wt. % GNPs is 0.8 MPa. As for the Pure UHMWPE, it survived testing at 0.3 MPa but failed at 0.5 MPa resulting in a PV limit of 0.6 MPa.m/s and a critical pressure of 0.3 MPa. Figure 7.7 shows the digital photographs of some selected samples after the wear test. The visual extent of wear can be seen increasing with contact pressure increase. Also, Figure 7.7C and F show pure and 1 wt. % GNPs reinforced UHMWPE that failed at

0.5 and 1 MPa respectively. The aluminum substrates can be seen shining since the polymer coatings have been totally removed.

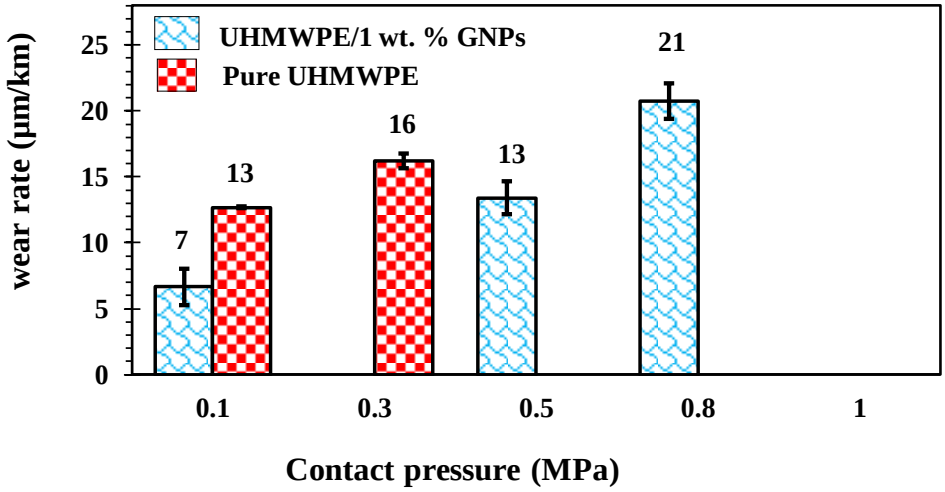

Figure 7.6: Average wear rate of pure and 1 wt. % GNPs reinforced UHMWPE coatings tested at 2 m/s and varied contact pressure under dry sliding condition

Figure 7.7: Pictures of coated thrust bearing after wear test at 2 m/s and varied contact pressure under dry sliding condition for pure UHMWPE coating at (A) 0.1 MPa, (B) 0.3 MPa., (C) 0.5 MPa and UHMWPE/ 1 wt. % GNPs coating at (D) 0.1 MPa, (E) 0.8 MPa and (E) 1 MPa

The SEM images of the pure and 1 wt. GNPs reinforced coatings before and after wear tests are shown in Figure 7.8. The surfaces of both coatings before wear test showed the typical orange-peel structure. Pinholes are minimal. This is an indication that the electrostatic coating method can deposit high-quality coatings. Also, UHMWPE alone or GNPs reinforced UHMWPE are suitable powders for this technique. The surface profile consists of ridges and valleys with a roughness (Ra) value of 2.61 ± 0.11 μm as determined by the optical profilometer. However, after the wear test, the surface became smoothened as shown in Figure 7.8B and D. Marks of material pull out signifying wear by adhesion can be seen on the wear track surfaces. This pull-out is more pronounced for the pure UHMWPE hence it has higher wear rate. Also, there is still the sign of the original surface profile of the reinforced coatings indicating that the wear magnitude is lesser as compared to the pure polymer coating. The SEM of the wear track indicates that the wear mechanism is mild adhesive wear. When contact pressure and sliding speed were increased, the samples were subjected to more severe testing condition (higher PV). The outcome of this is visible in the SEM image, Figure 7.9. The higher the PV, the higher the material pull out, hence the higher the adhesive wear rate.

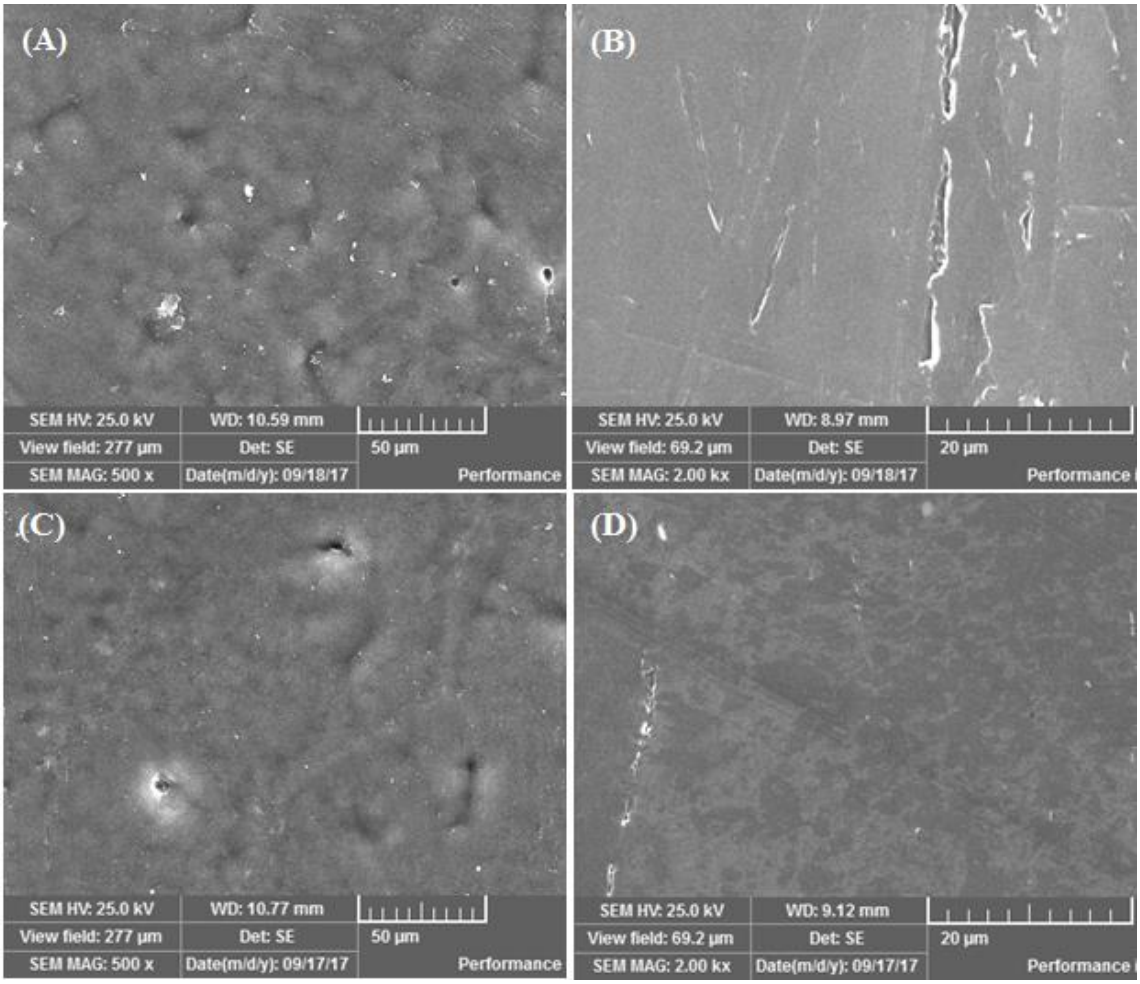

Figure 7.8: SEM images of pure UHMWPE coating (A) before wear test (B) after dry wear test at 0.1 MPa, 2 m/s, and UHMWPE/1 wt. % GNPs coating (C) before and after dry wear test at (D) 0.1 MPa, 2 m/s

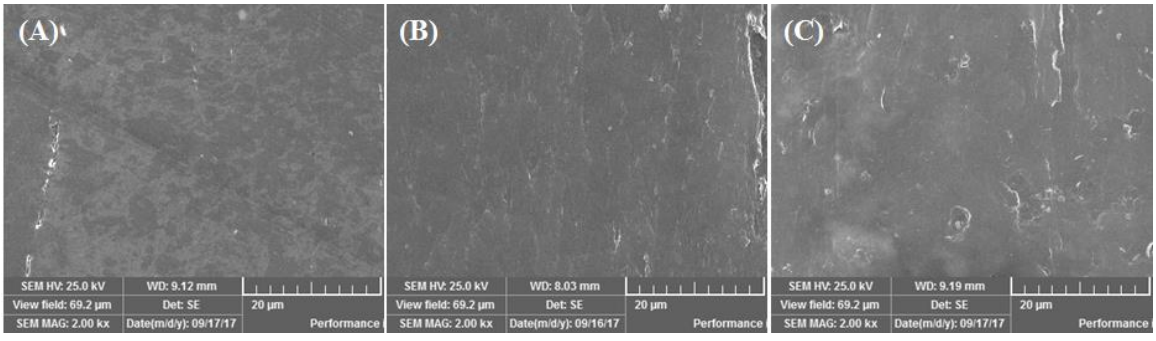

Figure 7.9: SEM images of UHMWPE/1 wt. % GNPs coating wear track at (A) 0.1 MPa, 2 m/s, 0.2 MPa.m/s, (B) 0.5 MPa, 1 m/s 0.5 MPa.m/s and (C) 0.5 MPa, 2 m/s, 1 MPa.m/s under dry sliding condition

7.2 Boundary lubrication tribological performance of the coated thrust bearing

7.2.1 The effect of sliding speed and contact pressure on friction

Figure 7.10, shows the typical plots of the dynamic COF of the samples tested at three different linear sliding speeds using base oil lubricant SN 150. A steady friction response was attained at about 100 m into the test. This implies that the break-in in all cases is about or less than 10 % of the total sliding distance. The samples have a quite stable dynamic COF but with a progressive decrease as the sliding distance increases. The initial high COF is a typical characteristic of boundary lubrication. As the sliding progressed, contact heat due to friction increased. This heats up the lubricant and reduced its viscosity with respect to sliding distance, thus reducing friction.

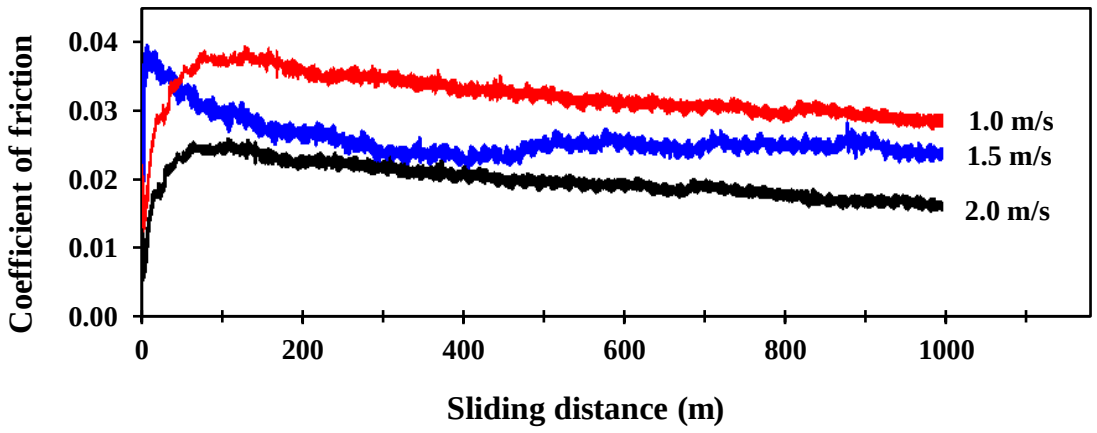

Figure 7.10: Typical COF plot of UHMWPE/1 wt. % GNPs coating tested at 1 MPa and varied sliding speed under base oil lubrication

As shown in Figure 7.11, the average COF of the samples decreased linearly with increase in the sliding speed. This can be attributed to the surface softening tendency at higher speed, which reduced tangential resistance. Also, at higher sliding speed, the contact temperature is higher resulting in lower lubricant viscosity, thereby lowering friction. The COF of the samples as shown in the figure has relatively less deviation an indication that the samples preparation and wear tests were well controlled. The COF of all the samples ranged from 0.034 to 0.022 and about ten times less than similar coatings tested in a dry wear condition as reported in the previous section of this chapter. This is due to the lubricating effect of the applied thin film of oil. The properties of the coating surface also contribute to the general low friction since boundary lubrication does not create a total contact pair separation. Most of the previous investigations on UHMWPE composites as bearings were done under water lubrication [175–177]. In one of the references, the COF of polyamide reinforced UHMWPE composite tested at 2.5 and 1 MPa and 0.5 m/s ranged from 0.07 to 0.055. The lubrication regime was termed elastohydrodynamic. The COF in the current research, simulating boundary lubrication, could have been lesser because base oil, such as SN 150 provides better lubrication than water.

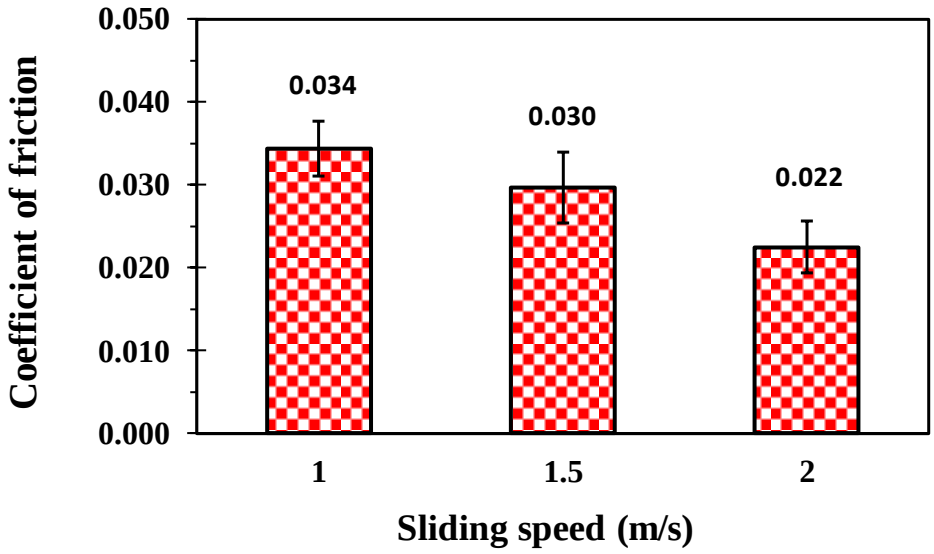

Figure 7.11: Average COF of UHMWPE/1 wt. % GNPs coating tested at 1 MPa and varied sliding speed under base oil lubrication

Figure 7.12 shows the dynamic COF plot of pure and 1 wt. % GNPs reinforced UHMWPE coatings at varied contact pressure. UHMWPE/ 1 wt. % GNPs, having performed best in the previous study, is the sample of focus for boundary lubrication tests. However, pure UHMWPE was also tested with similar test parameters to serve as a reference. The run-in period is quite short, a maximum of 120 m, for all the samples at all contact pressure. The friction plot is also steady till the end of the test at a distance of 1000 m except for samples that failed earlier than 1000 m. While UHMWPE/1 wt. % GNPs could survive the test up to 2.7 MPa, pure UHMWPE failed at 1 MPa. A sudden rise in COF beyond 0.1 after a short sliding distance indicated the failure of the coatings.

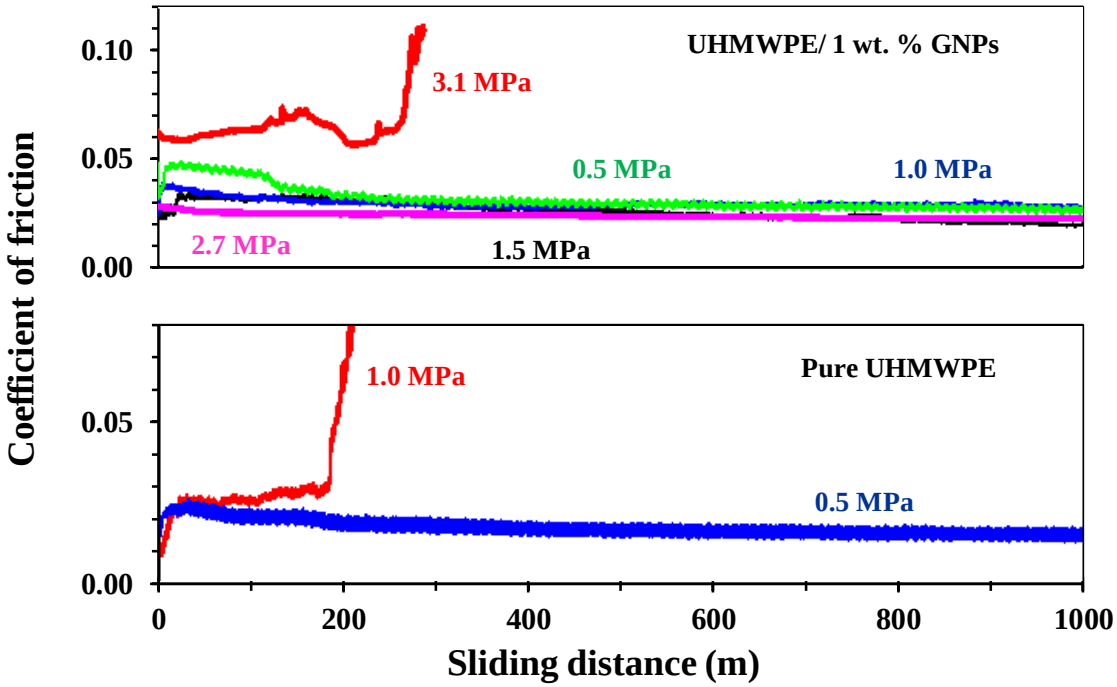

Figure 7.12: Typical COF plot of UHMWPE/1 wt. % GNPs and pure UHMWPE coatings tested at 1.5 m/s and varied contact pressure under base oil lubrication

For each sample, the average steady COF was determined from the COF plots of three trials and plotted in Figure 7.13. The chart shows that, for both the pure and reinforced UHMWPE, there was a slight reduction in the dynamic COF of the coatings as the pressure was increased. There was a significant rise in COF when contact pressure was increased to 3.1 MPa for the reinforced coating. It is understood that at higher pressure, the lubricant is squeezed out of the contact, thereby limiting the effect of lubrication. Also, the asperities are more pressed against the counterface leading to their flatness and higher adhesion that results in higher COF.

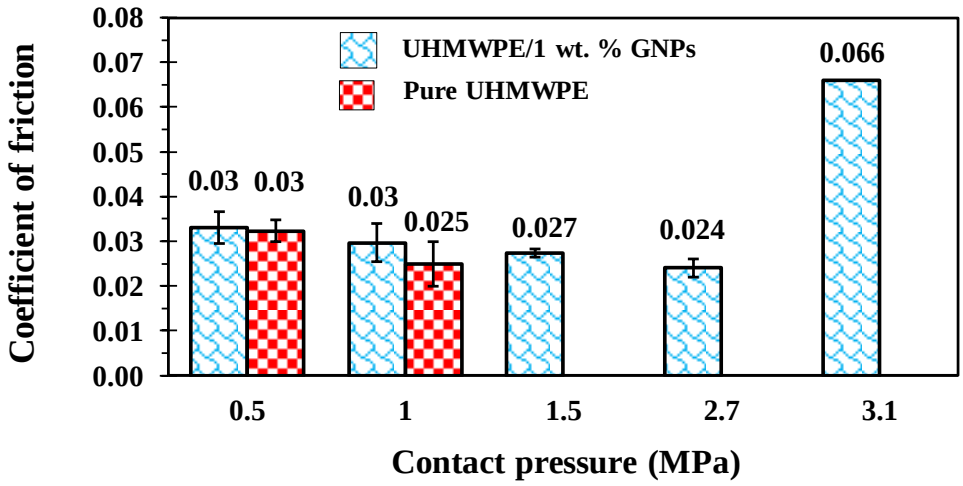

Figure 7.13: Average COF of pure and 1 wt. % GNPs reinforced UHMWPE coatings tested at 1.5 m/s and varied contact pressure under base oil lubrication

7.2.2 The effect of sliding speed and contact pressure on wear

In order to study the effect of sliding speed on the bearing sample coated with UHMWPE/ 1 wt. % GNPs, wear tests were conducted at 1, 1.5 and 2 m/s, each at three trials. Prior to each test, the mass of the sample was measured using a high precision weight balance with a precision of 10^{-5} g. The mass was also measured after the test to obtain the weight loss. The loss in mass was then used to obtain the wear rate. At an initial speed, 1 m/s, the wear rate recorded was 4.1 μm/km, a relatively low value for a sliding distance of 1 km. When the speed was increased to 1.5 m/s the wear rate decreased as shown in Figure 7.14. This might have occurred due to the significant peeling effect occurring at the lower speed as shown in Figure 7.15. However, when the speed was increased to 2 m/s, the wear rate increased. An increase in speed implies an increase in PV, which manifest itself as an increase in contact heating, thereby increasing wear rate by surface softening. However, it should be noted that all the sample sustained the test at all the sliding speeds. It has been observed that two contributing wear mechanisms determine material removal during the

wear test. These include peeling effect and adhesive wear (Figure 7.15). The peeling effect reduced with speed increase justifying why the wear rate at 1.5 m/s is less than at 1 m/s. However, at higher speed, there was a greater amount of adhesive wear resulting in an increase in the wear rate at 2 m/s.

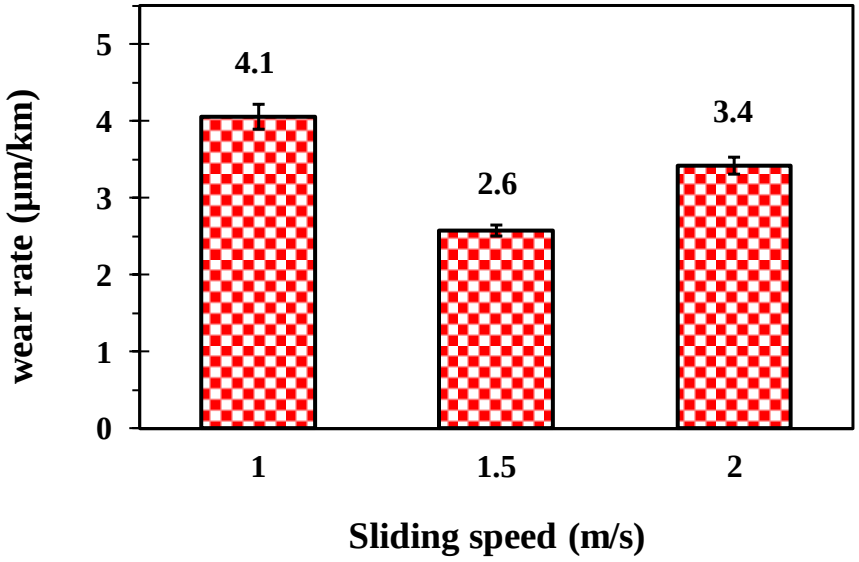

Figure 7.14: Average wear rate of UHMWPE/1 wt. % GNPs coating tested at 1 MPa and varied sliding speed under base oil lubrication

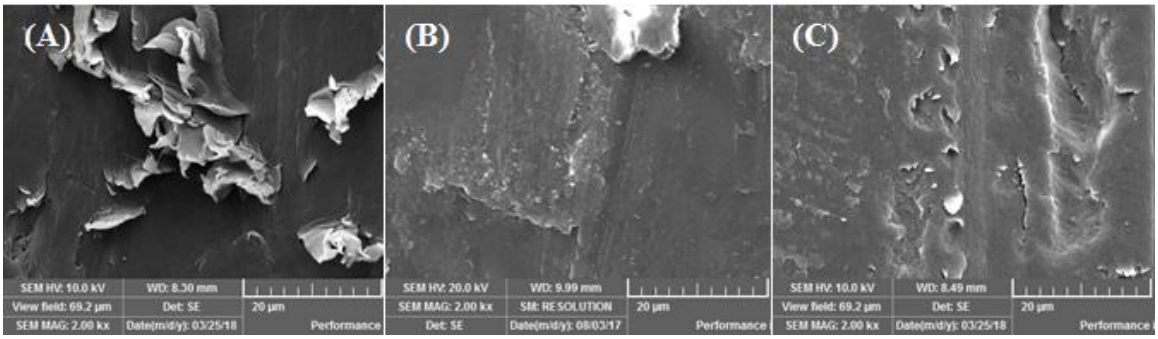

Figure 7.15: SEM images of wear track of UHMWPE/1 wt. % GNPs coating tested at (A) 1 m/s, (B) 1.5 m/s and (C) 2 m/s at constant pressure of 1 MPa under base oil lubrication

Contact pressure effect test was conducted on both UHMWPE/1 wt. % GNPs coating and the pure UHMWPE coating. Increase in pressure led to an increase in wear rate for both samples as shown in Figure 7.16A. This is expected as the increase in normal load results in more penetration of the counterface asperities in the coating causing a higher magnitude of plowing and plastic deformation. Also, an increase in pressure leads to the increase in the PV, which can cause surface softening allowing counterface asperities to plow through easily. UHMWPE/1 wt. % GNPs sample survived the test at contact pressures up to 2.7 MPa but failed at 3.1 MPa. The un-reinforced coating rather failed at 1 MPa (Figure 7.16B). The coating was totally removed and the aluminum substrate became totally visible. The increase in wear resistance of the reinforced sample over the pure UHMWPE can be attributed to the positive impact of the GNPs reinforcement, which has excellent mechanical, thermal and chemical properties [10,11].

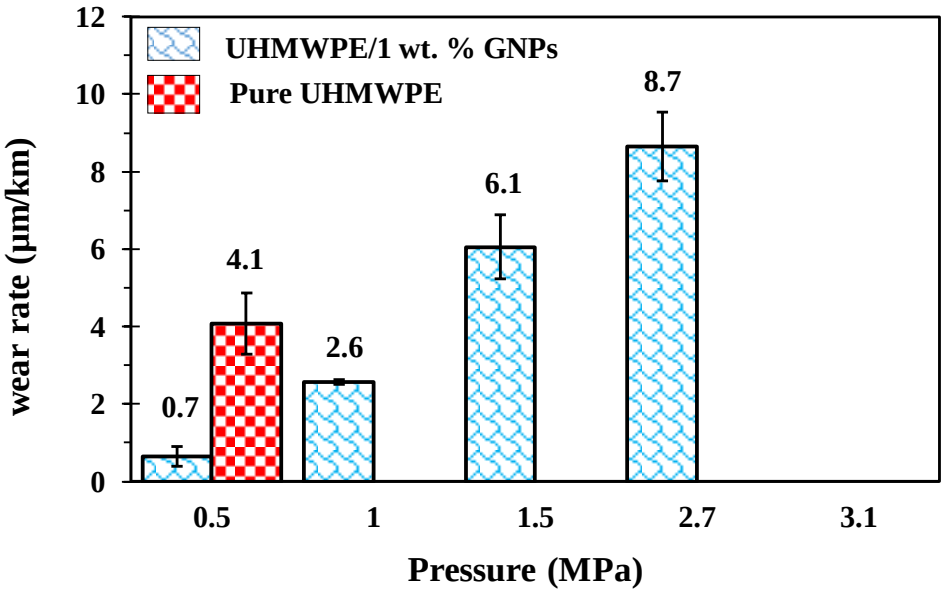

Figure 7.16: Average wear rate of UHMWPE/1 wt. % GNPs and pure UHMWPE coatings tested at 1.5 m/s and varied contact pressure under base oil lubrication

The asperities of the counterface, being much harder, plow through the asperities of the coating as shown in Figure 7.17. This is expected since the kind of lubrication employed here is boundary lubrication. A thin film of oil is not sufficient to create a total prevention of the counterface asperities from having contact with sample's asperities. Unlike in the dry wear test reported in the first section of this chapter, sample surface smoothening effect is minimal. The SEM images (Figure 7.17) show that a large proportion of the surface profile/features of the coating remains visible. The wear mechanism can be said to be a mixture of mild abrasive and mild adhesive wear. However, for the pure UHMWPE coating, which failed at 1 MPa, the wear mechanism is severe adhesive due to coating delamination. The SEM images confirm the relative wear rate between the pure and 1 wt. % GNPs reinforced UHMWPE coating that was reported earlier. For example, at 0.5 MPa, the original surface feature of pure UHMWPE is more altered than that of UHMWPE/ 1 wt. % GNPs (Figure 7.17A vs. C) and the plowing lines on the pure UHMWPE is more. Also comparing UHMWPE/ 1 wt. % GNPs at different loads (0.5 and 1.0 MPa), all the asperities have been removed from the sample tested at 1.0 MPa. It also has a smoother surface and higher amount of plastic deformation as visible in the SEM image (Figure 7.17C vs. D). Visual observation of the disc counterface after the wear tests indicates that there was no transfer of polymer film on to it. Figure 7.18 shows the surface profile of the counterface before and after six runs of wear tests. After each wear test, no significant wear or scratch was made on the counterface by the samples. This is because the coatings being polymer based are mild on the counterface coupled with the oil lubrication effect. Once the scratches are getting significant, the counterface is re-grinded to create a similar testing condition with respect to surface profile.

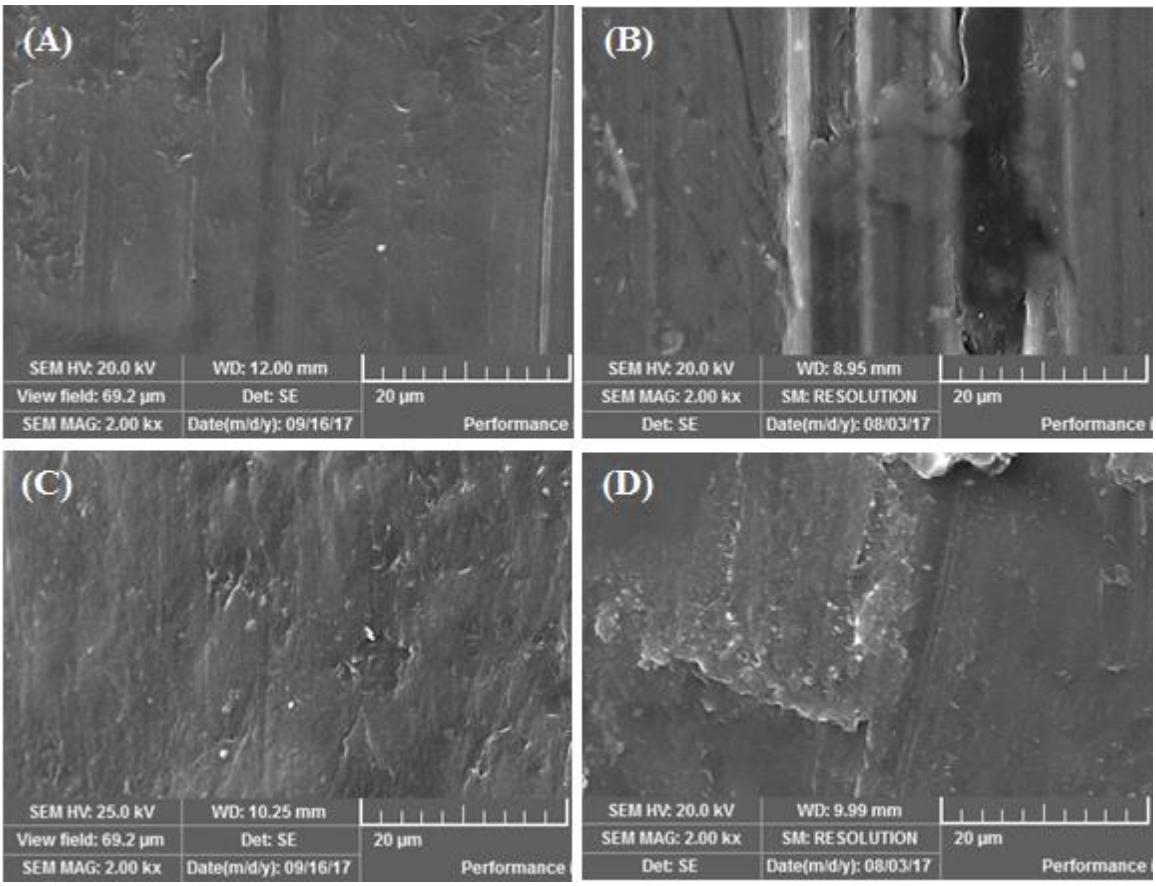

Figure 7.17: SEM images of wear track of pure UHMWPE coating at (A) 0.5 MPa, (B) 1.0 MPa and UHMWPE/1 wt. % GNPs coating (C) 0.5 MPa, (D) 1.0 MPa at constant speed of 1.5 m/s under base oil lubrication

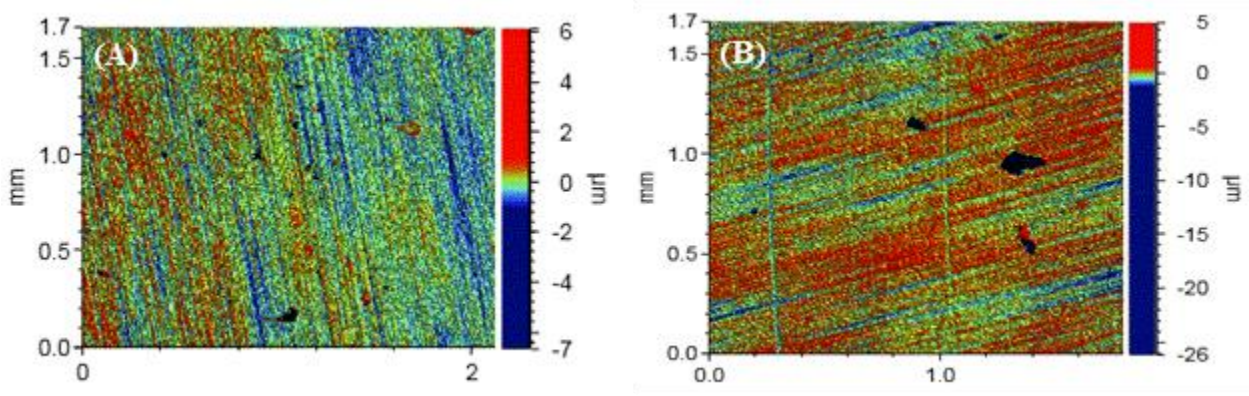

Figure 7.18: The counterface surface profile by optical profilometry (A) before (Ra = 0.30 µm) and (B) after 6 wear tests (Ra = 0.31) under base oil lubrication

7.2.3 Boundary lubrication with various types of oil

In order to study the compatibility of the current bearing sample with other types of lubricating oil, wear tests wear carried out under synthetic oil, vegetable oil, and base oil lubrication. The basic properties of the oils are shown in Table 7.1.

Table 7.1: Properties of lubricating oils [35,178–180]

Property	SN 150 base oil	Mobil1 0W-40, fully synthetic oil	Sunflower vegetable oil
Dynamic viscosity at 40 ^{o}C (mPa.s)	24 - 30	64	35
Dynamic viscosity at 100 ^{o}C (mPa.s)	4.5 – 4.7	11.5	8.2
Flash point (^{o}C)	200	230	316
Density (kg/m^{3})	868	850	917

The tests were conducted under the most severe combination of contact pressure and linear sliding speed of 1.5 MPa and 1.5 m/s respectively out of those used in the previous base oil lubrication wear tests. As shown in Figure 7.19, the run-in occurs within very short sliding distance and the dynamic friction reduce gradually with sliding distance.

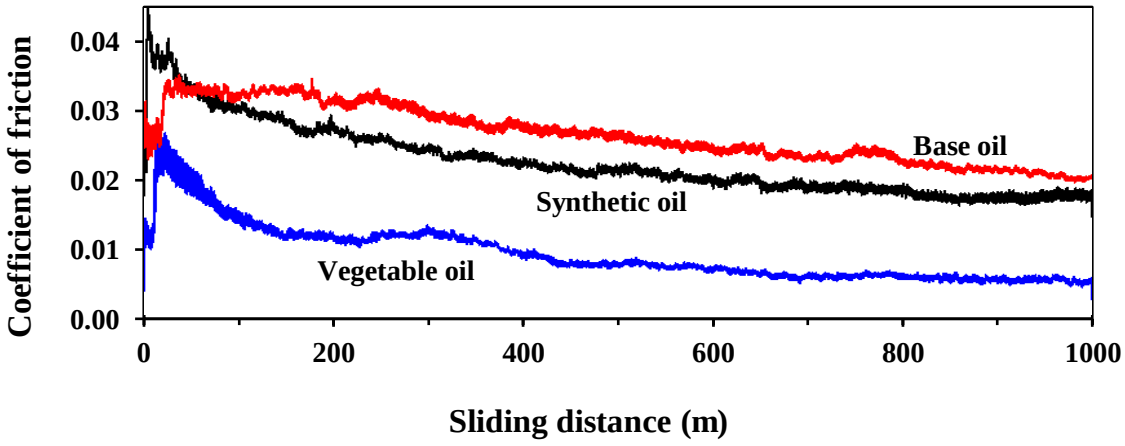

Figure 7.19: Typical COF plot of UHMWPE/1 wt. % GNPs coating tested under three different lubricating oils at 1.5 m/s and 1.5 MPa

The use of synthetic oil and vegetable oil resulted in a lower COF as compared to base oil. (Figure 7.20). Based on the Stribeck curve, an increase in Sommerfeld number ($\eta V/P$) results in a decrease in COF in the boundary lubrication regime [22]. In the boundary lubrication range, increase in viscosity will lead to decrease in COF. Hence tests with synthetic and vegetable oil are expected to produce lower COF than base oil since they have higher viscosity. However, the vegetable oil produced an extremely lower COF than the synthetic oil despite having lower viscosity. This might have resulted due to a better adhesion of the vegetable oil to contact surfaces, thereby providing a better lubrication. This is an indication that, vegetable oil, which is most environmentally friendly as compared to the other oils, is promising for the replacement of oils that have a harmful environmental effect. The excess low friction gives an important advantage of global interest. Lower energy is required during operation of low friction engine, which minimizes fuel consumption and emission. Also, lower friction can reduce wear rate significantly.

The wear rate also follows a similar trend as the COF chart. Slightly lower wear rate was recorded when synthetic oil was used compared to base oil. Also, the wear rate of the sample lubricated by vegetable oil is slightly lower than the one of synthetic oil (Figure 7.20).

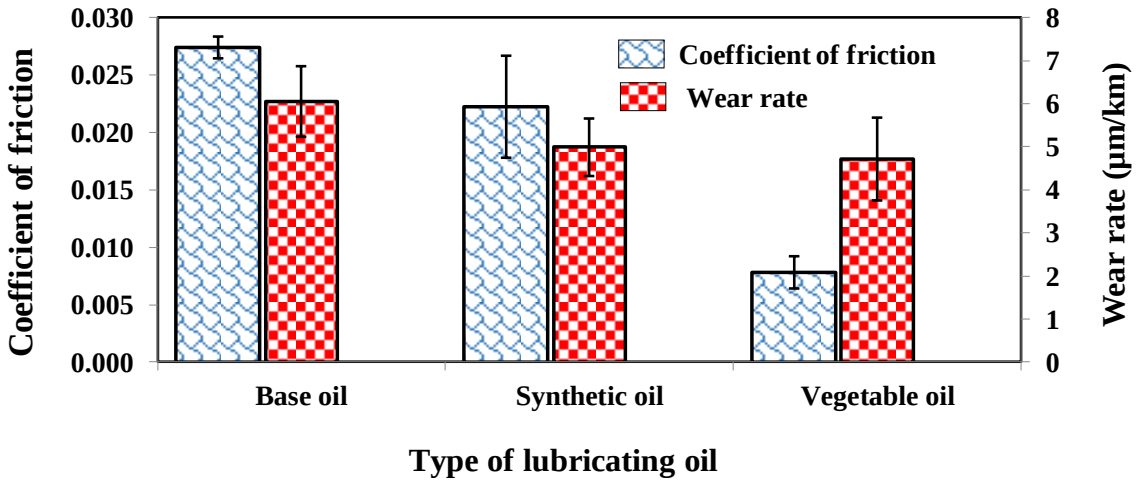

Figure 7.20: Average COF and wear rate of 1 wt. % GNPs reinforced UHMWPE coating tested at 1.5 m/s and 1.5 MPa under three different liquid lubricants

7.3 Conclusion

Pure and 1 wt. % GNPs reinforced UHMWPE nanocomposite coatings were successfully deposited on the aluminum thrust bearing. The samples were tested under dry and boundary lubrication condition using a ring on disc contact type. The effects of contact pressure and sliding speed on tribological performance were investigated.

In the dry wear test, COF decreased from 0.42 to 0.33 with an increase in sliding speed (1, 1.5 and 2 m/s). The wear rate increased from 8.7 to 13.4 µm/km. When contact pressure was varied (0.1, 0.5, 0.8 and 1 MPa), the COF of UHMWPE/ 1 wt. % GNPs coating reduced from 0.36 to 0.27. Pure UHMWPE had higher COF than UHMWPE/ 1 wt. %

GNPs at a similar testing condition. The wear rate increased with contact pressure for both samples, but UHMWPE/ 1 wt. % GNPs coating sustained a higher maximum contact pressure of 0.8 MPa as compared to pure UHMWPE coating that could only sustain 0.3 MPa.

When boundary lubrication tests were conducted, it was found that the UHMWPE/ 1 wt. % GNPs coating performed better in all the conditions it was subjected to as compared to the pure UHMWPE coating. The dynamic COF was low and decreased with increase in sliding speed and contact load. UHMWPE/ 1 wt. % GNPs coating had an abrasive wear mode and a low wear rate at all the test conditions. Investigating the effect of speed on wear rate showed an initial drop in wear rate, then it increased afterward due to change in wear mechanism. However, the wear rate increased with contact pressure consistently. The UHMWPE/ 1 wt. % GNPs coating sustained a maximum contact pressure of 2.7 MPa as compared to the pure UHMWPE coating that sustained only 0.5 MPa.

The investigation of the coating under different types of lubricating oils revealed that the coating is compatible with a wide range of oils such as base oil, synthetic oil, and vegetable oil. The COF and wear rate of the sample when synthetic oil was used were lower than those of base oil. The use of vegetable oil resulted in the lowest friction (~ 0.008) and wear rate (4.7 μm/km).

CHAPTER 8

CONCLUSIONS AND FUTURE RECOMMENDATIONS

8.1 Summary of results

The main objective of this research was to develop GNPs reinforced UHMWPE coatings to reduce the excessive friction and wear during the use of mechanical bearings in dry and boundary lubrication regime. In order to realize this objective, a feasibility study was initially carried out by synthesizing bulk UHMWPE/GNPs nanocomposites. The purpose of the study was to investigate whether GNPs can improve the friction and wear properties of UHMWPE. Nanocomposites of UHMWPE with GNPs reinforcement ranging from 0 to 0.5 wt. % were synthesized by ultra-sonication and hot pressing. Dry friction and wear tests were carried out to find out the optimum composition. The sample with the optimum composition was further tested at varied contact pressure to see the effect of contact pressure and determine the load-bearing capacity of the material. Effect of speed and PV limit were also investigated. From the results the following observations were made:

a. The fabrication process resulted in a stable phase and fully densified nanocomposite with relative density ranging from 99.2 to 99.5 %. The addition of GNPs did not result in a significant change in the hardness of the UHMWPE nanocomposite.
b. The addition of GNPs led to an increase in dynamic COF of the nanocomposite from 0.15 to 0.24.

c. In terms of wear resistance, the performance of UHMWPE/0.25 wt. % GNPs was optimal. It reduced wear rate from 4.5 μm/km to 3.1 μm/km (31 % reduction) as compared to pure UHMWPE.
d. Increase in the contact pressure (8, 12, 16 and 20 MPa) did not cause a significant change in the dynamic COF.
e. The wear rate increased linearly with contact pressure increase. The nanocomposite sustained the maximum contact pressure of 20 MPa (PV = 20*0.1= 2 MPa.m/s) without a severe wear rate.
f. When sliding speed was varied at a constant pressure of 12 MPa, there was a gradual increase in wear rate till a sliding speed of 0.5 m/s. Once the sliding speed was increased to 0.75 m/s a severe increase in wear rate by 757 % was observed. Hence the PV limit for this nanocomposite is 6 MPa.m/s.

After establishing from the first part (friction and wear assessment of bulk nanocomposite) of this research that GNPs has the potential of improving the wear resistance of UHMWPE, the nanocomposite material was developed as coatings on aluminum substrate disc samples. UHMWPE nanocomposites with GNPs reinforcement ranging from 0 to 2 wt. % were prepared and deposited on aluminum substrates using electrostatic spray gun. Friction and wear tests were then conducted on the coatings. The following observations were made.

a. The addition of GNPs to the UHMWPE coatings resulted in an increase in the microhardness from 10.0 to 13.0 HV (30 %).
b. The addition of GNPs, ranging from 0.25 to 2 wt. % did not cause a significant change in the dynamic COF of the coatings.

c. In terms of wear resistance, the performance of UHMWPE/1 wt. % GNPs was optimal. It reduced wear rate from 37 to 18.2 μm/km, (51 % reduction) as compared to pure UHMWPE.
d. Increase in the contact pressure (2, 4, 6 and 8 MPa) resulted in a progressive decrease in the dynamic COF of UHMWPE/1 wt. % GNPs from 0.32 to 0.20 (38 % reduction).
e. The wear rate increased linearly from 18.2 to 56.1 μm/km with contact pressure up to 6 MPa. The coating did not fail until contact pressure was increased to 8 MPa.
f. Friction and wear properties were also studied as a function of sliding speed (0.1, 0.5 and 1 m/s). Dynamic COF decreased from 0.27 to 0.14 (48 %). A durable thin transfer film that enhanced friction reduction was formed. The higher the speed, the more the surface of the counterface covered.
g. When sliding speed was varied at a constant pressure, 4 MPa, wear rate increased from 40.6 to 59 μm/km. However, the coating did not fail. The maximum PV sustained was 4 MPa.m/s.

One of the objectives of this research was to assess the friction property and wear resistance of the developed coating at elevated temperature. Pure and 1 wt. % reinforced UHMWPE were investigated at elevated temperatures ranging from 75 to 125 ^{o}C. The following observations were made:

a. The increase in temperature resulted in the decrease in COF from 0.13 to 0.09 (28 %) due to surface softening at increased temperature.
b. The wear rate increased from 52 μm/km at room temperature to 95 μm/km at 115 ^{o}C.

c. While pure UHMWPE failed at 75 ^{o}C, UHMWPE/ 1 wt. % GNPs showed outstanding performance by passing the wear test up to 115 ^{o}C. It confirms that the softening temperature of UHMWPE was improved above 125 ^{o}C.
d. When test temperature was increased to 125 ^{o}C, the UHMWPE/ 1 wt. % GNPs coating failed. Hence the critical temperature of the coating is 115 ^{o}C. This temperature is slightly higher than the required bearing temperature in some automobiles. Therefore, there is a potential in deploying the current coating as a commercial bearing coating.

Since this research focused on developing polymer coating with improved friction and wear resistance for mechanical bearing application, the sample (UHMWPE/1 wt. % GNPs) that performed best in the pin on disc wear tests was synthesized on a thrust bearing. UHMWPE/1 wt. % GNPs and pure UHMWPE coated thrust bearing samples were tested both under dry and boundary lubrication condition at varied speed and varied load.

The following conclusions were arrived at for the dry sliding wear test:

a. The COF of UHMWPE/1 wt. % GNPs decreased from 0.42 to 0.33 with an increase in sliding speed from 1 to 2 m/s while the wear rate increased from 8.7 to 13.4 µm/km.
b. When contact pressure was varied from 0.1 to 1 MPa, the COF of UHMWPE/ 1 wt. % GNPs coating reduced from 0.36 to 0.27. Pure UHMWPE had higher COF and wear rate than UHMWPE/ 1 wt. % GNPs. Generally, the wear rate increased with contact pressure for both sample, but pure UHMWPE failed at 0.5 MPa while UHMWPE/ 1 wt. % GNPs sustained 0.8 MPa but failed at 1 MPa.

The following conclusions were arrived at for the boundary lubrication wear test in base oil:

a. The COF of UHMWPE/ 1 wt. % GNPs coating reduced from 0.034 to 0.022 when speed was varied (1, 1.5 and 2 m/s). The wear rate initially decreased from 4.1 to 2.6 μm/km and then increased from 2.6 to 3.4 μm/km.
b. It was found that despite the use of limited lubrication, the UHMWPE/ 1 wt. % GNPs coating performed well in all the conditions it was subjected to as compared to pure UHMWPE. The dynamic COF was generally low and decreased with increase in contact pressure. The COF of UHMWPE/ 1 wt. % GNPs coating reduced from 0.03 to 0.024 when contact pressure was varied (0.5, 1, 1.5 and 2.7 MPa). Further testing at 3.1 MPa resulted in a higher friction, 0.066. UHMWPE/ 1 wt. % GNPs had more wear resistance than the pure UHMWPE. Generally, wear rate increased with contact pressure for both samples, but pure UHMWPE failed at 1 MPa while UHMWPE/ 1 wt. % GNPs did not fail even at 2.7 MPa but it failed at 3.1 MPa.

The following conclusions were arrived at when UHMWPE/ 1 wt. % GNPs coating was subjected to wear test at 1.5 m/s and 1.5 MPa in different lubricants.

a. The COF and wear rate of the sample when synthetic oil was used were lower than those of base oil. The use of vegetable oil resulted in the lowest friction (0.008) and wear rate (4.7 μm/km).

8.2 Conclusions

Polymer nanocomposite materials were successfully synthesized as both bulk material and coatings. They were subjected to wear tests at dry, lubricated, room and elevated temperatures using the POD and ROD contact types. The nanocomposite was also successfully deposited on aluminum alloy thrust bearing. The following conclusions were arrived at from the results:

- The addition of GNPs to UHMWPE led to the improvement in mechanical and tribological properties of the nanocomposites. It improved the wear resistance of both the bulk and nanocomposite coatings. While 0.25 wt. % GNPs was optimum amount of GNPs for improved tribological properties of the bulk nanocomposite, 1 wt. % GNPs was the optimum for the coating. There was 31 and 51 % reduction in were rate respectively due to GNPs addition. GNPs addition resulted in an increase in the COF of the bulk nanocomposite but slightly reduced friction in the coatings. It improved the softening temperature of UHMWPE/GNPs nanocomposite coating from 80 ^{o}C to a value above 115 ^{o}C.
- The Bulk nanocomposite with the optimum composition of GNPs, UHMWPE/ 0.25 wt. % GNPs had a load-bearing capacity of 86 N (20 MPa) and a PV limit of 6 MPa.m/s while the load-bearing capacity of the coating was 48 N (6 MPa) and its PV limit was 4 MPa.m/s under POD tests
- The coatings capacity depends on testing configuration. With POD, load-bearing capacity was 4 MPa but with ROD capacity was 0.8 MPa.
- The coating performed well in presence of base oil, which gives room for eliminating the use of synthetic oil having a negative environmental impact. The

coating is compatible with wide range of lubricant from base to synthetic and to vegetable.

- Generally, COF decreased with increase in contact pressure and sliding speed. The COF of UHMWPE/1 wt. % GNPs coating was lower than that of pure UHMWPE in the dry test condition. However, the reverse was the case in the lubricated test condition.
- The current coating is promising for automobile weight reduction by creating means for replacement of steel shafts and bearings with aluminum, thereby reducing weight and emission of harmful gases. The success in the deposition of the coating on aluminum thrust bearing is a great advancement. Hence there is a potential in deploying this coating as a commercial bearing coating.

8.3 Future recommendations

The developed UHMWPE/GNPs nanocomposite coating has shown excellent improvement in tribological properties. There is now a potential to put the material to use as mechanical bearing commercially due to the improved dry, boundary lubricated and elevated temperature friction and wear performance. However, more studies have to be conducted in order to upscale the coating for commercial application. Also, it will be of great addition if the elevated temperature performance can be improved further to create a higher margin between the operating temperature 110 ^{o}C and the critical temperature of the coating 115 ^{o}C.

Furthermore, in some cases, GNPs resulted in negative effect by increasing the COF in dry bulk nanocomposite wear test and in lubricated coating wear test. It will be great to explore means of reinforcement that can result in lower friction rather.

The following are therefore recommended for future studies related to this coating.

- Carrying out research and analysis that can enable the upscaling of this coating for commercial deployment.
- Investigate reinforcements that could provide improved friction reduction of UHMWPE in dry wear test condition including hybrid systems.
- Exploring reinforcement that can further improve the working temperature of the coating.

References

[1] http://www.nanomech.com.

[2] Radu C. The Most Common Causes of Bearing Failure and the Importance of Bearing Lubrication. RKB Technical Review 2010.

[3] Reinosa A. Automatic method and apparatus for preventing wear in an internal combustion engine. U.S. Patent 1998; 5,743231.

[4] http://www.freedoniagroup.com.

[5] Samad MA, Sinha SK. Dry sliding and boundary lubrication performance of a UHMWPE/CNTs nanocomposite coating on steel substrates at elevated temperatures. Wear 2011;270:395–402.

[6] Donnet C, Erdemir A. Historical developments and new trends in tribological and solid lubricant coatings. Surf Coatings Technol 2004;180–181:76–84.

[7] An Y, Tai Z, Qi Y, Yan X, Liu B, Xue Q, et al. Friction and wear properties of graphene oxide/ultrahigh-molecular-weight polyethylene composites under the lubrication of deionized water and normal saline solution. J Appl Polym Sci 2014;131.

[8] Bao Y, Zhang T, Gawne DT. Influence of composition and process parameters on the thermal spray deposition of UHMWPE coatings. J Mater Sci 2005;40:77–85.

[9] Rajput AW. An investigation into the production of UHMWPE fibres and coatings for protective apparel. PhD diss. Heriot-Watt University 2013.

[10] Jang BZ, Zhamu A. Processing of nanographene platelets (NGPs) and NGP nanocomposites: a review. J Mater Sci 2008;43:5092–101.

[11] Lahiri D, Dua R, Zhang C, de Socarraz-Novoa I, Bhat A, Ramaswamy S, et al.

Graphene nanoplatelet-induced strengthening of ultrahigh molecular weight polyethylene and biocompatibility in vitro. ACS Appl Mater Interfaces 2012;4:2234–41.

[12] Han J, Ding S, Zheng W, Li W, Li H. Microstructure and anti- wear and corrosion performances of novel UHMWPE/graphene-nanosheet composite coatings deposited by flame spraying. Polym Adv Technol 2013;24:888–94.

[13] Pascual FJ, Quiles L, Castell P, Puértolas JA. Tribological behaviour of functionalized 1-2 layered graphene/UHMWPE composites. Proc. 8th Iberian Conf. IBERTRIB 2015.

[14] Tai Z, Chen Y, An Y, Yan X, Xue Q. Tribological behavior of UHMWPE reinforced with graphene oxide nanosheets. Tribol Lett 2012;46:55–63.

[15] Chen Y, Qi Y, Tai Z, Yan X, Zhu F, Xue Q. Preparation, mechanical properties and biocompatibility of graphene oxide/ultrahigh molecular weight polyethylene composites. Eur Polym J 2012;48:1026–33.

[16] Bakshi SR, Balani K, Laha T, Tercero J, Agarwal A. The nanomechanical and nanoscratch properties of MWNT-reinforced ultrahigh-molecular-weight polyethylene coatings. JOM 2007;59:50–3.

[17] Punmia BC, Jain AK, Jain AK. Comprehensive design of steel structures. 2nd ed. Bangalore: Laxmi Publications; 1998.

[18] Bhushan B. Introduction to tribology. 2nd ed. New York: John Wiley & Sons; 2013.

[19] Clauss FJ. Solid lubricants and self-lubricating solids. New York: Academic Press; 2012.

[20] https://www.zklindia.com/product_category/roller-bearings

[21] http://machinedesign.com/whats-difference-between/what-s-difference-between-bearings-1.

[22] Samad MA. Environment-friendly polymeric boundary lubricants for mechanical bearing systems. PhD diss. National University of Singapore 2010.

[23] http://oilwise.co.za/the-label-game.

[24] Madanhire I, Mbohwa C. Lubricant Additive Impacts on Human Health and the Environment. Mitigating Environ. Impact Pet. Lubr., Springer; 2016, p. 17–34.

[25] http://www.substech.com/dokuwiki/doku.php?id=additives_in_lubricating_oils.

[26] Ahmed NS, Nassar AM. Lubricating oil additives. In: Tribology - Lubricants and Lubrication, INTECH Open Access Publisher; 2011;10:249–68.

[27] Kodjak D. Policies to reduce fuel consumption, air pollution, and carbon emissions from vehicles in G20 nations. Briefing Paper, Int Counc Clean Transp 2015.

[28] Hewstone RK. Environmental health aspects of lubricant additives. Sci Total Environ 1994;156:243–54.

[29] Arena F, Mezzana L, Antoine D, Hiroto S, Kevin L, Becker T. The Automotive CO 2 Emissions Challenge. Arthur D Little 2014. http://www.adlittle.com/en/insights/viewpoints/automotive-co2-emissions-challenge

[30] Bartz WJ. Lubricants and the environment. Tribol Int 1998;31:35–47.

[31] Sanchez FP, Bandivadekar A, German J. Estimated cost of emission reduction technologies for LDVs. Report, Int Counc Clean Transp 2012:1–136.

[32] Briscoe BJ, Sinha SK. Chapter 1. Tribological applications of polymers and their composites: Past, present and future prospects. Tribol. Polym. Nanocomposites

2008; 55:1–14.

[33] http://machinedesign.com/archive/fighting-friction-solid-film-coatings.

[34] Zhang G, Liao H, Li H, Mateus C, Bordes J-M, Coddet C. On dry sliding friction and wear behaviour of PEEK and PEEK/SiC-composite coatings. Wear 2006;260:594–600.

[35] Samad MA, Sinha SK. Nanocomposite UHMWPE–CNT polymer coatings for boundary lubrication on Aluminium substrates. Tribol Lett 2010;38:301–11.

[36] Burris DL, Boesl B, Bourne GR, Sawyer WG. Polymeric nanocomposites for tribological applications. Macromol Mater Eng 2007;292:387–402.

[37] Konovalova O, Suchanek J. Significance of of Polymer Nanocomposites in Triboengineering Systems. Proc. 4th Int. Conf. NANOCON 2012.

[38] Liu F, Wang Y, Li K, Jiang L, Wang X, Shao X, et al. Graphene Oxide / Ultrahigh Molecular Weight Polyethylene Composites : Ball-Milling Preparation Mechanical Performance and Biocompatibility Effects. Am J Biomed Sci and Eng 2015;1:51–7.

[39] Briscoe BJ, Sinha SK. Wear of polymers. Proc. Inst Mech Eng Part J J Eng Tribol 2002;216:401–13.

[40] Sinha SK. Wear failures of plastics. ASM Handbook, Mater Park OH ASM Int 2002;11:1019–27.

[41] Erdemir A. Rolling-contact fatigue resistance of hard coatings on bearing steels. Argonne National Lab., IL (US); 1999.

[42] Gilmore R, Baker MA, Gibson PN, Gissler W, Stoiber M, Losbichler P, et al. Low-friction TiN–MoS 2 coatings produced by dc magnetron co-deposition. Surf

Coatings Technol 1998;108:345–51.

[43] Jahanmir S, Hunsberger AZ, Heshmat H. Load Capacity and Durability of H-DLC Coated Hydrodynamic Thrust Bearings. J Tribol 2011;133:31301.

[44] Voevodin AA, O'neill JP, Zabinski JS. Tribological performance and tribochemistry of nanocrystalline WC/amorphous diamond-like carbon composites. Thin Solid Films 1999;342:194–200.

[45] Marrocco T, Driver LC, Harris SJ, McCartney DG. Microstructure and properties of thermally sprayed Al-Sn-based alloys for plain bearing applications. J Therm Spray Technol 2006;15:634–9.

[46] Siu JHW, Li LKY. An investigation of the effect of surface roughness and coating thickness on the friction and wear behaviour of a commercial MoS 2–metal coating on AISI 400C steel. Wear 2000;237:283–7.

[47] Yeo SM. Tribology of polymeric coatings for aggressive bearing applications PhD diss. University of Illinois at Urbana-Champaign 2013.

[48] Sung HC. Tribological characteristics of various surface coatings for rotary compressor vane. Wear 1998;221:77–85.

[49] Neville A, Morina A, Haque T, Voong M. Compatibility between tribological surfaces and lubricant additives—how friction and wear reduction can be controlled by surface/lube synergies. Tribol Int 2007;40:1680–95.

[50] Harris SJ, Weiner AM, Tung SC, Simko SJ, Militello MC. A diamond-like carbon film for wear protection of steel. Surf Coatings Technol 1993;62:550–7.

[51] Wang Y, Lim S, Luo JL, Xu ZH. Tribological and corrosion behaviors of Al2O3/polymer nanocomposite coatings. Wear 2006;260:976–83.

[52] Lee J-Y, Lim D-S. Tribological behavior of PTFE film with nanodiamond. Surf Coatings Technol 2004;188–189:534–8.

[53] McCook NL, Burris DL, Bourne GR, Steffens J, Hanrahan JR, Sawyer WG. Wear resistant solid lubricant coating made from PTFE and epoxy. Tribol Lett 2005;18:119–24.

[54] Satyanarayana N, Sinha SK, Ong BH. Tribology of a novel UHMWPE/PFPE dual-film coated onto Si surface. Sensors Actuators A Phys 2006;128:98–108.

[55] Fusaro RL. Tribological properties of polymer films and solid bodies in a vacuum environment. Annual meeting of the American Society of Lubrication Engineers 1987.

[56] Song H-J, Li N, Yang J, Min C-Y, Zhang Z. Preparation and tribological behaviors of poly (ether ether ketone) nanocomposite films containing graphene oxide nanosheets. J Nanoparticle Res 2013;15:1–10.

[57] Pan B, Zhao J, Zhang Y, Zhang Y. Wear Performance and Mechanisms of Polyphenylene Sulfide/Polytetrafluoroethylene Wax Composite Coatings Reinforced by Graphene. J Macromol Sci Part B 2012;51:1218–27.

[58] Li Y, Ma Y, Xie B, Cao S, Wu Z. Dry friction and wear behavior of flame-sprayed polyamide1010/n-SiO 2 composite coatings. Wear 2007;262:1232–8.

[59] Song H-J, Zhang Z-Z, Men X. Effect of nano-Al2O3 surface treatment on the tribological performance of phenolic composite coating. Surf Coatings Technol 2006;201:3767–74.

[60] Zhang G, Liao H, Coddet C. Friction and wear behavior of PEEK and its composite coatings. Rev Artic Tribol Interface Eng Ser 2008;55:458–82.

[61] Wang ZZ, Gu P, Zhang Z. Indentation and scratch behavior of nano-SiO 2/polycarbonate composite coating at the micro/nano-scale. Wear 2010;269:21–5.

[62] Kim J, Im H, Cho MH. Tribological performance of fluorinated polyimide-based nanocomposite coatings reinforced with PMMA-grafted-MWCNT. Wear 2011;271:1029–38.

[63] Ma W, Gong F, Liu C, Tao G, Xu J, Jiang B. SiO2 reinforced HDPE hybrid materials obtained by the sol–gel method. J Appl Polym Sci 2014;131

[64] Sinha SK, Lee CB, Lim SC. Tribological performance of UHMWPE and PFPE coated films on aluminium surface. Tribol Lett 2008;29:193–9.

[65] Samad MA, Sinha SK. Mechanical, thermal and tribological characterization of a UHMWPE film reinforced with carbon nanotubes coated on steel. Tribol Int 2011;44:1932–41.

[66] Kurtz SM. Chapter 1 - A Primer on UHMWPE. In: Kurtz SMBT-TUH, editor., San Diego: Academic Press; 2004, p. 1–12.

[67] Rocha M, Mansur A, Mansur H. Characterization and accelerated ageing of UHMWPE used in orthopedic prosthesis by peroxide. Materials (Basel) 2009;2:562–76.

[68] Ma P-C, Siddiqui NA, Marom G, Kim J-K. Dispersion and functionalization of carbon nanotubes for polymer-based nanocomposites: A review. Compos Part A Appl Sci Manuf 2010;41:1345–67.

[69] Liao M, Koide Y. Carbon-Based Materials: Growth, Properties, MEMS/NEMS Technologies, and MEM/NEM Switches. Crit Rev Solid State Mater Sci 2011;36:66–101.

[70] Magrez A, Kasas S, Salicio V, Pasquier N, Seo JW, Celio M, et al. Cellular Toxicity of Carbon-Based Nanomaterials. Nano Lett 2006;6:1121–5.

[71] Mauter MS, Elimelech M. Environmental Applications of Carbon-Based Nanomaterials. Environ Sci Technol 2008;42:5843–59.

[72] Wood W. Processing, wear, and mechanical properties of polyethylene composites prepared with pristine and organosilane-treated carbon nanofibers. PhD diss. Washington State University 2012.

[73] Enomoto K, Yasuhara T, Kitakata S, Murakami H, Ohtake N. Frictional Properties of Carbon Nanofiber Reinforced Polymer Matrix Composites. New Diam Front Carbon Technol 2004;14:11–20.

[74] Sui G, Zhong WH, Ren X, Wang XQ, Yang XP. Structure, mechanical properties and friction behavior of UHMWPE/HDPE/carbon nanofibers. Mater Chem Phys 2009;115:404–12.

[75] Cho MH, Bahadur S. A study of the thermal, dynamic mechanical, and tribological properties of polyphenylene sulfide composites reinforced with carbon nanofibers. Tribol Lett 2007;25:237–45.

[76] Kausar A. Advances in Polymer/Fullerene Nanocomposite: A Review on Essential Features and Applications. Polym Plast Technol Eng 2017;56:594–605.

[77] Phillips JP, Deng X, Stephen RR, Fortenberry EL, Todd ML, McClusky DM, et al. Nano-and bulk-tack adhesive properties of stimuli-responsive, fullerene–polymer blends, containing polystyrene-block-polybutadiene-block-polystyrene and polystyrene-block-polyisoprene-block-polystyrene rubber-based adhesives. Polymer (Guildf) 2007;48:6773–81.

[78] Li F, Li Y, Ge Z, Zhu D, Song Y, Fang G. Synthesis and optical limiting properties of polycarbonates containing fullerene derivative. J Phys Chem Solids 2000;61:1101–3.

[79] Balayeva NO, Mamiyev ZQ. Synthesis and characterization of Ag2S/PVA-fullerene (C60) nanocomposites. Mater Lett 2016;175:231–5.

[80] Alzari V, Zaragoza-Galán G, Nuvoli D, Illescas J, Rivera E, Sanna V, et al. Preparation and interaction study between fullerene and graphene in a polymeric matrix. Compos Sci Technol 2015;110:217–23.

[81] Jeyranpour F, Alahyarizadeh G, Minuchehr A. The thermo-mechanical properties estimation of fullerene-reinforced resin epoxy composites by molecular dynamics simulation – A comparative study. Polymer (Guildf) 2016;88:9–18.

[82] Ruoff RS, Tse DS, Malhotra R, Lorents DC. Solubility of fullerene (C60) in a variety of solvents. J Phys Chem 1993;97:3379–83.

[83] Iijima S. Helical microtubules of graphitic carbon. Nature 1991;354:56.

[84] Bakshi SR, Agarwal A. An analysis of the factors affecting strengthening in carbon nanotube reinforced aluminum composites. Carbon N Y 2011;49:533–44.

[85] Zoo Y-S, An J-W, Lim D-P, Lim D-S. Effect of carbon nanotube addition on tribological behavior of UHMWPE. Tribol Lett 2004;16:305–9.

[86] He H, Klinowski J, Forster M, Lerf A. A new structural model for graphite oxide. Chem Phys Lett 1998;287:53–6.

[87] Zhu Y, Murali S, Cai W, Li X, Suk JW, Potts JR, et al. Graphene and graphene oxide: synthesis, properties, and applications. Adv Mater 2010;22:3906–24.

[88] Tong Y, Bohm S, Song M. Graphene based materials and their composites as

coatings. Austin J Nanomedicine Nanotechnol 2013;1:1003.

[89] Lin L-Y, Kim D-E, Kim W-K, Jun S-C. Friction and wear characteristics of multi-layer graphene films investigated by atomic force microscopy. Surf Coatings Technol 2011;205:4864–9.

[90] Qi K, Sun Y, Duan H, Guo X. A corrosion-protective coating based on a solution-processable polymer-grafted graphene oxide nanocomposite. Corros Sci 2015;98:500–506.

[91] Puértolas JA, Kurtz SM. Evaluation of carbon nanotubes and graphene as reinforcements for UHMWPE-based composites in arthroplastic applications: A review. J Mech Behav Biomed Mater 2014;39:129–45.

[92] Lee C, Wei X, Li Q, Carpick R. Elastic and frictional properties of graphene. Phys Status Solidi B, Basic Solid State Phys 12AD;246:2562–7.

[93] Marchetto D, Held C, Hausen F, Wählisch F, Dienwiebel M, Bennewitz R. Friction and wear on single-layer epitaxial graphene in multi-asperity contacts. Tribol Lett 2012;48:77–82.

[94] Hsieh C-T, Chen W-Y. Water/oil repellency and work of adhesion of liquid droplets on graphene oxide and graphene surfaces. Surf Coatings Technol 2011;205:4554–61.

[95] Balandin AA, Ghosh S, Bao W, Calizo I, Teweldebrhan D, Miao F, et al. Superior thermal conductivity of single-layer graphene. Nano Lett 2008;8:902–7.

[96] Ghosh S, Calizo I, Teweldebrhan D, Pokatilov EP, Nika DL, Balandin AA, et al. Extremely high thermal conductivity of graphene: Prospects for thermal management applications in nanoelectronic circuits. Appl Phys Lett

2008;92:151911.

[97] Baena JC, Wu J, Peng Z. Wear Performance of UHMWPE and Reinforced UHMWPE Composites in Arthroplasty Applications: A Review. Lubricants 2015;3:413–36.

[98] Gao Y, Liu L-Q, Zu S-Z, Peng K, Zhou D, Han B-H, et al. The effect of interlayer adhesion on the mechanical behaviors of macroscopic graphene oxide papers. ACS Nano 2011;5:2134–41.

[99] Gómez-Navarro C, Burghard M, Kern K. Elastic properties of chemically derived single graphene sheets. Nano Lett 2008;8:2045–9.

[100] Berman D, Erdemir A, Zinovev A V, Sumant A V. Nanoscale friction properties of graphene and graphene oxide. Diam Relat Mater 2015;54:91–6.

[101] Lee W, Lee JU, Jung BM, Byun J-H, Yi J-W, Lee S-B, et al. Simultaneous enhancement of mechanical, electrical and thermal properties of graphene oxide paper by embedding dopamine. Carbon N Y 2013;65:296–304.

[102] Ghosh S. Thermal Conduction in Graphene and Graphene Multilayers PhD diss. University of California, Riverside 2009.

[103] Mittal V. Functional polymer nanocomposites with graphene: A review. Macromol Mater Eng 2014;299:906–31.

[104] Hernandez Y, Nicolosi V, Lotya M, Blighe FM, Sun Z, De S, et al. High-yield production of graphene by liquid-phase exfoliation of graphite. Nat Nanotechnol 2008;3:563–8.

[105] Park S, Ruoff RS. Chemical methods for the production of graphenes. Nat Nanotechnol 2009;4:217–24.

[106] McAllister MJ, Li J-L, Adamson DH, Schniepp HC, Abdala AA, Liu J, et al. Single sheet functionalized graphene by oxidation and thermal expansion of graphite. Chem Mater 2007;19:4396–404.

[107] Xiao J, Xu Y, Yang S. High-Performance Supercapacitors Based on Novel Graphene Composites. In: A. Rashid bin Mohd Yusoff editor Graphene-based Energy Devices, Wiley-VCH Verlag GmbH & Co. KGaA 2015, p. 145–70.

[108] Berger C, Song Z, Li X, Wu X, Brown N, Naud C, et al. Electronic confinement and coherence in patterned epitaxial graphene. Science 2006;312:1191–6.

[109] Wu H, Zhao W, Hu H, Chen G. One-step in situball milling synthesis of polymer-functionalized graphene nanocomposites. J Mater Chem 2011;21:8626–32.

[110] Jiang X, Drzal LT. Reduction in percolation threshold of injection molded high-density polyethylene/exfoliated graphene nanoplatelets composites by solid state ball milling and solid state shear pulverization. J Appl Polym Sci 2012;124:525–35.

[111] Liu Y, Wu H, Chen G. Enhanced mechanical properties of nanocomposites at low graphene content based on in situ ball milling. Polym Compos 2014;37:1190–7.

[112] Jang B, Yang L, Wong S-C, Bai Y. Process for producing nano-scaled graphene plates. U.S. Patent Application 2004;10/858814.

[113] Zhao W, Wu F, Wu H, Chen G. Preparation of colloidal dispersions of graphene sheets in organic solvents by using ball milling. J Nanomater 2010;2010

[114] Kun P, Wéber F, Balázsi C. Preparation and examination of multilayer graphene nanosheets by exfoliation of graphite in high efficient attritor mill. Open Chem 2011;9:47–51.

[115] Yan L, Lin M, Zeng C, Chen Z, Zhang S, Zhao X, et al. Electroactive and

biocompatible hydroxyl-functionalized graphene by ball milling. J Mater Chem 2012;22:8367–71.

[116] Sun P, Kuga S, Wu M, Huang Y. Exfoliation of graphite by dry ball milling with cellulose. Cellulose 2014;21:2469–78.

[117] Wang D, Bierwagen GP. Sol–gel coatings on metals for corrosion protection. Prog Org Coatings 2009;64:327–38.

[118] Gray JE, Luan B. Protective coatings on magnesium and its alloys — a critical review. J Alloys Compd 2002;336:88–113.

[119] Norrman K, Ghanbari-Siahkali A, Larsen NB. 6 Studies of spin-coated polymer films. Annu Reports Sect "C", Physical Chem 2005;101:174–201.

[120] Yimsiri P, Mackley MR. Spin and dip coating of light-emitting polymer solutions: Matching experiment with modelling. Chem Eng Sci 2006;61:3496–505.

[121] Siemann U. Solvent cast technology – a versatile tool for thin film production. Scatt. Methods Prop. Polym. Mater. SE - 1, vol. 130, Springer Berlin Heidelberg; 2005, p. 1–14.

[122] https://en.wikipedia.org/wiki/Polymer_solution_casting.

[123] Lee M. Solution-casting of Disulfonated Poly (arylene ether sulfone) Multiblock Copolymer Films for Proton Exchange Membranes. PhD diss. Virginia Tech 2009.

[124] Knoop HE. Process for solvent casting a film. U.S. Patent 1987;4664859.

[125] Liu J, Casavant MJ, Cox M, Walters DA, Boul P, Lu W, et al. Controlled deposition of individual single-walled carbon nanotubes on chemically functionalized templates. Chem Phys Lett 1999;303:125–9.

[126] http://nano.columbia.edu/files/cise/spintheory_0.pdf.

[127] Sahu N, Parija B, Panigrahi S. Fundamental understanding and modeling of spin coating process: A review. Indian J Phys 2009;83:493–502.

[128] Lim S-L, Chen E-C, Chen C-Y, Ong K-H, Chen Z-K, Meng H-F. High performance organic photovoltaic cells with blade-coated active layers. Sol Energy Mater Sol Cells 2012;107:292–7.

[129] Blankenburg L, Schultheis K, Schache H, Sensfuss S, Schrödner M. Reel-to-reel wet coating as an efficient up-scaling technique for the production of bulk-heterojunction polymer solar cells. Sol Energy Mater Sol Cells 2009;93:476–83.

[130] Hu Z, Zhang J, Xiong S, Zhao Y. Performance of polymer solar cells fabricated by dip coating process. Sol Energy Mater Sol Cells 2012;99:221–5.

[131] Hussmann EK. Dip coatings: characteristics, properties, applications. Opt. Surf. Technol., International Society for Optics and Photonics; 1983, p. 152–9.

[132] Girotto C, Rand BP, Genoe J, Heremans P. Exploring spray coating as a deposition technique for the fabrication of solution-processed solar cells. Sol Energy Mater Sol Cells 2009;93:454–8.

[133] Bailey AG. The science and technology of electrostatic powder spraying, transport and coating. J Electrostat 1998;45:85–120.

[134] Fredrickson G, Pham L, Feng J, Anderson N, Eidenschink T, O'connor T. System and method for electrostatic-assisted spray coating of a medical device. U.S. Patent Application 2007;11/412774.

[135] Krebs FC. Fabrication and processing of polymer solar cells: A review of printing and coating techniques. Sol Energy Mater Sol Cells 2009;93:394–412.

[136] Kim J-S, Chung W-S, Kim K, Kim DY, Paeng K-J, Jo SM, et al. Performance

Optimization of Polymer Solar Cells Using Electrostatically Sprayed Photoactive Layers. Adv Funct Mater 2010;20:3538–46.

[137] Powder Coatings Electrostatic vs Fluid Bed. Br Coatings Fedearation http://www.coatings.org.uk/Sectors/Powder_Coatings_Electrostatic_vs_Fluid_Bed_.aspx.

[138] Coating application guide. Wattyl Ind Coatings 2010:1–7. http://www.wattylindustrial.com.au/documents/industrial/information/3 COATING APPLICATION GUIDE v2.pdf.

[139] Aziz F, Ismail AF. Spray coating methods for polymer solar cells fabrication: A review. Mater Sci Semicond Process 2015;39:416–25.

[140] Barletta M, Lusvarghi L, Mantini FP, Rubino G. Epoxy-based thermosetting powder coatings: Surface appearance, scratch adhesion and wear resistance. Surf Coatings Technol 2007;201:7479–504.

[141] Barletta M. Dry sliding wear response of some industrial powder coatings. Tribol Int 2011;44:1236–50.

[142] Barletta M, Gisario A, Rubino G, Tagliaferri V. Electrostatic spray deposition (ESD) of 'self organizing' TiO2-epoxy powder paints: Experimental analysis and numerical modeling. Surf Coatings Technol 2006;201:3212–28.

[143] Sharma R, Trigwell S, Biris AS, Sims RA, Mazumder MK. Effect of ambient relative humidity and surface modification on the charge decay properties of polymer powders in powder coating. Ind Appl IEEE Trans 2003;39:87–95.

[144] Mazumder MK, Sims RA, Biris AS, Srirama PK, Saini D, Yurteri CU, et al. Twenty-first century research needs in electrostatic processes applied to industry and

medicine. Chem Eng Sci 2006;61:2192–211.

[145] Barletta M, Gisario A, Tagliaferri V. Electrostatic spray deposition (ESD) of polymeric powders on thermoplastic (PA66) substrate. Surf Coatings Technol 2006;201:296–308.

[146] http://en.wikipedia.org/wiki/Aluminium_carbide.

[147] Sims RA, Mazumder MK, Liu X, Chok W, Mountain JR, Wankum DL, et al. Electrostatic effects on first pass transfer efficiency in the application of powder coatings. Ind Appl IEEE Trans 2001;37:1610–7.

[148] Barletta M, Tagliaferri V. Influence of process parameters in electrostatic fluidized bed coating. Surf Coatings Technol 2006;200:4619–29.

[149] Barletta M, Tagliaferri V. Electrostatic fluidized bed deposition of a high performance polymeric powder on metallic substrates. Surf Coatings Technol 2006;200:4282–90.

[150] Zhu S, Zhang Y, Li Q, Wei L, Guan S. Influence of polytetrafluoroethylene (PTFE) content on mechanical and tribological properties of poly (ether ether ketone)/PTFE coatings prepared by electrostatic powder spraying technique. High Perform Polym 2014;27:3–9.

[151] Zouari M, Kharrat M, Dammak M, Barletta M. Scratch resistance and tribological performance of thermosetting composite powder coatings system: A comparative evaluation. Surf Coatings Technol 2015;263:27–35.

[152] Lahiri D, Hec F, Thiesse M, Durygin A, Zhang C, Agarwal A. Nanotribological behavior of graphene nanoplatelet reinforced ultra high molecular weight polyethylene composites. Tribol Int 2014;70:165–9.

[153] Mohammed AS, Ali A Bin. Investigating the effect of water uptake on the tribological properties of organoclay reinforced UHMWPE nanocomposites. Tribol Lett 2016;62.

[154] Abdul Samad M, Satyanarayana N, Sinha SK. Tribology of UHMWPE film on air-plasma treated tool steel and the effect of PFPE overcoat. Surf Coatings Technol 2010;204:1330–8.

[155] http://harrickplasma.com/applications/surface-modification.

[156] Bückle H. Use of the hardness test to determine other material properties. Sci Hardness Test Its Res Appl 1973:453.

[157] Shepelev O, Kenig S. Effect of Modified Graphene on Properties of Polypropylene Nanocomposites. Graph Graphene, Their Polym Nanocomposites 2012:447.

[158] Chieng BW, Ibrahim NA, Wan Yunus WMZ, Hussein MZ, Silverajah VS. Graphene nanoplatelets as novel reinforcement filler in poly (lactic acid)/epoxidized palm oil green nanocomposites: Mechanical properties. Int J Mol Sci 2012;13:10920–34.

[159] Pang W, Ni Z, Chen G, Huang G, Huang H, Zhao Y. Mechanical and thermal properties of graphene oxide/ultrahigh molecular weight polyethylene nanocomposites. RSC Adv 2015;5:63063–72.

[160] Maksimkin A V, Kaloshkin SD, Tcherdyntsev V V, Chukov DI, Shchetinin I V. Effect of high-energy ball milling on the structure and mechanical properties of ultra-high molecular weight polyethylene. J Appl Polym Sci 2013;130:2971–7.

[161] Ferrari AC. Raman spectroscopy of graphene and graphite: Disorder, electron–phonon coupling, doping and nonadiabatic effects. Solid State Commun 2007;143:47–57.

[162] Matis M, Kosidlo U, Tonner F, Glanz C, Kolaric I. Electrochemical Exfoliation: A Cost-Effective Approach to Produce Graphene Nanoplatelets in Bulk Quantities. Graph Graphene, Their Polym Nanocomposites 2012:139.

[163] Ferrari AC, Meyer JC, Scardaci V, Casiraghi C, Lazzeri M, Mauri F, et al. Raman spectrum of graphene and graphene layers. Phys Rev Lett 2006;97:187401.

[164] Zavgorodnev Y V, Chvalun SN, Nikolaeva GY, Sagitova EA, Pashinin PP, Gordeyev SA, et al. Raman study of uniaxial deformation of single-crystal mats of ultrahigh molecular weight linear polyethylene. J. Phys. Conf. Ser., vol. 594, IOP Publishing; 2015, p. 12010.

[165] Lawal D, Bin Ali A, Mohammed AS. Tribological investigations of carbon nanotube-reinforced polymer (UHMWPE) nanocomposites using Taguchi methodology. J Appl Polym Sci 2016;133.

[166] Huang G, Ni Z, Chen G, Zhao Y. The Influence of Irradiation and Accelerated Aging on the Mechanical and Tribological Properties of the Graphene Oxide/Ultra-High-Molecular-Weight Polyethylene Nanocomposites. Int J Polym Sci 2016;2016.

[167] Gang W, Chunhua Z, Xinze Z. Friction and Wear Characteristics of UHMWPE Studied by Orthogonal Method. Adv. Tribol., Springer; 2009, p. 847–50.

[168] Boon PC, Md. Akil H, Md. Nasir R. Dry Sliding Wear Behaviour of Talc-reinforced UHMWPE Composite for Implant Application. Sains Malaysiana 2015;44:819–25.

[169] Quaglini V, Dubini P. Friction of polymers sliding on smooth surfaces. Adv Tribol 2011;2011.

[170] Zhang J, Polycarpou AA, Economy J. An improved tribological polymer-coating system for metal surfaces. Tribol Lett 2010;38:355–65.

[171] GreeneTweed. Plastic Bearing Design Guide. www.gtweed.com.

[172] Samyn P, Van Schepdael L, Leendertz JS, Gerber A, Van Paepegem W, De Baets P, et al. Large-scale friction and wear tests on a hybrid UHMWPE-pad/primer coating combination used as bearing element in an extremely high-loaded ball-joint. Tribol Int 2006;39:796–811.

[173] Glaeser W. Materials for tribology. vol. 20. Elsevier; 1992.

[174] http://www.hotrod.com/articles/engine-oil-temperature.

[175] Liu CZ, Ren LQ, Tong J, Green SM, Arnell RD. Effects of operating parameters on the lubricated wear behavior of a PA-6/UHMWPE blend: a statistical analysis. Wear 2002;253:878–84.

[176] Liu CZ, Wu JQ, Li JQ, Ren LQ, Tong J, Arnell AD. Tribological behaviours of PA/UHMWPE blend under dry and lubricating condition. Wear 2006;260:109–15.

[177] Xiong D, Ge S. Friction and wear properties of UHMWPE/Al2O3 ceramic under different lubricating conditions. Wear 2001;250:242–5.

[178] https://www.mobil.com/english-au/passenger-vehicle-lube/pds/glxxmobil-1-0w40.

[179] Shahidi F. Bailey's Industrial Oil and Fat Products, 6 Volume Set. vol. 4. Chapter; 2005.

[180] Fasina OO, Colley Z. Viscosity and specific heat of vegetable oils as a function of temperature: 35 C to 180 C. Int J Food Prop 2008;11:738–46.

VITAE

Name	**Ismaila Kayode Aliyu**
Nationality	Nigerian
Address	c/o Supol Jimoh Aliyu (retd), Police Mounted Troop, P.M.B. 1394, Kulende, ILORIN, Kwara State, Nigeria
Date of Birth	18/05/1980
Email	ismaaelei@gmail.com
Academic Background	**Ph.D. (Mechanical Engineering), December 2017.** *Specialized in Materials and Manufacturing*. King Fahd University of Petroleum and Minerals, Dhahran, Saudi Arabia. **M.Sc. (Mechanical Engineering), May 2013.** *Specialized in Materials and Manufacturing*. King Fahd University of Petroleum and Minerals, Dhahran, Saudi Arabia. **B.Eng. (Mechanical Engineering), November, 2007.** *Specialized in Design and Production.* University of Ilorin, Ilorin, Nigeria.